Yale University

EliScholar – A Digital Platform for Scholarly Publishing at Yale

Yale Graduate School of Arts and Sciences Dissertations

Fall 10-1-2021

Investigating the Effect of Allostery on Downstream Biology of the Epidermal Growth Factor Receptor

Deepto Mozumdar
Yale University Graduate School of Arts and Sciences, deepto.moz@gmail.com

Follow this and additional works at: https://elischolar.library.yale.edu/gsas_dissertations

Recommended Citation

Mozumdar, Deepto, "Investigating the Effect of Allostery on Downstream Biology of the Epidermal Growth Factor Receptor" (2021). *Yale Graduate School of Arts and Sciences Dissertations*. 382.
https://elischolar.library.yale.edu/gsas_dissertations/382

This Dissertation is brought to you for free and open access by EliScholar – A Digital Platform for Scholarly Publishing at Yale. It has been accepted for inclusion in Yale Graduate School of Arts and Sciences Dissertations by an authorized administrator of EliScholar – A Digital Platform for Scholarly Publishing at Yale. For more information, please contact elischolar@yale.edu.

Abstract

Investigating the Effect of Allostery on Downstream Biology of the

Epidermal Growth Factor Receptor

Deepto Mozumdar

2021

The Epidermal Growth Factor Receptor (EGFR) is a member of the receptor tyrosine kinase (RTK) family of human proteins with a critical role in transducing diverse extracellular chemical information to initiate multiple cellular signaling cascade in the cell that are essential for normal cell development. Aberrant activation of this receptor via mutation or overexpression misregulates this flow of information and is implicated in a multiple human carcinoma. Thus, understanding the molecular mechanisms by which chemical information is encoded and decoded in EGFR is imperative both from a basic cell biology and therapeutic standpoint.

In this thesis consisting of four chapters, I describe my graduate work studying the structure of a portion of EGFR called the juxtamembrane segment (JM) and investigating its role in modulating and controlling the downstream biology of the receptor.

Chapter 1: This chapter provides an introduction, overview and in-depth discussion of the literature pertaining to the critical role of JM in modulating EGFR biology through its manifold functions in kinase activation, allosterically encoding structural changes in the various domains of EGFR, and its interactions with diverse intracellular components.

Chapter 2: In this chapter I describe my work utilizing a chemical biology tool called Bipartite Tetracysteine Display to study to the structure of the JM of a constitutively active variant of EGFR, namely EGFRvIII that is implicated in most cases of Glioblastoma Multiforme. Through my studies I illustrate how the assembly of unique structures within the JM segment of this oncogenic receptor supports the constitutive activity of this protein.

Chapter 3: In this chapter I describe my work utilizing tools in chemical biology, biochemistry and cell biology to demonstrate that the assembly of discrete coiled coil structures within the JM segment of EGFR is necessary and sufficient for controlling the path of endocytic trafficking of the receptor and its intracellular lifetime. Furthermore, I demonstrate how the assembly of these discrete JM structures also predicts kinase-independent effects of oncogenic EGFR mutations (implicated in Non-Small Cell Lung Cancer) and clinically relevant tyrosine kinase inhibitors that promote efficient, lysosome-based EGFR degradation.

Chapter 4: *This chapter describes preliminary experiments that were performed on two projects that were initiated in the early and later parts of Ph.D. research. The first project seeks to investigate the role of receptor multimerization on the JM structure of EGFR. The second ongoing project seeks to investigate the effect of JM structure on the interactome of WT and oncogenic EGFR using APEX2-based proximity labeling and mass spectrometry. For both projects, I discuss my rationale, experimental design and preliminary results and provide my thoughts for future directions.*

Investigating the Effect of Allostery on Downstream Biology of the

Epidermal Growth Factor Receptor

A Dissertation

Presented to the Faculty of the Graduate School

of

Yale University

in Candidacy for the Degree of

Doctor of Philosophy

by

Deepto Mozumdar

Dissertation Director: Alanna Schepartz

December 2021

© 2021 by Deepto Mozumdar

All Rights Reserved

Acknowledgements

There are so many people whom I am greatly indebted to for my success in graduate school.

First, I am immensely grateful for the wonderful mentorship of my thesis advisor, Professor Alanna Schepartz. Throughout my graduate research, Alanna has provided me with unwavering inspiration and support both in my scientific pursuits and on a personal front. Alanna's first priority has always been her students and she has fostered an incredibly positive, inclusive and collaborative lab atmosphere. Alanna's confidence in my ability to succeed, even in my moments of failure or doubt, has been the key driving force for my progress – her consistently high expectations have caused me to push myself and improve throughout my graduate research. Needless to say, I am better scientist because of her.

I would like to thank my other thesis committee members Professor Sarah Slavoff and Professor Scott Miller for their guidance. I would also like to thank Professor Jonathan Ellmann and Professor William Jorgenson for their help and support in my dissertation progress. I would also like to thank Professor Joseph Wolenski, Professor Steve Ruzin and Dr. Denise Schichnes for support with the confocal microscope (without which I would be missing my third chapter)

I will be forever grateful for my brilliant labmates in the Schepartz lab past and present. I am indebted to my mentors: to Dr. Amy Elizabeth Doerner, Dr. Julie Sinclair, Dr. Kim Quach and Dr. Allison Walker for their guidance in my dissertation research – for teaching me everything about working with mammalian cells, cell biology and so much more; To Dr. Rebecca Wissner who has supported me in countless ways, helped me navigate the complexity of scientific research and being a constant source of inspiration in the early years of my graduate research. I am grateful for the guidance and support of past graduate students and post-docs, Dr. Alexander David Thompson, Dr. Wesley Robertson, Dr. Angela Steinaur, Dr. Aaron Zwicker, Dr. Aarushi Gupta and Dr. Omer Ad for their support and guidance. I would like to thank Dr. Susan Knox for her constant support and guidance in the many years we worked together. I would like to thank Dr. Jonathan Tyson for the many hours we spent talking science and dreaming up new directions for academic research. I would like to thank present graduate students: Sol Chang for being an amazing partner on the EGFR project – it is with her constant help and support that I have been able to carry forward the EGFR project. I would like to thank Sebasthian Santiago, Riley Fricke, Tent Tangpradabkul, Riley Fricke, Leah Tang Roe, Cameron Swenson, Isaac Knudson, Madeline Zoltek, Dr. Shuai Zheng and Dr. Andrew Cairns for being the most amazing lab members, for the many scientific discussion and the LOLs. I would like to thank Kelsey Zhang for her constant support with the cell lab and mammalian cell culture. I would like to thank Dr. Samantha Pixie Piszkeiwicz for her unbridled support as a scientist and on countless other fronts. I would like to thank Patrick Ginther for the countless discussions in science and life and many early morning coffee and lunch runs. I would like to thank the many undergrads students who helped me in my research – Alexandra Forman, Justin Zhang and Diane Rafizadeh. Finally, I would like to thanks Neville Dadina for being an amazing labmate and a wonderful friend. Our discussions have provided constant humor and color and scientific inspiration in my life.

I would like to acknowledge the vital support of Karen K. Wong – she has looked out for my well-being in UC Berkeley on countless occasions and I am indebted to her for her support (and the many baked goods that kept me going through late nights in lab!). I would like to thank Michelle Ferrara for her constant support and guidance and Carol MacDonald-Phillips for keeping the lab

running back at Yale. I would like to thank the administrative staff both at UC Berkeley and Yale for their constant support and help.

Over the course of my graduate life both at Yale and UC Berkeley, I was fortunate to have shared my time with some amazing friends who have carried me through graduate school. I would like to thank Dr. Raktim Roy for providing me with scientific inspiration, guidance and critique that has helped shape many aspects of my scientific thinking. I would like to thank Dr. Gourab Banerjee for his constant encouragement and support in every stage of my graduate research (and reminding me that 29 is a suit exhaustive card game!). I would like to thank Dr. Subhajyoti Chaudhuri for being a wonderful mentor, for his advice and counsel in navigating graduate school (and for the countless insightful life stories). I am indebted to the constant care and support provided by Dr. Ipsita Ghosh in my years in graduate school (and for the countless impromptu getaways to NYC). I would like to thank Dr. Titas Sengupta for her academic mentorship and for inspiring me with her persistence and dedication to science. I would like to thanks Dr. Sanghamitra Majumdar and Dr. Subhashish Mandal for their love and support (and for their amazing cooking, for driving me to so many places on our group adventures). This group of friends has molded me into the person and scientist I am. Our countless adventures and memories are a treasure that I will forever cherish. I thank all the great friends I made during my time in New Haven and Berkeley – I honestly cannot imagine getting through this without you. Life away from home wasn't so bad thanks to all our silly shenanigans. I would like to thank the love and support of my 'Changers' intramural basketball and trivia crew of Raymond Ehlers, Angele Delevoye, Noreen Gentry, Julie Cheung and Varun Jorapur. It has been a genuine pleasure playing with them and I immensely cherish the memories made on our countless 'Ball, Burger and Beer' adventures. I would like to thank Luis Lorenzo Perez, Thomas Bonczek, Rodrigo Bento, Mingrui Xu, Mehdi El Hailoush, Vanessa Bittner for our countless summer barbecue and late-night GPSCY adventures in New Haven. To all friends in the Chemistry Department at Yale and UC Berkeley, thank you for the cheer and many scientific discussions.

I would like to thank every single one of my teachers in school, college and graduate school for shaping me as a person, for believing in me, for nurturing my curiosity and guiding me to the path of science. I am indebted to each and every one of them for where I am today. I would like to particularly thank Ms. Virender Kaur, Ms. Shubhra Dabas, Ms. Florence Joseph, Ms. Sharmishtha Sanyal, Ms. Tarang Chaudhary, Ms. Anuradha Gupta, Dr. Rashmi Sachdeva, Dr. Rakhi Thareja, Dr. Vibha Sharma and Dr. Ekta Kundra, Dr. Elsa Yan, Dr. Victor Batista, Dr. Gary Brudvig, Dr. Ziad Ganim and Dr. Nilay Hazari. I would like to thank Dr. Sushil Mishra who first taught me how to use a pipette and guiding me in my first steps in scientific research. I am indebted to Dr. Pramit K. Chowdhury for letting me work in his lab for my undergraduate research and for his constant support and encouragement.

Finally, I am eternally grateful for the unconditional love and support of my family. I thank my brother Aaloke who has been a constant source of love and humor and my closest confidante in difficult moments in my life. I thank my grandparents for showering my life with love and care and inspiring me with their life and example. I would like to thank my aunts and uncles in India and in the US who have provided me a home away from home and filled my life with joy and humor. Most importantly I would like to thank my parents, who in every stage of my life, have provided me with unbridled support and encouragement that has kept me afloat and has inspired me to push myself ahead in life. They were the first to nurture my curiosity that seeded my love of science. Needless to say, I wouldn't be here without my parents, but the truth is that any success in my life is simply a testament to the love and countless sacrifices in theirs.

Table of Contents

Figures and Tables

Chapter 1

Chapter 2

Chapter 3

Chapter 4

Chapter 1. The juxtamembrane region of the epidermal growth factor receptor is a critical modulatory element of growth factor dependent signaling.

Disclosure and authorship

This chapter contains material that was written together with Sol H.-H. Chang, and is being prepared for a submission as a review to *Trends in Biochemical Sciences.*

Chapter 1. The juxtamembrane region of the epidermal growth factor receptor is a critical modulatory element of growth factor dependent signaling.

1.1. Introduction

The epidermal growth factor receptor [1,2] (EGFR; also referred to as ErbB1 [3]/ HER) is a member of the receptor tyrosine kinase (RTK) family of human proteins [4,5], and functions as a conduit for the flow of information across the cell membrane [6]. In normal physiology, chemical information encoded by multiple extracellular growth factors [3,7,8] is allosterically communicated through EGFR into the cell interior, to effect diverse signaling outcomes that support cell growth and survival [4,6]. Misregulation of this information flow *via* mutation or overexpression of EGFR, is associated with multiple human cancers and disease pathologies [9–11]. Given its critical role both from a physiological and therapeutic standpoint, it has been a long standing goal to decipher the molecular mechanisms by which chemical information is encoded and decoded in EGFR.

EGFR is a 1186 amino acid long transmembrane protein consisting of five connected domains/ segments, namely the extracellular domain (ECD), the transmembrane (TM) and juxtamembrane (JM) domains, the tyrosine kinase (TK) domain and the C-terminal tail (C-tail) [6] **(Figure 1.1.A**). Upon binding EGFR specific growth factors [7], the ECD undergoes conformational rearrangements [12–14] that are propagated through the membrane-embedded TM helix [15–17] and adjacent cytosolic JM [17–21] region to induce assembly of the intracellular kinase domain into a catalytically competent asymmetric dimer conformation [22,18,19] (**Figure 1.1.B**). Thereafter, the catalytically active kinase auto-phosphorylates the C-tail at multiple tyrosine residues [3,4,6] and these phosphorylated tyrosines recruit diverse adaptor proteins to initiate multiple cellular signaling cascades in the cell [3,4,6] (**Figure 1.1B,C**). Our current

understanding of how the different parts of EGFR function in the mechanism of growth factor induced receptor activation, is based on high resolution structural studies of the isolated EGFR domains (ECD [12–14,23], TM [15,24], JM [15,18,19], TK domains [18,22]), low resolution electron microscopy of the near full length/ full-length EGFR protein [25,26] together with computational analyses [16]. For detailed discussions of EGFR biochemical mechanisms and structures that have been elucidated, we direct the reader to other extensive reviews on the subject [4–6,27].

Complicating the analysis of information transfer by EGFR is the fact that the receptor ECD binds seven different growth factors that activate EGFR in mammalian systems [7,8] – these are namely, epidermal growth factor (EGF), transforming growth factor-alpha (TGF-α), epigen (EPI), epiregulin (ER), betacellulin (BC), heparin-binding EGF (HB-EGF), and amphiregulin (AR) (**Figure 1.1.C**). It is well known that the different EGFR specific growth factors upon binding EGFR initiate diverse growth factor-dependent signals in the cell interior [14,28–30]. Lesser is known about how the chemical information encoded by the diverse growth factors is decoded by EGFR into distinct outcomes of signaling and cell state. Preliminary clues can be gleaned from high resolution structures of the EGFR ECD bound to a subset of these growth factors (EGF [13,26], TGF-α [12,26], EPI [14] and ER [14]), that reveal that these diverse EGFR specific growth factors induce distinct structures locally within the ECD. Understanding how growth factor dependent differences in ECD structure are then (1) allosterically propagated through the intervening segments of the EGFR protein and (2) decoded into distinct intracellular signals has been a focus of research in the Schepartz lab [17,20,31,21].

At the centre of this focus is the juxtamembrane region of EGFR [18,19]– this intervening segment (spanning ~ 37 amino acid residues) is right in the middle of the allosteric network that

extends from the ECD to the tyrosine kinase domain and plays critical roles in multiple aspects of EGFR signaling. In this section of my thesis, I will discuss the existing body of literature on the EGFR JM, focusing on (i) the mechanistic roles of the JM in signal transduction, (ii) the allosteric coupling of JM structure to the different EGFR domains and finally (iii) the interactions of the JM with various intracellular components. Through this discussion, I hope to highlight the fact that the JM region, through its various structures and interactions, acts as an essential signal modulatory unit in the EGFR protein.

1.2. The juxtamembrane segment of the is necessary for EGFR kinase assembly and activation. Several pieces of biochemical [18,19,32–35] and biophysical [18,19] evidence have illustrated the indispensable role of the EGFR JM in receptor activation. Initial biochemical analyses of EGFR kinase constructs with varying JM segment deletions revealed a clear activatory role of the JM – As compared to EGFR kinase constructs where the complete JM was present, constructs lacking the JM segment either in part or in entirety displayed (i) reduced dimerization *in vitro* [18], (ii) reduced tyrosine kinase activity (~65-95% *in vitro*; 95% *in cellula*) [33] and reduced catalytic efficiency (~10-70 fold reduction in k_{cat}/ K_M *in vitro*) [18]. Likewise, C-tail autophosphorylation activity was reduced *in cellula* for constructs lacking part of/ the entire JM or where the entire JM is replaced by an unstructured $(GGS)_{10}$ sequence, as compared to the analogous intact full length/ intact intracellular domain constructs [32–34].

Biophysical analysis of the JM region either in conjunction with the kinase domain (using crystallography) [18,19,22] or in isolation (using NMR) [18,36] have revealed finer structural details of the individual elements of the JM that contribute to kinase assembly and activation. The analysis of crystal structures of EGFR [19] and HER4 [18,37] kinase domains constructs with their respective juxtamembrane segments revealed a conserved C-terminal portion of the

JM (EGFR residues 664-682; dubbed JM-B) (**Figure 1.2.A**) that stabilizes the EGFR kinases in the catalytically competent asymmetric dimer conformation [22]. In this conformation, the JM-B of the 'receiver'/ 'acceptor' kinase wraps tightly around/ cradles the C-lobe of the 'activator'/ 'donor' kinase to provide additional stabilizing interactions between the two kinase domains thereby enhancing their dimerization in solution (**Figure 1.2.B**) [18,19]. This was further corroborated by mutagenesis of either all of the JM-B residues (except T669) individually to alanine [19] or the interacting kinase domain C-lobe residues to either alanine or to reverse charge [18] in the full length receptor – both of which had the effect of drastically reducing growth factor dependent auto-phosphorylation activity *in cellula* [19]. Interestingly, the surface of the kinase domain bound by the JM-B (residues 664-668) in the active state [18,19] is roughly equivalent to the surface used by a portion of the C-tail (residues 986-990) to bind the kinase domain in its inactive state (as seen in the crystal structure of an inactive kinase dimer [18]). The authors in the study [18] suggested that the binding of the C-tail to the kinase in the inactive state sterically occludes JM-B binding to facilitate kinase autoinhibition when the catalytically competent asymmetric dimer is not formed.

Notably however, the JM-B portion of the JM segment by itself is insufficient for complete activation of the EGF receptor kinases – As compared to kinase constructs where the complete JM was present, the constructs lacking most of/ the complete N-terminal portion of the JM (residues 645-664; dubbed JM-A) (**Figure 1.2.A**) had (i) reduced kinase dimerization (~40 fold increase in K_D) [18] (ii) reduced tyrosine kinase activity (~65% *in vitro*; 95% *in cellula*) [33] and reduced catalytic efficiency (observed as ~10 fold decrease in k_{cat}/ K_M *in vitro*) [18]. The isolated JM-A forms an amphipathic helix as detected by NMR [18,36] and also observed in a crystal structure of an EGFR kinase construct containing the complete JM [19]. Furthermore,

mutagenesis of arginine residues in the JM-A $_{655}$LRRLL$_{659}$ helix motif (R656, R657) to glycine, that weakens α-helicity [38] was found to abrogate phospho-EGFR activity *in cellula* [18]. NMR experiments using a peptide containing two copies of the JM-A attached by a short flexible linker [18] revealed that the JM-A helices in this polypeptide assemble into a stable antiparallel coiled coil dimer in solution which the authors proposed was necessary for driving proper kinase assembly and activity *in vitro* (**Figure 1.2.B**). The assembly of the JM-A helices into an antiparallel coiled coil was also documented in subsequent NMR and molecular modeling studies of a polypeptide consisting of the JM and the directly preceding Transmembrane domain (TM) segment (residues 618-673) [15,16]. It was observed that the coiled coil assembly of the JM-A helices is directly coupled to dimerization of TM helices at an N-terminal G-x-x-x-G motif that occurs in response to growth factor induced rearrangements in the ECD [15,16] providing a clear picture of the allosteric network extending from the ECD to the JM.

Taken together the biochemical and biophysical data discussed so far implicate both the JM-A and JM-B as essential for driving proper kinase assembly and activation – The JM-A forms an antiparallel coiled coil dimer (which is coupled to structural rearrangements in the ECD and TM induced by EGF binding) to enhance kinase proximity and dimerization [15,16,18] while the JM-B provides additional stabilizing interactions to support formation of the catalytically competent asymmetric kinase dimer [18,19] (**Figure 1.2.B**). While it is clear that the JM is essential for kinase activation, it is challenging to study the structure and dynamics of the JM at a high resolution in the context of the full length receptor in the dynamic environment of a mammalian cell prompting two important questions. First, is the assembly of the JM-A helices into an antiparallel coiled coil structure (as observed by NMR) [15,18] also observed in the full length receptor in cells as a conduit for relaying growth factor binding by the ECD to support

intracellular kinase activation? Secondly, how does a single structure [15,16,18,19] support the subtle differences in growth factor induced ECD arrangements [12–14] to elicit diverse signaling outcomes [14,29,30] by the receptor? To answer both questions, additional lines of evidence need to be considered.

1.3. Using chemical biology tools to reveal the role of the JM-A coiled coil structure in allosterically communicating growth factor identity. In order to interrogate the JM structure and its role in communicating growth factor identity in full-length EGFR *in cellula*, Schepartz and colleagues made use of a chemical biology tool called Bipartite Tetracysteine Display [39,40]. This tool reports on protein conformation and association by exploiting the bis-arsenical dye ReAsH [41,42] as a fluorogenic sensor. ReAsH bound through arsenic to two ethanedithiol ligands is non fluorescent [41,43] and lights up only when coordinated to four cysteine (Cys) side chains in an encoded tetracysteine motif that is reconstituted when the protein is predictably folded and assembled [39,40] (**Figure 1.2.C**). The strict spatial requirement of the assembly of a proper tetracysteine ReAsH binding site in order to observe ReAsH fluorescence [39,40] makes the assay uniquely suited to visualise predicted interactions within the protein containing the encoded tetracysteine motif in the complex environment of a mammalian cell [39,40].

In an initial study, starting from the NMR structure of the JM-A based peptide [18], Scheck and colleagues designed a series of full length EGFR variants with rationally placed Cys-Cys pairs in the JM region to test the hypothesis that the intracellular JM-A segment assembles into an antiparallel coiled coil upon EGF binding in *cellula* [20]. Using this approach, the authors observed that upon binding EGF, the JM-A of EGFR adopts an antiparallel coiled coil conformation [20], analogous to the structure observed previously by NMR [18] (**Figure 1.2.D**).

In this ‘EGF-type’ conformation the JM-A coiled coil dimer is characterized by a hydrophobic mini-leucine zipper interface (formed by L655, L658 and L659) and decorated on the outside by charged residues (K652, R656, R657, E661 and E663) [18,20]. Notably this particular assembly of the JM-A was detected only when EGFR was bound to EGF (and HB-EGF) and not (i) when EGFR was bound to TGF-α or NRG, (ii) when JM-A helicity was interrupted by R656G/R657G mutations and (iii) when assembly of the asymmetric kinase dimer was abrogated by a V924R mutation [20]. Taken together the authors demonstrated the formation of an antiparallel coiled coil structure in the JM-A of EGFR *in cellula* that uniquely encodes EGF (and HB-EGF) binding by the ECD and supports the catalytically competent assembly of the kinase domain [20].

In a more comprehensive subsequent study, using a combination of molecular modeling of the JM helices *in silico* and bipartite tetracysteine display *in cellula*, Doerner and colleagues revealed the conformation of the JM-A when EGFR is bound to its seven different growth factors [21]. Using RosettaDock [44] followed by iterative Monte Carlo randomization, the authors observed *in silico* that the JM-A helices are able to stably assemble into several classes of anti-parallel assemblies [21] (**Figure 1.2.E**). Some of these assemblies were found to be consistent with the EGF-type structure predicted by NMR *in vitro* [18] and observed by Bipartite Tetracysteine Display *in cellula* [20]. However, the *in silico* modeling also predicted a completely separate class of antiparallel coiled coil assemblies that resembles an ‘‘inside-out’’version of the ‘EGF-type’ structure related by a 150 disrotatory rotation about each helix axis [20]. Using Bipartite Tetracysteine Display, the authors observed that this JM-A coiled coil conformation is adopted only when EGFR is bound to TGF-α, EPI, ER and AR and not with EGF or HB-EGF [20]. In this alternate ‘TGF-α-type’ conformation the JM-A interface is dominated by polar interactions at the antiparallel interface with the hydrophobic leucine

residues pointing outwards [20]. The authors also found that when bound to BC, both the EGF-type and TGF-α-type were detected in the JM-A, which is supported by the assembly of the JM-A into a third intermediate coiled coil interface predicted *in silico* [20]. Notably the type of coiled coil structure adopted by the JM-A in response to growth factor binding by the ECD, namely EGF-type (with EGF, HB-EGF) or TGF-α-type (with TGF-α, EPI, ER and AR) correlates directly with cell state and downstream signaling outcomes elicited by these growth factors [14,29,30]. Taken together, the assembly of discrete antiparallel coiled coil structures within the JM-A not only links ligand-induced reorganization of the ECD to support kinase domain activation but also uniquely specifies growth factor identity in context of the full length EGF receptor in cells [20,21] (**Figure 1.2.F**). How do the alternate JM-A coiled coil structures tie into the larger allosteric network of EGFR? For this additional lines of evidence need to be considered.

1.4. Allosteric coupling of the JM-A coiled coil structures to the extracellular and TM domains of EGFR. As discussed previously EGF binding by the ECD induces well documented conformational rearrangements in the TM that are directly coupled to the formation of the 'EGF-type' coiled coil structure in the JM-A [15,16,18]. Much lesser is known *in vitro* about what happens to the TM when the other growth factors (such as TGF-α) are bound by the ECD. Overlaying crystal structures of the EGFR ECD bound to EGF [13] and TGF-α [12] reveal clear differences in the arrangement of domain IV of the ECD [20] (that immediately precedes the TM). How are these differences in ECD arrangement then transmitted through the TM to induce the formation of the alternate JM-A coiled coil structures?

In order to test the hypothesis that differences in TM conformation propagate growth factor induced rearrangements from the ECD to the JM-A, Sinclair and colleagues used a diverse set

of chemical biology and computational tools to probe the TM structure [17]. First, the authors used a series of EGFR variants harboring single Cys substitutions within the TM, to evaluate growth factor dependent changes in the extent of inter-chain Cys-Cys crosslinking (**Figure 1.3.A**) [17] similar to an approach used previously by Springer and colleagues [45]. The authors observed that the extent of inter-chain Cys-Cys crosslinking in the N-terminal segment of the TM (particularly at residues 624-629) differed significantly depending on the growth factor bound to the ECD (high with EGF, HB-EGF, BC; low with TGF-α, AR) [17] suggesting growth factor dependent differences in TM helix association. Next, starting from an NMR structure of the TM-JM fragment [15] the authors used a combination of *in silico* molecular modeling (RosettaMPDock) [44,46,47] and Monte Carlo simulations (MPRelax) [46–48] to identify helical conformations in the TM that are consistent with the assembly of the JM-A into the two distinct 'EGF-type' and 'TGF-α-type' coiled coil structures detected *in cellula* (**Figure 1.3.A**) [20,21]. The authors observed that *in silico* the TM helices assemble into discrete dimer populations that differ in both cross-location and cross-angle to support assembly of the alternate JM-A structures – TM helix dimers with smaller cross-angles at multiple cross locations support assembly of the EGF-type coiled coil structure in the adjacent JM, whereas helix dimers with larger cross-angles at fewer cross locations induce the TGF-α-type coiled coil (**Figure 1.3.A**) [17]. Finally using bipartite tetracysteine display the authors demonstrated that by rationally altering the cross-angle in the TM via mutation, the assembly of the JM-A could be biased into either the EGF-type or TGF-α-type or coiled coil structure independent of growth factor identity [17]. Overall the alternate coiled coil structures formed within the JM-A are directly coupled to the assembly of the TM helices into distinct conformations specified by cross location and cross angle **(Figure 1.3.A**) [17].

1.5. Allosteric coupling of the JM-A coiled coil structures to the mutational/ pharmacological status of the EGFR kinase domains. It is well known that mutations in the EGFR kinase domain are most frequently implicated in patients with non-small-cell lung cancer (NSCLC) [49]. One common mutation (L834R) induces ligand-independent activation and oncogenic signaling [50,51] that accounts for nearly 7–8% of all EGFR mutations found in patient populations [52–54]**.** Patients whose tumors harbor L858R EGFR often respond to first-generation tyrosine kinase inhibitors (TKIs) such as erlotinib (OSI-774) [55,56] and gefitinib (ZD1839/Iressa) [57,58] that act by competing reversibly with ATP [59,60]. However these patients frequently regress due to a second kinase domain mutation (T766M) that lowers inhibitor potency [61,62]**.** This double mutant (L834R/ T766M EGFR) can be targeted by second- and third-generation TKIs such as afatinib (BIBW-2992) [63,64], rociletinib (CO-1686) [65,66] **,** WZ4002 [67] and osimertinib (AZD-9291) [68–70] that bind to the kinase of the mutant EGFR by irreversibly alkylating a conserved active site cysteine side chain (C797).

Using bipartite tetracysteine display, Lowder and colleagues found that perturbations within the intracellular kinase domain either due to oncogenic mutation or specific TKI binding are propagated over long distances to allosterically modulate the coiled coil assembly of the JM-A helices [31] – The authors found that the JM-A helices of EGFR bearing the oncogenic mutation L834R constitutively assemble into the EGF type structure *in cellula* (**Figure 1.3.B**) [31]. In contrast the JM-A helices in EGFR variants bearing the L834R/T766M double mutations constitutively assemble into a TGF-α-type coiled coil structure as detected *in cellula* (**Figure 1.3.B**) [31]. Furthermore when cells expressing the double mutant L834R/T766M EGFR are treated with 2nd gen TKIs such as afatinib (BIBW-2992), the coiled coil structure remains unaffected [31]. In contrast treatment with double mutant selective 3rd gen TKIs such as

WZ-4002, CO-1686 (rociletinib) and AZD9291 (Tagrisso/ osimertinib) have the effect of entirely flipping the coiled coil structure into the alternate 'EGF-type' structure [31] (**Figure 1.3.B**). While the exact structural mechanism by which the transition of the JM-A from one coiled coil state to another is mediated by oncogenic mutations/ 3rd gen TKI binding, remains a subject of ongoing investigation, overall it is evident that the JM-A structure is allosterically linked to the pharmacological status of the kinase domain (**Figure 1.3.B**) [31].

1.6. The juxtamembrane region is a hotspot for interactions with diverse intracellular components that regulate EGFR biology. The JM region of EGFR is a hotspot of interactions with diverse intracellular cellular components (membrane lipids and intracellular proteins), many of which modulate EGFR signaling and downstream biology. One of these is the interaction of the JM-A with the inner leaflet of the lipid bilayer of the cell membrane as revealed by detailed biochemical [15,18] and computational analyses [16]. This interaction is twofold – Firstly, the three leucine side chains within the $_{655}$LRRLL$_{659}$ helical motif of the JM-A [18] are found to be buried in the hydrophobic part of the lipid membrane [15,16]. Second, positively charged residues within the juxtamembrane segmentv(in addition to those in the kinase domain) interact electrostatically with negatively charged anionic phospholipids present in the inner leaflet of the cell membrane [15,16,71]. This interaction provides an additional layer of receptor auto-inhibition in the absence of growth factor activation, by reducing the proximity of JM-A helices from adjacent monomers thereby preventing their dimerization and [15,16,18,72]. The JM region has also been shown to interact with many intracellular proteins, such as Calmodulin [32,72–76], Nck adaptor protein [77], GαS [78], PKC [79–84], p38MAPK [85,86], PI4K [87], AP2 [88,89], TRAF4 [90], ARNO [91] and PKD[92]. **Table 1.1** lists the details of the experiments evaluating these interactions, the binding sites of these protein interactors and their observed/ proposed biological effects. Notably the JM sequence also contains multiple sites and cryptic motifs that are recognized by intracellular machineries to elicit receptor upregulation (T669;

phosphorylation by p38MAPK reduces the downregulation of EGFR [85,86]), receptor downregulation (T654; phosphorylation by protein kinase C attenuates EGFR activity [79,80,82,84]), a dileucine motif (L679, L680; recognized by AP-2 for clathrin mediated endocytosis [88,89]), motifs for basolateral sorting [93,94] and nuclear translocation [95,96]. (**Figure 1.4.)**

1.7. Conclusion. In this chapter we have discussed the evidence in the literature that points to the importance of the juxtamembrane region of EGFR in multiple aspects of growth factor induced receptor activation. Within the juxtamembrane, both the JM-A and JM-B are essential for driving proper kinase assembly and activation – During the course of growth factor activation of EGFR, the JM-A forms an antiparallel coiled coil dimer to enhance kinase proximity and dimerization [15,16,18] while the JM-B provides additional stabilizing interactions to support formation of the catalytically competent asymmetric kinase dimer [18,19]. The JM-A is also critical for communicating growth factor identity – the JM-A can assemble into discrete antiparallel coiled coil structures to uniquely specify the identity of the ECD bound growth factor in context of the full length EGF receptor in cells [20,21]**.** Furthermore, the JM-A structure is allosterically controlled by the confirmation within the TM segment helices specified by cross location and cross angle [17]. The JM-A structure is also allosterically coupled to the mutational/ pharmacological status of the kinase domain [31]. Lastly, the JM is a hotspot for interactions with diverse intracellular cellular lipid and protein components with potential roles in modulating EGFR signaling and downstream biology. Overall, in this chapter, we discuss how the JM segment of EGFR through its various structures and interactions, acts as an essential signal modulatory unit in the EGFR protein and is not simply a passive connector of the extracellular sensory (ECD) and intracellular effector (kinase) domains.

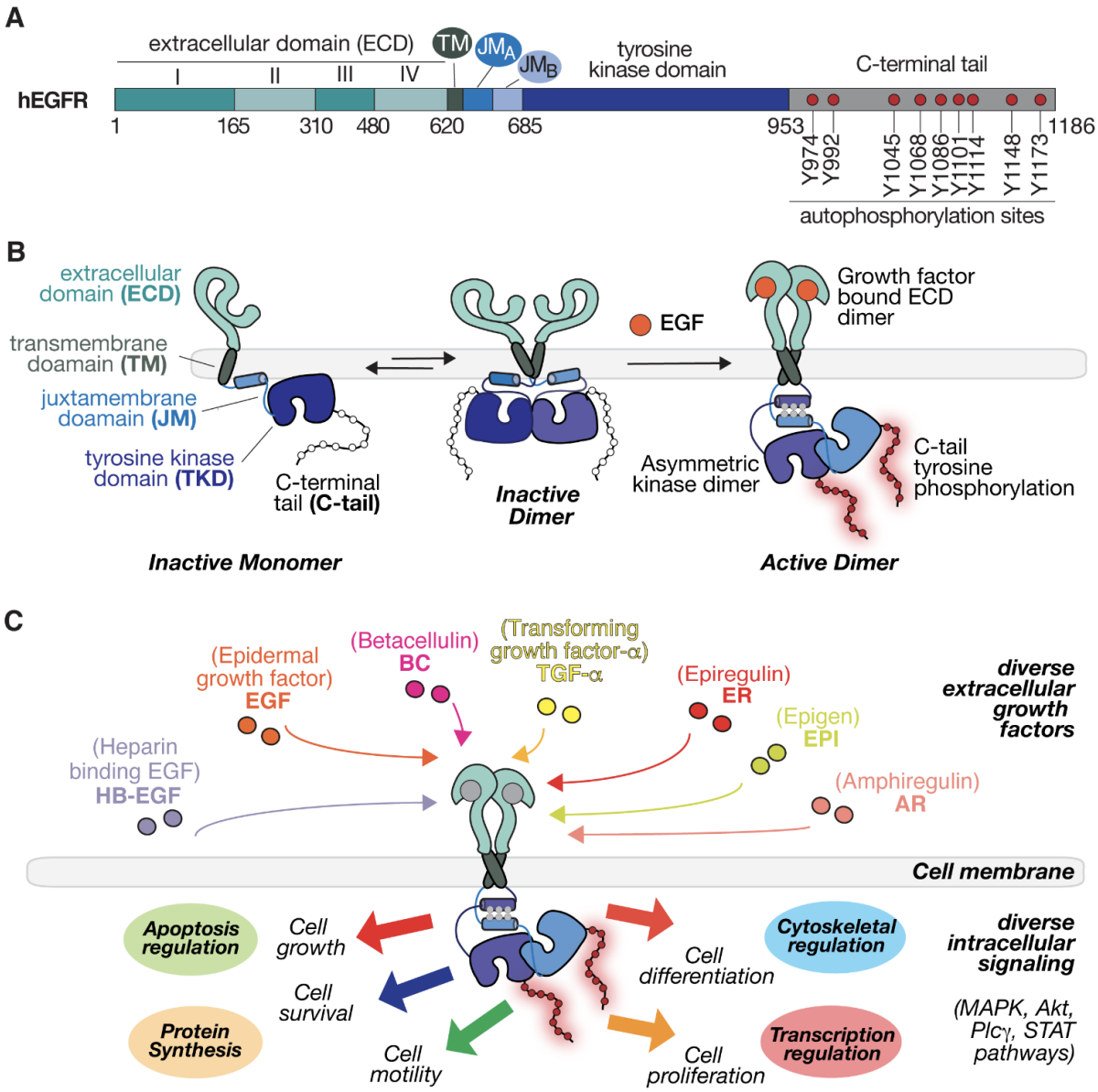

Figure 1.1. The Epidermal growth factor receptor – structure, mechanism of activation and intracellular signaling. (A) Schematics illustrating the distinct regions and domains of EGFR. **(B)** Schematic illustrating the mechanism of EGF induced activation of EGFR. **(C)** Schematic illustrating the diverse growth factor induced intracellular signaling of EGFR. EGFR binds to seven different kinds of extracellular growth factor to initiate multiple intracellular signaling cascades that are critical for diverse cellular functions.

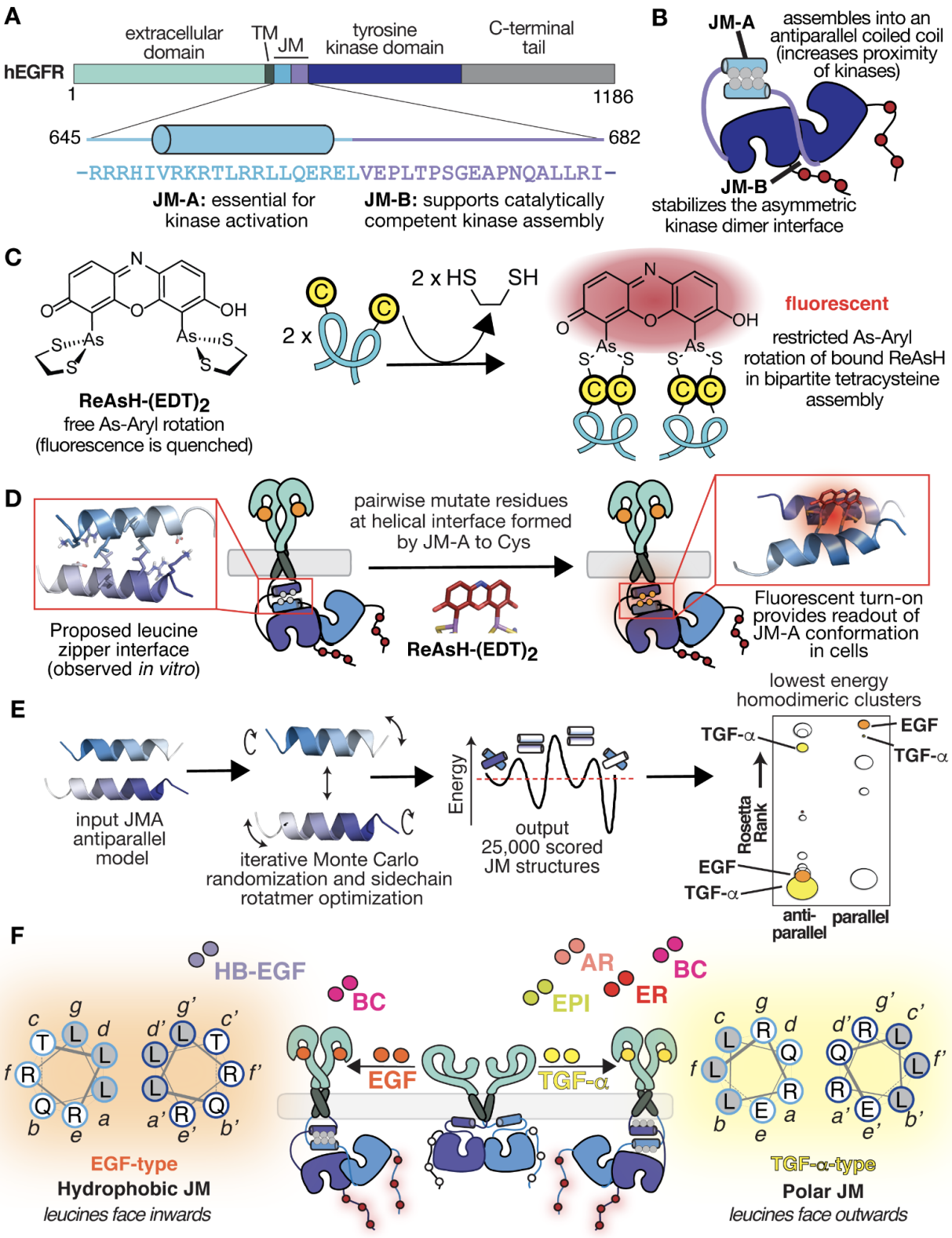
A
extracellular domain
TM
JM
tyrosine kinase domain
C-terminal tail
hEGFR
1
1186
645
682
-RRRHIVRKRTLRRLLQERELVEPLTPSGEAPNQALLRI-
JM-A: essential for kinase activation
JM-B: supports catalytically competent kinase assembly
B
JM-A
assembles into an antiparallel coiled coil (increases proximity of kinases)
JM-B
stabilizes the asymmetric kinase dimer interface
C
ReAsH-(EDT)2
free As-Aryl rotation
(fluorescence is quenched)
2 x
2 x HS
SH
fluorescent
restricted As-Aryl rotation of bound ReAsH in bipartite tetracysteine assembly
D
Proposed leucine zipper interface (observed in vitro)
pairwise mutate residues at helical interface formed by JM-A to Cys
ReAsH-(EDT)2
Fluorescent turn-on provides readout of JM-A conformation in cells
E
input JMA antiparallel model
iterative Monte Carlo randomization and sidechain rotatmer optimization
Energy
output 25,000 scored JM structures
lowest energy homodimeric clusters
TGF-α
EGF
Rosetta Rank
anti-parallel
parallel
F
HB-EGF
BC
AR
BC
EPI
ER
EGF
TGF-α
EGF-type
Hydrophobic JM
leucines face inwards
TGF-α-type
Polar JM
leucines face outwards

Figure 1.2. The juxtamembrane segment of EGFR is essential for kinase activation and for allosterically encoding growth factor identity in cells. (A) Schematics illustrating the domain location and sequence of the JM-A and JM-B portions of the juxtamembrane domain of EGFR. **(B)** The JM-A and JM-B portions of the juxtamembrane segment are both essential for catalytically competent assembly and activation of the EGFR kinase *in vitro*– the JM-A assembles into an antiparallel coiled coil structure *in vitro* to increase proximity and dimerization of kinase domains; the JM-B provides stabilizing interactions to the asymmetric kinase dimer interface. **(C)** The fluorogenic dye ReAsH is quenched when bound to two ethanedithiol ligands because of free rotation about the carbon-sulfur bond. When bound to proteins containing four proximal Cys thiols in bipartite tetracysteine motif, rotation is inhibited and the ReAsH fluoresces providing a readout on conformation. **(D)** Schematic summary of the methodology used to apply bipartite tetracysteine display to probe the assembly of the JM-A coiled coil structure of EGF activated EGFR in cells. **(E)** Schematic summary of the computational methodology used to identify other stable antiparallel coiled coil structures that can be adopted by the JM-A. **(F)** Alternate coiled coil structures formed within the JM-A of EGFR are sufficient for allosterically encoding the identity of the growth factor bound to the extracellular domain – schematic summary of the results of the bipartite tetracysteine display experiments. Helical wheel diagrams showing axial views of inter-helix JM-A segment packing in EGF- and TGF-α-type coiled coils.

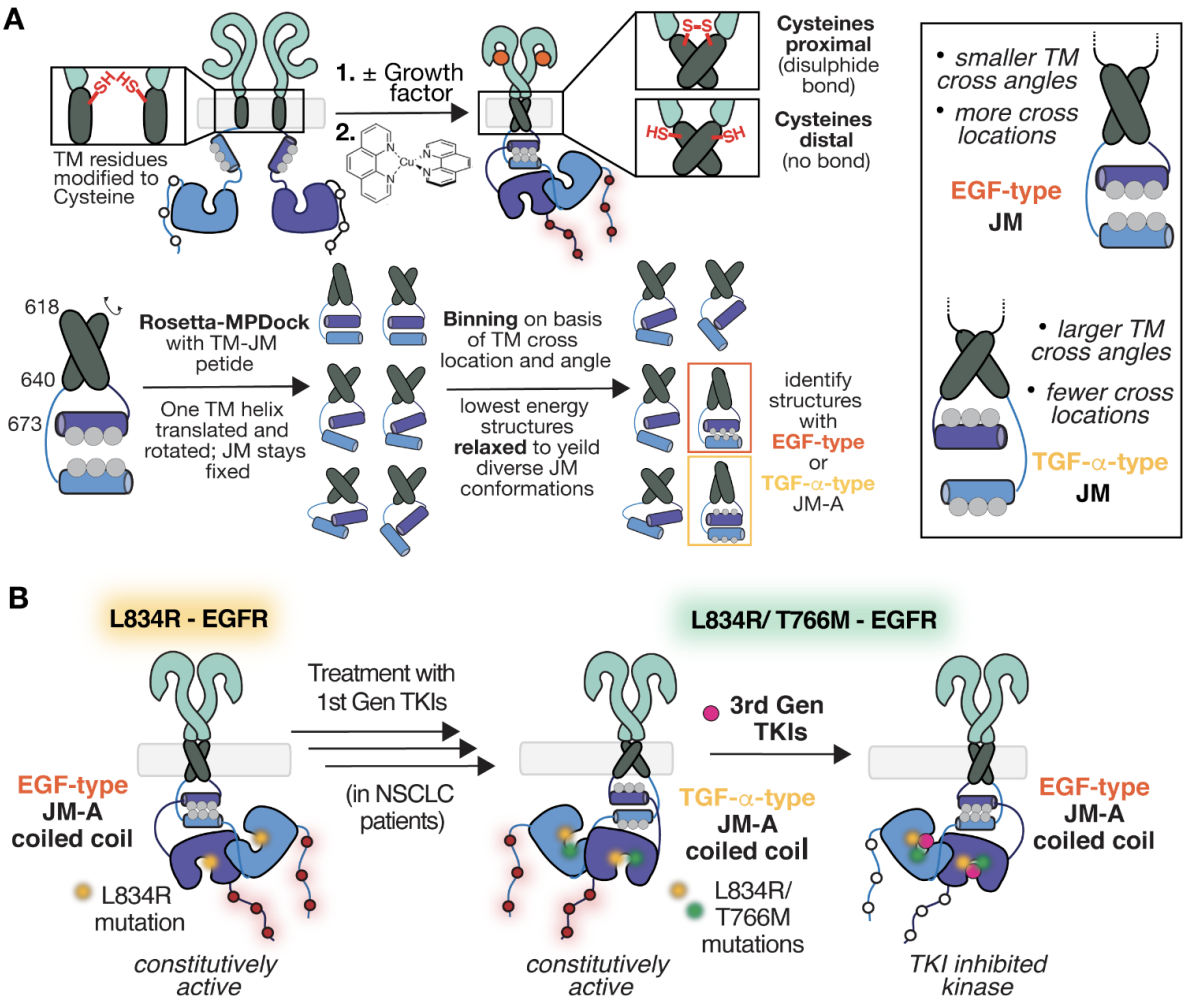

Figure 1.3. The JM-A coiled coil structure is allosterically connected to the structure of the TM domain and pharmacological status of the kinase domain. (A) Schematic summary of disulphide cross-linking experiments and *in silico* modeling of the TM-JM segment to evaluate the allosteric coupling of the TM and JM segments. The JM-A coiled coil structure is controlled by the cross angle and cross-location of the TM helices. **(B)** Oncogenic mutations L834R and L834R/ T766M lock the JM-A into the EGF-type or TGF-α-type coiled coil structures respectively. Treatment with third generation tyrosine kinase inhibitors (TKIs) specific for L834R/ T766M EGFR flip the coiled coil structure of L834R/ T766M EGFR from the TGF-α-type structure into the EGF-type structure.

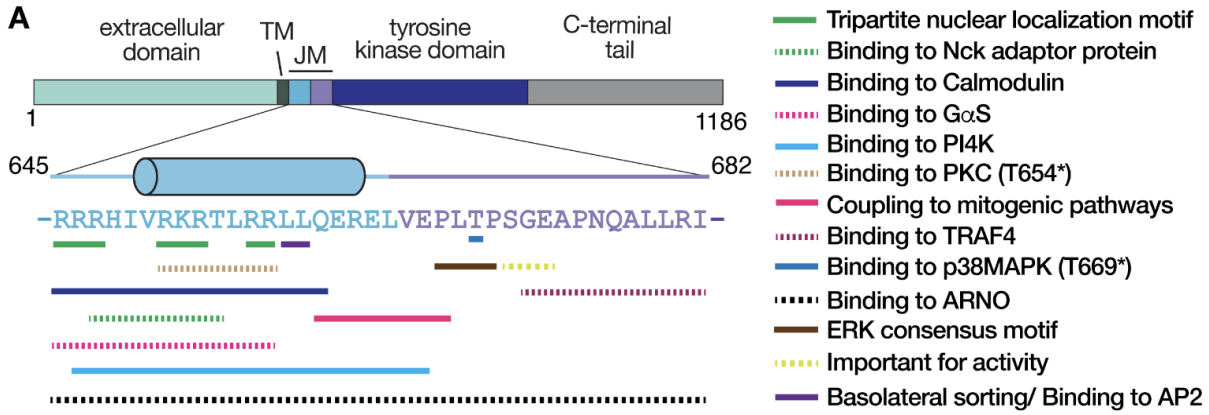

Figure 1.4. Sequence motifs and protein binding sites in the juxtamembrane region. Schematic illustrating the location and sequence of known cryptic motifs and protein binding sites in the juxtamembrane segment of EGFR. See also **Table 1.1.**

Table 1.1. Protein interactions with the juxtamembrane domain of EGFR

Protein interactor	Interaction site in JM	Experimental Method and Constructs used	Biological effect/ Experimental summary	Ref.
Calmodulin (CaM)	R645–Q660	Cross-linking/ CaM and GST-JM peptide (645–660)	CaM binding to JM is dependent on intracellular Ca^{2+}	[73]
	R647, T654	SPR/CaM and immobilized GST-JM peptide (644–688)	pT654 inhibit CaM binding (with T654D, and PKC treatment)	[32]
	R645-Q660	Radioactive probe conjugated to a JM peptide (645–660)	Intracellular Ca^{2+}/CaM induces dissociation of JM from a PC/PS membrane	[72]
	R645-Q660	Fluorescence probe conjugated JM (645–660)		[74]
	R645-Q660	FRET/ EGFR TM-JM peptide (R622–Q660)	Intracellular Ca^{2+}/CaM induces dissociation of JM from a POPC membrane containing PIP2	[76]
	R645-Q660	EGFR activation *in cellula* and western blotting/ (CaM antagonist treatment/ CaM-KO cells/ chelation of Ca^{2+}/ mutagenesis of CaM-binding domain)	Abrogating CaM binding/ depleting intracellular Ca^{2+} inhibits EGFR activation	[75]
Nck adaptor protein	H648, I649, R647-T654	^{13}C-^{1}H HSQC/ JM peptide (645-672) or (644-674) titrated with unlabeled GB1-Nck1-2	The JM segment of EGFR interacts with Nck.	[77]
GαS	R645-R657	IP and western blotting of GαS with JM peptides (645-657) or (679-692)	Treatment with JM peptides induces phosphorylation of GαS	[78]
PI4K	R645-E663	IP and western blotting of of PI4K with EGFR JM peptide (645-663)	Treatment with JM peptide increases PI4P activity	[87]
Protein kinase C (PKC)		A431 cells/ P-32 labeling phosphorylation assay	PKC is related to phosphorylation of the EGFR	[80,81]
	T654	A431 cells/ P-32 labeling phosphorylation assay	PKC phosphorylates the JM of EGFR at T654	[79,82]
	T654	A432/ B82 cells transfected with WT or T654A-EGFR/ I-125 EGF binding assay	EGF binding by WT EGFR is lost for upon PKC activation (by phorbol esters)	[83]
	T654	CHO cells transfected with WT or T654E-EGFR/ I-125 EGF binding assay	EGF binding by WT EGFR is lost upon PKC activation; T654E-EGFR has lower C-tail pY activity compared to WT-EGFR upon PKC activation.	[84]

p38MAPK	T669	A431 cells/ P-32 labeling phosphorylation assay	p38MAPK phosphorylates the EGFR JM at T669 and changes its binding and kinase state.	[85]
	T669	MDA-MB-468 or CHO-K1 cells transfected with WT or T669A-EGFR/ Western blotting & P-32 labeling phosphorylation assay	p38MAPK phosphorylates the EGFR JM at T669; T669 phosphorylation by p38MAPK induces EGFR internalization.	[86]
AP-2	L679, L680	NR6 cells transfected with WT or L679A,L680A-EGFR Internalization/ recycling assay with I-125 EGF; radioactivity measurement, Lamp-1 immunostaining and confocal microscopy.	The dileucine motif in the EGFR juxtamembrane formed by L679, Leu680 is critical for the post-endocytic endosomal sorting of EGFR to lysosomes/ degradation pathway	[88,89]
TRAF4	G672-I682	HeLa cells with WT EGFR or Δ672-682 EGFR; EGFR phosphorylation assay by immunoblotting; HSQC of ^{15}N TRAF4 with EGFR peptide (672-682)	TRAF4 binds to the EGFR JM-B (672-682) and is essential for EGF-induced activity of EGFR	[90]
ARNO	R645-I682	Microscale thermophoresis (MST) between EGFR-JM and Sec7 domain of ARNO ^{1}H, ^{15}N-HSQC of EGFR-JM titrated with ARNO-Sec7	ARNO binds to the JM region of EGFR and competes with the binding interaction of the JM with CaM and anionic phospholipids	[91]
Protein kinase D (PKD)	T654, T669	CHO-K1 cells with eGFP-EGFR for Raster image correlation spectroscopy (RICS) or T654/T669 phospho-mimetics or PKD1 mutant with kinase activity abrogated (K612W)	PKD1 phosphorylates the EGFR JM at T654/T669; T654/T669 phosphorylation by PKD shifts the monomer-dimer equilibrium of EGF-bound EGFR towards the monomeric state.	[92]

Chapter 2. Discrete coiled coil rotamers form within the EGFRvIII juxtamembrane domain

Disclosure and authorship

This text of this chapter contains material adapted from a peer-reviewed publication:

"Discrete coiled coil rotamers form within the EGFRvIII juxtamembrane domain.", Mozumdar, D., Doerner, A., Zhang, J.Y., Rafizadeh, D.N., Schepartz, A., *Biochemistry*, **2020**, 59, 3965-3972

Chapter 2. Discrete coiled coil rotamers form within the EGFRvIII juxtamembrane domain

2.1. ABSTRACT

Mutations in the ECD of EGFR are implicated in the development of glioblastoma multiforme (GBM), a highly aggressive form of brain cancer [97–100]. Most notable in GBM pathology is the variant of EGFR known as EGFRvIII, that results from an in-frame deletion of exons 2-7, which encode EGFR ECD residues 6-273 [101–103]. This deleted region includes an auto-inhibitory tether [23], whose absence, alongside unique disulfide interactions [104] within the truncated ECD, supports constitutive assembly of an active asymmetric kinase dimer [22,97,100]. Previous studies have shown that growth factors binding to the ECD of wild type (WT) EGFR leads to the formation of two distinct coiled coil dimers in the JM-A segment whose identities correlate with downstream phenotype [17,20,21]. One coiled coil contains leucine residues at the interhelix interface (EGF-type), whereas the other contains charged and polar side chains (TGF-α-type) [17,20,21]. It has been proposed that growth factor-dependent changes in the ECD structure and adjacent TM helix are transduced into distinct coiled coil structures in the JM-A region [17,20,21]. Herein we demonstrate that in the absence of this growth factor-induced signal, the JM-A of EGFRvIII is able to adopt both EGF-type and TGF-α-type structures, providing direct evidence for this hypothesis [105]. These studies confirm that the signals that define the identity of the JM-A coiled coil begin within the ECD, and support a model in which growth factor-induced conformational changes are transmitted from the ECD through the TM helices to favor different coiled coil isomers within the JM.

2.2. Introduction – EGFRvIII a prominent mutation in GBM is constitutively activated.

EGFRvIII is the most common EGFR mutation associated with glioblastoma multiforme (GBM) [99,106–109], a high-grade brain tumor associated with exceptionally high fatality [110]. Multiple studies have correlated the EGFRvIII expression with poor survival [111,112]. Unlike EGFR variants in NSCLC that bear mutations within the kinase domain [50,51,113–115] that can be targeted selectively with TKIs [63,65,67,68,116,117], EGFRvIII contains a wild type (WT) kinase domain, hindering the development of selective inhibitors [100,118–121].

EGFRvIII is generated by an in-frame deletion of 801 base pairs from exons 2-7 of the ECD [100–103] (**Figure 2.1.A**). As a result, the receptor lacks residues 6-273, which include most of ECD domains I and II. Included in this region is one of three residues (Y246) that interacts with D563 and K585 on domain IV to hold the WT receptor in an autoinhibited conformation [12,13,23,122] (**Figure 2.1.B,D**). The absence of the Y246 autoinhibitory latch causes EGFRvIII to be constitutively activated [12,13,108,123] (**Figure 2.1.B**). EGFRvIII also lacks the domain II dimerization arm that in WT EGFR is necessary for growth factor-induced ECD dimerization [12,13] (**Figure 2.1.C,D**). Despite this absence EGFRvIII is able to dimerize via formation of disulphide bonds between cysteine residues exposed as a result of ECD truncation [104]. This disulfide-induced extracellular dimerization event, like growth factor-induced dimerization, supports intracellular formation of an asymmetric kinase dimer that signals constitutively through the MAPK and AKT pathways (among others) to initiate oncogenic activity in the cell [98,106–108,124].

The EGFR ECD does more than simply bind growth factors and promote dimerization - it is an essential component of an allosteric pathway linking growth factor binding to kinase activation [6,27]**.** Previous studies have shown that growth factors binding by WT EGFR leads to the

assembly of two distinct coiled coil structures in the EGFR JM-A [17,20,21]. One of these structures dubbed the 'EGF-type coiled coil' is favored when WT EGFR is activated by epidermal growth factor (EGF) and heparin-binding EGF-like growth factor (HB-EGF), and is distinguished by a hydrophobic, leucine-rich coiled coil interface observed by NMR [15,18]. The other coiled coil structure dubbed the 'TGF-α-type coiled coil' is favored when WT EGFR is activated by transforming growth factor-α (TGF-α), epigen, epiregulin, and amphiregulin, and is distinguished by electrostatic interactions at the helical interface with leucines decorating the outside surface [21] (**Figure 2.1.E**). Formation of EGF- and TGF-α-type coiled coils within the EGFR JM-A correlate with distinct intracellular phenotypes, including the direction of endocytic trafficking, receptor lifetime, and the relative flux through alternative downstream signaling pathways [21,29]. Given that EGFRvIII is activated constitutively (even in the absence of growth factor induced ECD rearrangements), it provides a unique opportunity to interrogate the relative stabilities of the EGFR JM-A segment in the absence of signals emanating from a WT ECD. Here we utilize bipartite tetracysteine display [39,40] to demonstrate that in the absence of growth factor-induced signals, the JM of EGFRvIII is able to constitutively adopt both EGF-type and TGF-α-type structures [105]. Our studies provide further evidence for an allosteric pathway that links growth factor-induced binding to the extracellular domain to JM coiled coil structure and kinase activation.

2.3. Using bipartite tetracysteine display to probe the structure of the EGFRvIII JM-A.

Our initial experiments sought to probe the existence and structure of the coiled coil formed in the JM-A region of intact EGFRvIII dimers *in cellula*. To do so, we made use of the chemical biology tool bipartite tetracysteine display (**Figure 2.1.F**) [39,40]. This tool exploits the bis-arsenical dye ReAsH [41] as a fluorogenic sensor that lights up only when bound to four

cysteine (Cys) side chains in a discrete molecular array [43]. Our previous work identified a set of CysCys-containing WT EGFR variants whose dimers bind ReAsH and fluoresce only when the JM is assembled into either an EGF-type coiled coil (CC_H-1) or the isomeric TGF-α-type coiled coil (CC_H-10) [17,20,21] (**Figure 2.2.A**). The resulting ReAsH fluorescence, detected using TIRF microscopy (TIRF-M), provides an in-cell readout of JM structure within intact EGF receptors [17,20,21]. Visualizing ReAsH fluorescence using TIRF-M restricts fluorophore excitation and emission to a small (100–200 nm) cell surface plane and diminishes the signal from non-specific cytosolic ReAsH staining [20].

To probe for formation of the EGF-type or the TGF-α-type coiled-coil within the JM of intact EGFRvIII receptors, the CC_H-1 or CC_H-10 CysCys mutations were integrated into the EGFRvIII sequence to generate vIII-CC_H-1 and vIII-CC_H-10, respectively (**Figure 2.2.B**). In control experiments, we confirmed that vIII-CC_H-1 and vIII-CC_H-10 (each carrying an N-terminal FLAG-tag) were expressed in CHO-K1 cells, localized to the cell surface, and underwent the expected phosphorylation at C-tail residues Y1068 and Y1086 in the absence and presence of saturating (16.7 nM) EGF or TGF-α (**Figure 2.5.**).

In the bipartite tetracysteine display experiments, CHO-K1 cells expressing vIII-CC_H-1 or vIII-CC_H-10 were stimulated with growth factor (or not), incubated with ReAsH, washed, and immuno-stained. Receptor expression was monitored using a fluorescently labeled antibody to an N-terminal FLAG epitope. Using TIRF-M, the level of both cell surface ReAsH fluorescence (red) and EGFR expression (green) was quantified across multiple cells (67 - 161) expressing either EGFR or EGFRvIII variants. The cell-surface ReAsH fluorescence detected (over background) was normalized to the surface EGFR-expression detected (over background) to calculate the fold-increase in ReAsH fluorescence (**Figure 2.3.A,B**). Cells expressing WT-CC_H-1

or WT-CC_H-10 displayed levels of normalized ReAsH fluorescence relative to background that mirrored previous reports [17,20,21] (**Figure 2.3.A,B**). By contrast, cells expressing vIII-CC_H-1 or vIII-CC_H-10 showed an almost 2-fold increase in normalized ReAsH fluorescence relative to background both in the absence of any growth factor (1.86 ± 0.09 and 1.79 ± 0.09, respectively) as well as when treated with EGF (1.81 ± 0.10 and 1.70 ± 0.08) or TGF-α (1.80 ± 0.08 and 1.84 ± 0.10) (**Figure 2.3.A,B**). The fold-increase in ReAsH fluorescence observed for cells expressing vIII-CC_H-1 or vIII-CC_H-10 was comparable to that observed when WT-CC_H-1 or WT-CC_H-10 are activated with EGF and TGF-α, respectively [17,20,21]. Previous work examining the JM-A coiled coil status of WT EGFR activated with different growth factors [17,20,21], or of constitutively active EGFR kinase domain mutants [31], has always revealed a preference formation of a single JM-A coiled coil structure over the other. The absence of this preference in the case of EGFRvIII is consistent with two fundamentally different scenarios: The first possible explanation is that the structure of the constitutively active EGFRvIII is a mixture of dimers containing the EGF-type and TGF-α-type JM coiled coils (if not others). The second possibility is that the JM of constitutively active EGFRvIII can easily assume multiple different conformations including but not limited to the EGF-type and TGF-α-type JM coiled coils; the associated increased flexibility could also support ReAsH binding and induced fluorescence (**Figure 2.2.C**).

To differentiate between these two possibilities, we designed a third set of CysCys containing EGFRvIII variant, namely vIII-CC_H-4 (**Figure 2.2.A,B**). In vIII-CC_H-4 the four Cys residues within the JM are located too far apart to bind ReAsH in either the EGF-type or TGF-α-type conformation [20]. In the EGF-type structure, the Cys residues are located at positions *g* and *e* (as well as *g'* and *e'*); in the TGF-α-type structure the Cys residues are located at positions *g*

and *b* (as well as *g'* and *b'*). If the JM-A of EGFRvIII adopts either the EGF-type or the TGF-α-type antiparallel coiled coil, then cells expressing vIII-CC_H-4 should show little or no ReAsH fluorescence. Conversely, if the JM-A of EGFRvIII flexibly adopts multiple different conformations, then cells expressing vIII-CC_H-4 should show high ReAsH fluorescence. In control experiments, we verified that vIII-CC_H-4 was expressed in CHO-K1 cells and constitutively phosphorylated at C-tail positions Y1068 and Y1086 (**Figure 2.5.**).

Using bipartite tetracysteine display, the fold increase of ReAsH fluorescence of CHO-K1 cells expressing variants WT-CC_H-4 and vIII-CC_H-4 was evaluated in the absence and presence of EGF and TGF-α. As expected, with cells expressing WT-CC_H-4, no significant fold increase in ReAsH fluorescence is observed when the cells are activated with either EGF (1.09 ± 0.05) or TGF-α (1.06 ± 0.06) or not stimulated with any growth factor (1.01 ± 0.04) [20] (**Figure 2.3.A,B**). Interestingly, cells expressing vIII-CC_H-4 also showed little or no ReAsH labeling and fluorescence both without growth factor activation (1.19 ± 0.06) and when the cells were stimulated with either EGF (1.17 ± 0.06) or TGF-α (1.19 ± 0.09). These results favor a model in which the EGFRvIII JM assembles constitutively into a mixture of two different antiparallel coiled coils of roughly equal stability. The data are less consistent with a model in which the JM segment of EGFRvIII can easily assume multiple different conformations.

2.4. Conclusion.

WT EGFR interacts through its ECD with seven different growth factors [7,8]. These factors induce different structures within the cytoplasmic juxtamembrane segment (JM) of the dimeric receptor and propagate different growth factor-dependent signals to the cell interior [17,20,21]. Previous work has defined a model to explain how EGFR supports growth factor-dependent differences in intracellular signaling. This model begins with small but significant growth

factor-dependent differences in the structure of the bound ECD, especially in domain IV as it tracks into the TM helix [12,13,17,20]. These differences lead to TM helix dimers that differ in both cross location and cross angle [17]. TM helix dimers characterized by smaller cross angles at multiple cross locations induce the EGF-type coiled coil in the adjacent JM-A, whereas helix dimers with larger cross angles at fewer cross locations induce the TGF-α -type coiled coil (**Figure 2.4.A**) [17]. EGFRvIII provides a unique opportunity to test this model, as kinase activation occurs constitutively in the absence of either growth factor binding or activating kinase domain mutations. Here we make use of bipartite tetracysteine display to demonstrate that in the absence of this growth factor-induced signal, the JM-A of EGFRvIII adopts both EGF-type and TGF-α-type structures within the juxtamembrane segment [105]. We show that in the absence of growth factor-induced ECD rearrangements, the JM-A adopts a well-ordered configuration that appears to be a mixture of EGF-type and TGF-α-type structures [105] (**Figure 2.4.A**). These results suggest that the EGF-type and TGF-α-type JM-A coiled coils possess roughly equal stability in the context of the intact full-length receptor (**Figure 2.4.B**). Overall, our work provides further evidence for an allosteric pathway linking structural changes induced by growth factor-induced binding by the ECD to coiled coil assembly in the JM-A and consequent kinase activation.

2.5. Methods and Materials

Materials. Unlabeled recombinant human epidermal growth factor (EGF) (#CB40052) was purchased from Corning. Unlabeled recombinant human transforming growth factor-α (TGF-α) (#T7924) and mouse monoclonal (M2) anti-FLAG primary antibody (#F1804) were purchased from Sigma. 2,3-dimercapto-1-propanol (BAL) (#AC115300250) was purchased from Acros Organics. Rabbit monoclonal anti-phospho-EGF receptor Tyr1173 (53A5) (#4407), rabbit polyclonal anti-phospho- EGF receptor Tyr1086 (#2220), rabbit polyclonal anti-phospho-EGF receptor Tyr1068 (#2234), rabbit anti-α-tubulin (#2155) primary antibodies as well as goat polyclonal anti-Rabbit, HRP-conjugated (#7074) and goat polyclonal anti-mouse, HRP-conjugated (#7076) secondary antibodies were purchased from Cell Signaling Technology. CHO-K1 cells were purchased from the American type Culture Collection (ATCC). Dulbecco's phosphate buffered saline (DPBS) (#14190), fetal bovine serum (FBS) (#26140079), penicillin-streptomycin (10,000 U/mL) (#15140122), ReAsH-EDT_2 (#T34562) and goat polyclonal anti-mouse, AlexaFluor488-conjugated secondary antibodies (#A10667) were purchased from ThermoFisher Scientific. EGFR UniProtKB accession ID: P00533.

Plasmids and Cloning. All plasmids used in bipartite tetracysteine display and related assays are derived from a parent plasmid (pcDNA3.1), generously donated by the Kuriyan Group (University of California, Berkeley), which contains the sequence of full-length WT EGFR with an N-terminal FLAG tag [18,22]. Mutations and deletions were introduced into pcDNA3.1 using Quikchange Lightning site-directed mutagenesis (Agilent) and primers (Integrated DNA Technologies) listed in **Table 2.1**.

Cell Culture. CHO-K1 cells were purchased from ATCC and maintained at 37°C, 5% CO2, in F12K Medium (Corning) supplemented with 10% fetal bovine serum and pen-strep (100

I.U./mL penicillin and 100mg/mL streptomycin). Cell densities were determined with a Cellometer Auto T4 automated counter. Transient transfection of CHO-K1 cells was performed via use of the Transit-CHO Transfection Kit, according to the manufacturer's instructions (Mirus Bio LLC).

Bipartite Tetracysteine Display. ReAsH labeling was performed as described previously [17,20,21], by treating CHO-K1 cells that were transiently transfected with plasmids containing the appropriate EGFR variants in the presence of an endocytosis/ATP synthesis inhibition cocktail in F12-K media (10 mM NaN_3, 2 mM NaF, 5mM 2-deoxy-D-glucose), for 1hr at 37°C. Cells were then stimulated without/with 100ng/mL of EGF (16.7nM) or TGF-α (16.7nM) for 30 min at 4°C prior to labeling. Cells were then washed once with endocytosis/ATP synthesis inhibition cocktail in F12K media before incubation with ReAsH labeling solution (2mM ReAsH, 20mM BAL in F12K media) for 60 min at 37°C. Cells were then washed and incubated with endocytosis inhibitor-containing F12K media supplemented with 100 mM BAL for 10 min at 37°C. The media was removed, and the cells were fixed using 4% paraformaldehyde for 25 min at room temperature. Cells were then washed with DPBS and blocked with 10% BSA in DPBS for 30 min at 37°C. Cells were then labeled with primary antibody (mouse anti-Flag, 1:1000 dilution in 10% BSA in DPBS) for 1hr at 37°C, washed three times with 10% BSA in DPBS, then incubated with secondary antibody (AlexaFluor488-conjugated goat anti-mouse, 1:2000 dilution in 10% BSA in DPBS) for 1hr at 37°C. Cells were then washed two times with 10% BSA in DPBS, washed once with DPBS, then nuclear stained with Hoechst-33342 (1.62mM in DPBS) for 5 min at 37°C. Cells were then washed once with DPBS and stored in DPBS at 4°C prior to imaging. Labeled cells were then analyzed via TIRF microscopy, conducted on a Leica Microsystems AM TIRF MC DMI6000B fitted with an EM-CCD camera (Hamamatsu) with HCX

PL APO 63x/1.47 oil corrective objectives, as described previously [17,20,21]. Images were analyzed as described previously [17,20,21]. Briefly, raw data from TIRF microscopy were analyzed using ImageJ 643. Fluorescence intensities of ReAsH and AlexaFluor 488 (EGFR levels) were quantified, and the fold increase of ReAsH fluorescence relative to background was normalized for EGFR expression levels. Normalized values of ReAsH fold-increases were plotted using Prismv7.0 (for Mac, GraphPad Software, La Jolla California USA, www.graphpad.com), where n represents number of cells quantified, and error bars represent the standard error of the mean. One-way ANOVA followed by a Dunnett multiple comparisons test was performed.

Autophosphorylation analysis. Western blot analysis of EGFR autophosphorylation in transiently transfected CHO-K1 cells was performed as described previously [17,20,21]. CHO-K1 cells, transiently transfected with a plasmid encoding the appropriate EGFR variant, were collected ($5x10^5$ cells), resuspended in 200 mL of serum free F12K media, stimulated with 100ng/mL of EGF (16.7nM) or TGF-α (16.7nM) for 5 min at 37°C (or not), pelleted, washed with serum-free F12K media, pelleted again, then lysed in 100 mL of lysis buffer (50mM Tris, 150mM NaCl, 1mM EDTA, 1mM NaF, 1% Triton X-100, pH 7.5, 1x complete protease inhibitor cocktail (Roche), 1x PhosStop), on ice for 1hr. Clarified cell lysates were then subjected to reducing 10% polyacrylamide SDS-PAGE electrophoresis and transferred to immuno-blot PVDF membranes. Membranes were blocked with 5% milk in TBS-T Buffer (50mM Tris, 150mM NaCl, 0.1% Tween, pH 7.4) for 1hr followed by an overnight incubation at 4°C with the indicated primary (rabbit or mouse) antibodies. Blots were then washed with TBS-T and incubated with either anti-rabbit or anti-mouse goat HRP-conjugate secondary antibodies (Cell Signaling Technology) for 1hr at room temperature, then washed with TBS-T. Blots were then visualized

using Clarity Western ECL reagents (BioRad). Displayed blot images have been adjusted for brightness/contrast using ImageJ/ FIJI [125] and have been cropped to highlight band signals for full-length EGFR (~170 kDa) or EGFRvIII (~145 kDa).

Table 2.1: Mutagenesis Primers*

S.No.	Primer Name	Sequence (5'-3')
1.	EGFRvIII, forward	5'-cgagccgtgatctgtcaccacataattTTTCTTTTCCTCCAGTCCGGAGC-3'
2	EGFRvIII, reverse	5'-gacaagggctccggactggaggaaaagaaaAATTATGTGGTGACAGATCACGGCTC-3'

Mutagenesis primers for the insertion of cysteines to generate the CC_H-1, CC_H-4, and CC_H-10 variants of EGFRvIII have been previously described [20,21].

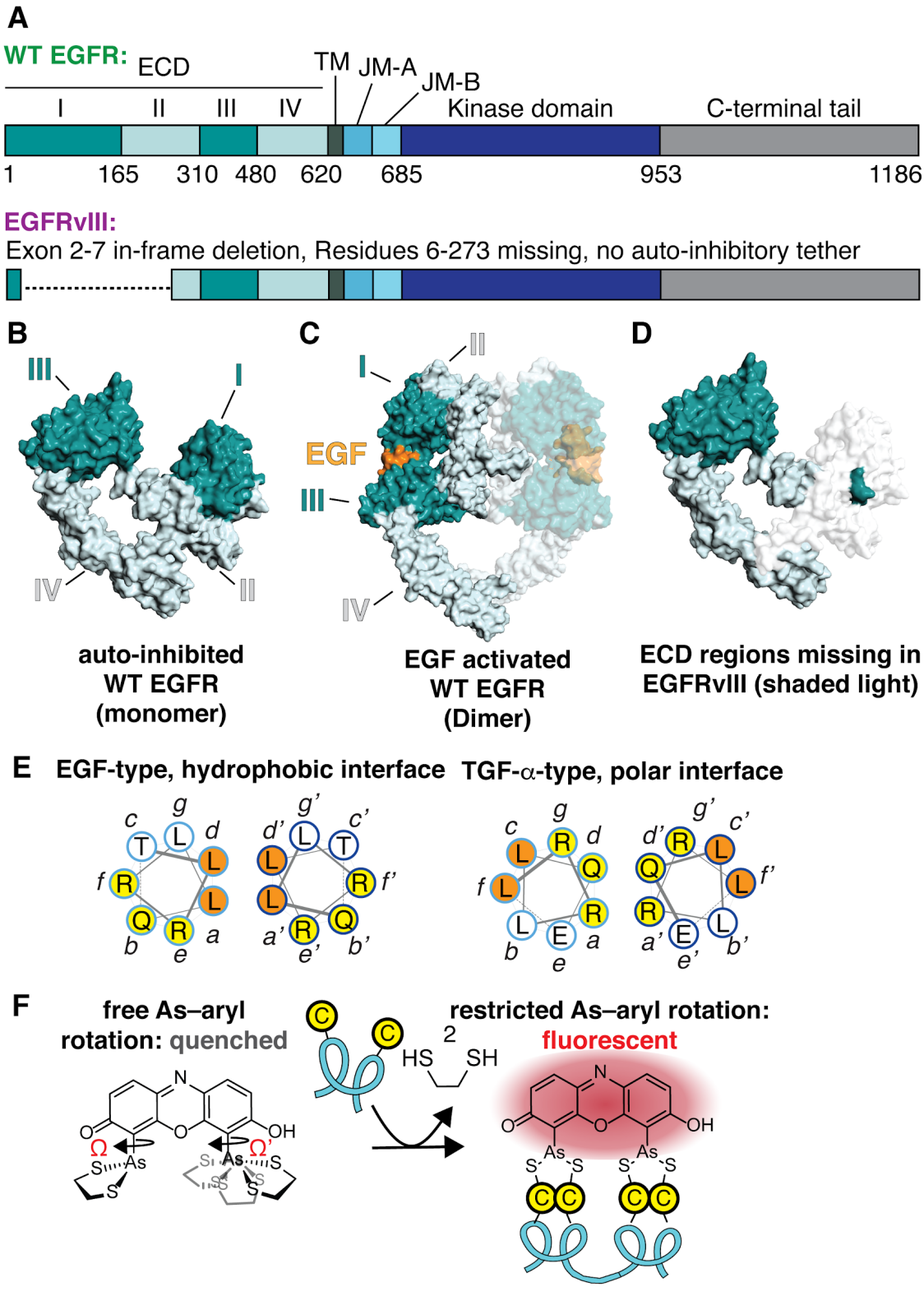
A
WT EGFR:
ECD
TM
JM-A
JM-B
I
II
III
IV
Kinase domain
C-terminal tail
1
165
310
480
620
685
953
1186
EGFRvIII:
Exon 2-7 in-frame deletion, Residues 6-273 missing, no auto-inhibitory tether
B
C
D
EGF
auto-inhibited WT EGFR (monomer)
EGF activated WT EGFR (Dimer)
ECD regions missing in EGFRvIII (shaded light)
E
EGF-type, hydrophobic interface
TGF-α-type, polar interface
F
free As–aryl rotation: quenched
restricted As–aryl rotation: fluorescent
HS
SH
2
OH

Figure 2.1. Comparison between wild type (WT) epidermal growth factor receptor (EGFR) and EGFRvIII. (A) Schematics illustrating the distinct regions and domains of WT EGFR and EGFRvIII. EGFRvIII lacks amino acid residues 6-273 of the extracellular domain (ECD) (dashed line). **(B)** Surface model of the auto-inhibited conformation of the WT EGFR ECD (PDB ID: 1NQL). Subdomains are color-shaded for visualization (I, III: deep teal; II, IV: pale cyan). The ECD is held in an auto-inhibited conformation by intramolecular interactions between residues in domains II and IV. **(C)** Surface model of the WT EGFR ECD dimer bound to EGF (PDB ID: 3NJP). Domains are color-shaded as previously indicated to visualize subdomain movement upon EGF binding. One of the dimeric partners is shaded light for clearer visualization. **(D)** Surface model of the auto-inhibited EGFR ECD with the portions missing in EGFRvIII shaded light. The ECD deletion prevents formation of auto-inhibitory intramolecular interaction between domain II and IV. **(E)** Helical wheel diagrams showing axial views of inter-helix juxtamembrane segment packing in EGF- and TGF-α-type coiled coils. **(F)** The fluorogenic dye ReAsH is quenched when bound to two ethanedithiol ligands because of free rotation about the carbon-sulfur bond. When bound to proteins containing four proximal Cys thiols, rotation is inhibited and the fluorescence is de-quenched.

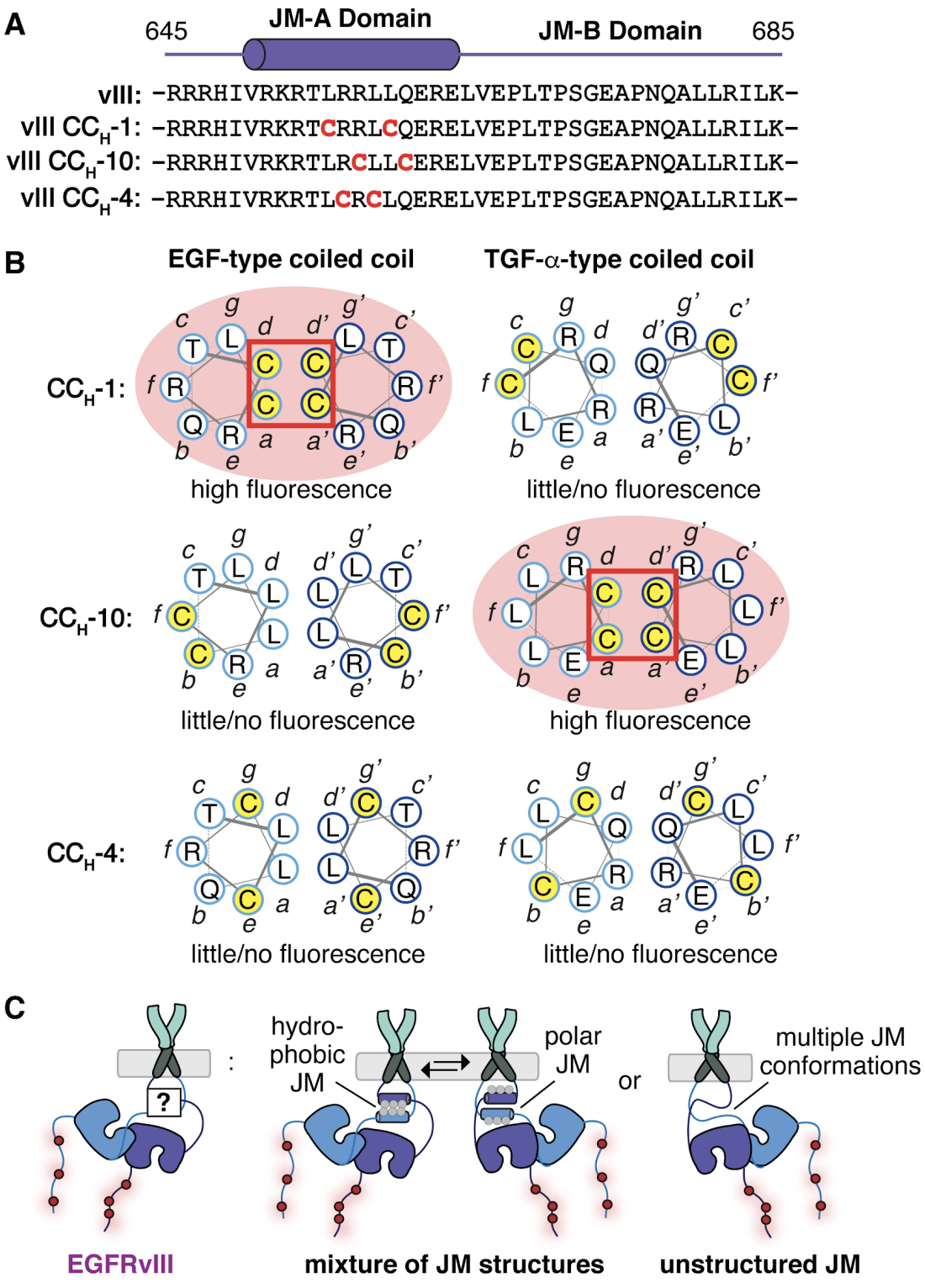
A
645
JM-A Domain
JM-B Domain
685
vIII: -RRRHIVRKRTLRRLLQERELVEPLTPSGEAPNQALLRILK-
vIII CC_H-1: -RRRHIVRKRTCRRLCQERELVEPLTPSGEAPNQALLRILK-
vIII CC_H-10: -RRRHIVRKRTLRCLLCERELVEPLTPSGEAPNQALLRILK-
vIII CC_H-4: -RRRHIVRKRTLCRCLQERELVEPLTPSGEAPNQALLRILK-
B
EGF-type coiled coil
TGF-α-type coiled coil
CC_H-1:
high fluorescence
little/no fluorescence
CC_H-10:
little/no fluorescence
high fluorescence
CC_H-4:
little/no fluorescence
little/no fluorescence
C
?
:
hydro-
phobic
JM
polar
JM
or
multiple JM
conformations
EGFRvIII
mixture of JM structures
unstructured JM

Figure 2.2. Probing EGFRvIII JM structure using bipartite tetracysteine display. (A) Sequence of the juxtamembrane (JM) regions of vIII (WT EGFR numbering) alongside those of vIII CC_H-1, CC_H-10 and CC_H-4. JM residues in the vIII sequence that are mutated to Cys in vIII-CC_H-1, vIII-CC_H-10 and vIII-CC_H-4 are colored red. **(B)** Helical wheel diagrams illustrating axial views of idealized inter-helix packing in EGF- and TGF-α-type coiled coils. The helical diagrams shaded with red background indicate a conformation that is suitable for ReAsH binding with the individual vIII variants. **(C)** Two models to account for ReAsH binding by both vIII-CC_H-1 and vIII-CC_H-10.

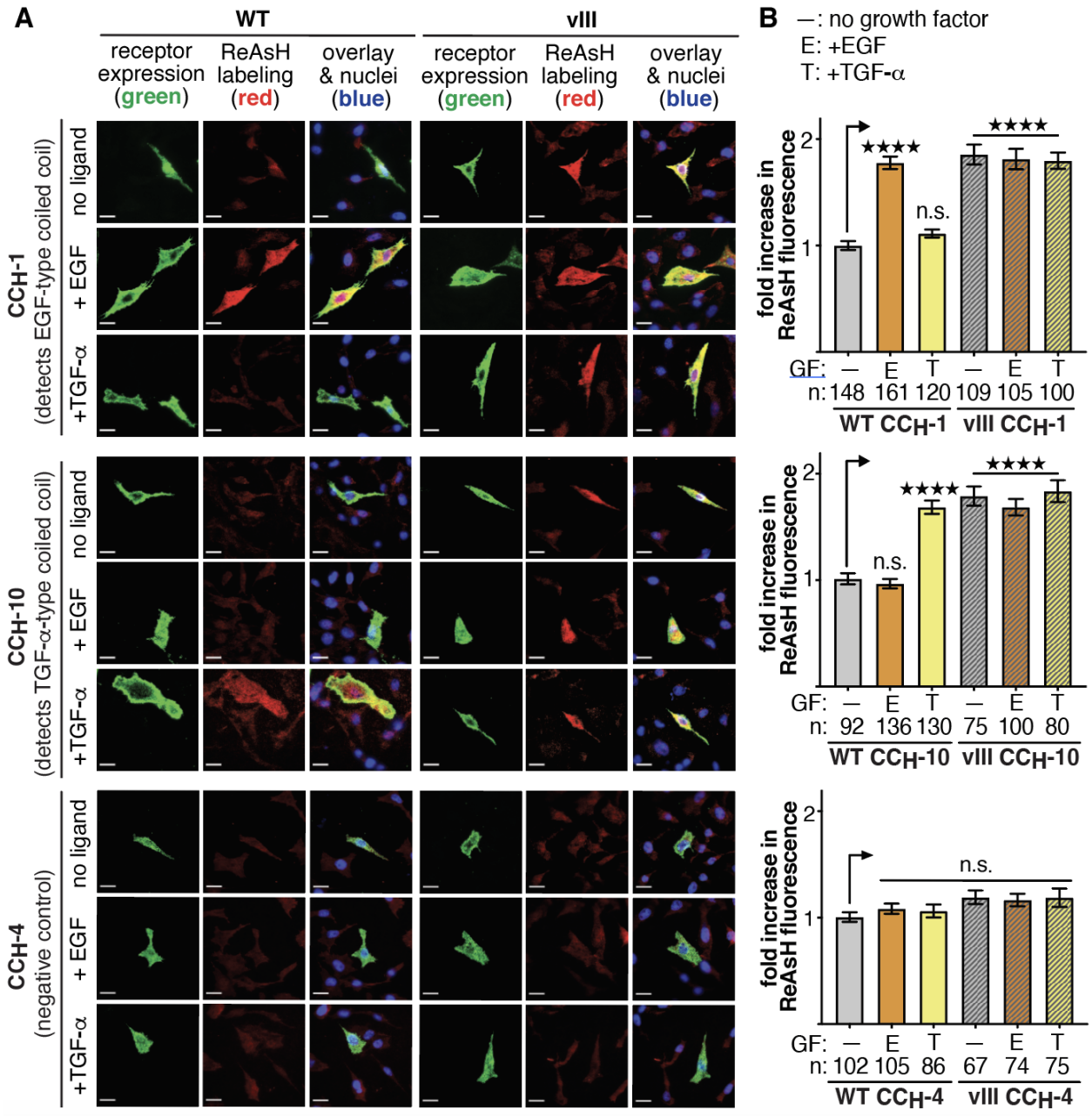
A
WT
vIII
receptor expression (green)
ReAsH labeling (red)
overlay & nuclei (blue)
receptor expression (green)
ReAsH labeling (red)
overlay & nuclei (blue)
CCH-1 (detects EGF-type coiled coil)
CCH-10 (detects TGF-α-type coiled coil)
CCH-4 (negative control)
no ligand
+ EGF
+TGF-α
B
—: no growth factor
E: +EGF
T: +TGF-α
fold increase in ReAsH fluorescence
GF: — E T — E T
n: 148 161 120 109 105 100
WT CCH-1
vIII CCH-1
n.s.
GF: — E T — E T
n: 92 136 130 75 100 80
WT CCH-10
vIII CCH-10
GF: — E T — E T
n: 102 105 86 67 74 75
WT CCH-4
vIII CCH-4

Figure 2.3. The juxtamembrane segment of EGFRvIII exists as a mixture of EGF- and TGF-α-type coiled coils. (A) Representative TIRF-M images of CHO-K1 cells illustrating ReAsH labeling (red fluorescence) and expression (green fluorescence) of FLAG-tagged CC_H-1, CC_H-10 and CC_H-4 variants of WT EGFR and EGFRvIII in the absence and presence of EGF or TGF-α stimulation (16.7 nM). Scale bars represent 10 μm. **(B)** Bar Plots illustrating the quantification of TIRF-M results from 'n' cells as a fold-increase in expression-corrected ReAsH fluorescence over background. Error bars represent s.e.m., ****p<0.0001, ***p<0.001, **p<0.01, *p<0.05 from one-way ANOVA with Dunnett's post-analysis accounting comparison to the WT control for each case without growth factor treatment. n.s., not significant. See also **Figure 2.5**.

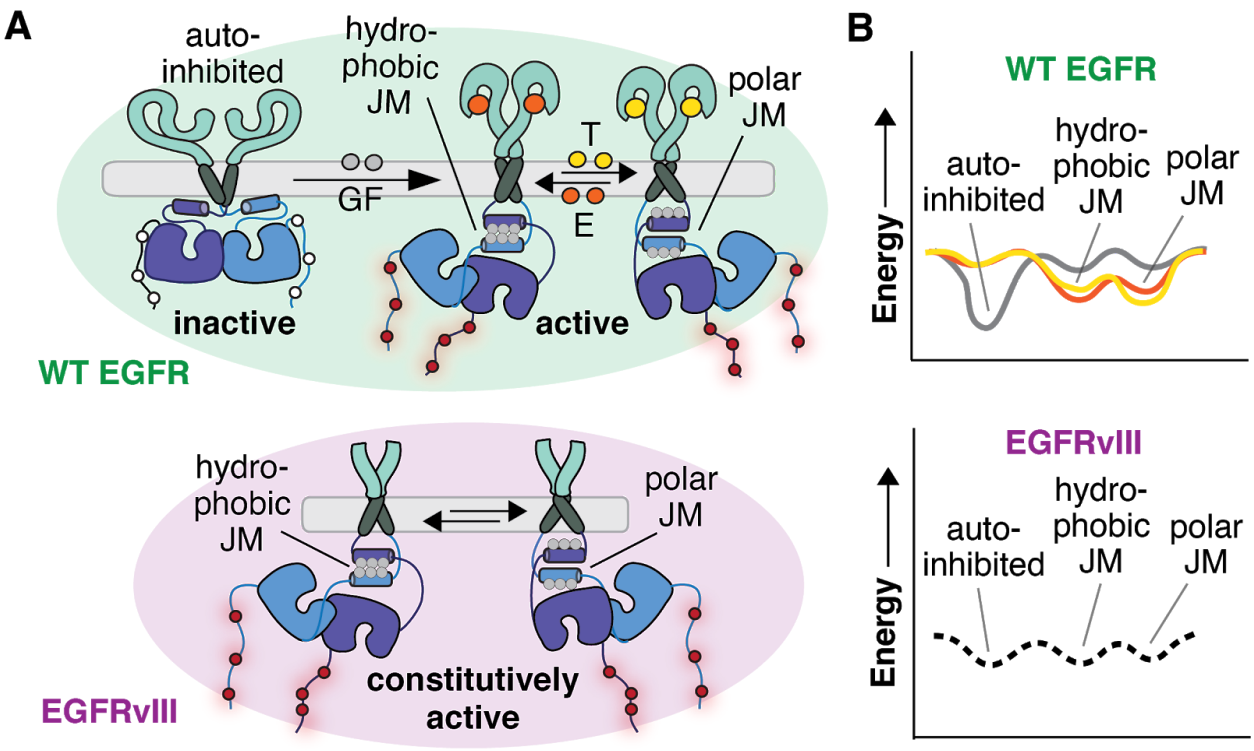

Figure 2.4. (A) Cartoon illustrating the preferred conformation of the JM coiled-coil in WT EGFR and EGFRvIII. In WT EGFR, the JM conformation is influenced by the identity of the growth factor bound to the ECD. When bound to EGF, the JM adopts an antiparallel coiled coil characterized by a leucine-rich, hydrophobic interface, when bound to TGF-α, the antiparallel coiled coil is characterized by a polar interface. In the constitutively active EGFRvIII, in the absence of growth factor-induced ECD rearrangements, both EGF-type and TGF-α coiled coil conformations are adopted. **(B)** Hypothetical energy well diagrams illustrating the different energy landscapes of the JM region in WT EGFR and EGFRvIII.

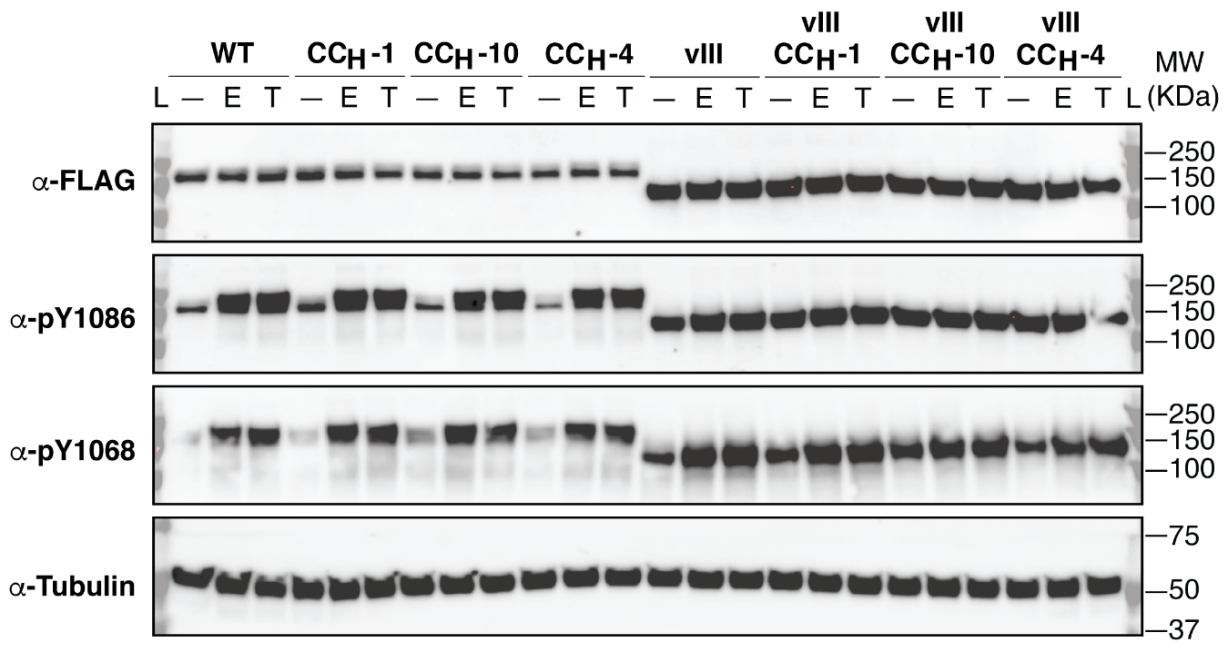

Figure 2.5. **CC_H-1, CC_H-10 and CC_H-4 variants of WT EGFR and EGFRvIII are expressed and phosphorylated as expected**. Immunoblots comparing the relative expression and activity (as judged by the level of receptor autophosphorylation at Y1068, Y1086) of CC_H-1, CC_H-10 and CC_H-4 variants of WT EGFR and EGFRvIII with the corresponding EGFR variant lacking CysCys substitutions within the JM. In each case, transiently transfected CHO-K1 cells were stimulated with 100ng/mL (16.7nM) EGF or TGF-α (or serum free media) for 5min at 37°C.

Chapter 3. Investigating the role of the JM-A coiled coil structure on EGFR trafficking and degradation.

Disclosure and authorship

This text of this chapter contains material adapted from a manuscript submitted to the peer-reviewed journal eLife for review:

"Coiled coil control of growth factor and inhibitor-dependent EGFR trafficking and degradation", Mozumdar, D., Chang, S. H.-H., Quach, K., Doerner, A., Schepartz, A.

Chapter 3. Investigating the role of the JM-A coiled coil structure on EGFR trafficking and degradation.

3.1. ABSTRACT.

EGFR exhibits biased intracellular signaling – growth factor or mutation-dependent changes in the conformation and/or dynamics of the receptor elicit distinct intracellular outcomes of EGFR signaling, biology and cell fate. We report that a two-state coiled coil switch located within the juxtamembrane segment (an essential component of the cytosolic dimer interface) controls many outcomes associated with activated EGFR. The position of this allosteric switch (defined by the identity of the JM-A coiled coil structure) controls the path of EGFR endocytic trafficking and whether or not the receptor is degraded in lysosomes. The identity of the JM-A coiled coil structure also predicts kinase-independent effects of oncogenic EGFR mutations (L834R/ T766M) and the ability of clinically relevant tyrosine kinase inhibitors (TKIs) to promote efficient, lysosomal degradation of oncogenic EGFR. These findings provide a model for biased intracellular signaling by EGFR, insights into kinase-independent activities of the receptor and clinically relevant TKIs, and identify new strategies for modulating EGFR lifetime.

3.2. Introduction.

Receptor tyrosine kinases in the EGFR family play diverse and critical roles in cell proliferation, differentiation, and migration [3,4,6]. Aberrant activation of EGFR family members, *via* overexpression or mutation, is associated with many human cancers [10,11,126]. Although much work on EGFR has focused on its activation by EGF [1], EGFR is activated by at least seven different growth factors including TGF-α, EPI, ER, BC, HB-EGF, and AR [7,8], and transmits these activation events into distinct intracellular phenotypes [28,29,127–129]. Growth factor-dependent biased signaling through EGFR has been previously attributed to differences

in the physical properties of the growth factors [28,127,129] or their receptor complexes [128–130]. EGFR is also activated constitutively by mutations in the kinase domain, the extracellular domain, or elsewhere [6,10,11,126]; these mutations are causally linked to many human cancers [126].

Previous work has shown that the binding of most growth factors to the ECD of EGFR induces the formation of one of two rotationally isomeric coiled coils within the juxtamembrane segment (JM) [21], an essential element of the cytoplasmic dimer interface [18,19]. Binding of EGF or HB-EGF induce a coiled coil in the JM-A defined by a leucine-rich inter-helix interface (EGF-type) [20], whereas AR, EPI, ER, or TGF-α induce an isomeric structure whose interface is charged and polar (TGF-α-type) [21]. JM coiled coil preference is also influenced allosterically, by point mutations within one of the G-x-x-x-G motifs of the TM helix [17], oncogenic ECD [105] and kinase domain mutations [31], and, in the case of drug-resistant L834R/T766M EGFR, the pharmacologic status of its kinase domain [31].

While it is clear that the structure of the JM-A segment is coupled allosterically to the different EGFR domains, this very coupling complicates strategies to investigate how and whether distinct coiled coil structures in the JM-A influence outcomes associated with biased signaling. To better understand the relationship between JM-A coiled coil structure and EGFR biology, we designed a set of kinase-active EGFR mutants that effectively shift the equilibrium between JM coiled coil isomers. These EGFR mutants assemble into dimers that favor one coiled coil or the other in a manner that is independent of the activating growth factor. Using these and other "decoupling" mutants, we demonstrate that coiled coil identity alone is *necessary and sufficient* for defining the pathway of EGFR trafficking into degradative (Rab7+) or recycling (Rab11+) endosomes and ultimately whether EGFR is degraded within lysosomes. The identity of the

coiled coil in the JM-A also predicts the trafficking and lifetime of oncogenic EGFR mutants and reveals kinase-independent effects of FDA-approved small molecule TKIs. These discoveries increase our understanding of the molecular mechanism used for biased signaling in ErbB-family receptors and suggest new strategies for purposefully controlling protein traffic and lifetime along the endocytic pathway.

3.3. Results

3.3.1. Design of EGFR decoupling mutants via mutations in the JM structure. We initially sought to identify and design a set of functional, full-length EGFR variants that could be used to isolate the cellular role of the JM-A by decoupling the coiled coil structure of the JM-A from growth factor identity [21,17,20]. It is well known that salt bridges at the *e* and *g* positions of model coiled coils influence stability and orientation [131], while changes at the *a* and *d* positions influence oligomeric state [132]. These studies suggested that the relative stability of the EGF- and TGF-α-type coiled coils formed within an intact EGFR dimer could be controlled by the presence/ absence of salt-bridging residues for a specific coiled coil structure at positions *e* and *g* (**Figure. 3.1.A**). We hypothesized that by rationally removing interactions that stabilized a given JM-A coiled coil structure would raise its free energy relative to the other and shift the equilibrium between the two structures (**Figure 3.2.A**). The result would be a set of EGFR variants that favored only a single JM-A coiled coil structure, regardless of the identity of the growth factor bound to the ECD. Such a design strategy would necessitate that two interconverting coiled coil structures are equally favorable – indeed our previous work with EGFRvIII revealed that the EGF- and TGF-α-type coiled coil structures are equally favorable when no growth factor-dependent signal emerges from the extracellular domain [105].

To test this hypothesis, a pair of EGFR variants (E661R and KRAA) were generated that contained one or two amino acid substitutions to selectively disrupt salt bridges unique to either the TGF-α- or EGF-type JM coiled coils (**Figure. 3.1.A** and **Figure. 3.2.B**). In E661R EGFR, a single charge-reversing mutation is located at distal *c* and *c'* positions of the heptad repeat when the JM folds into an EGF-type coiled coil, but at proximal *e* and *e'* positions when it folds into a TGF-α-type structure. Thus the JM-A in E661R EGFR should favor the EGF-type structure because it lacks a TGF-α-type-specific salt-bridge. By contrast, in KRAA EGFR, the two charge-eliminating substitutions K652A/ R656A are located at distal *c,g* and *c',g'* positions of the coiled coil repeat when the JM is assembled into the TGF-α-type structure, but at proximal *e*, *a* positions when assembled into the EGF-type structure. Thus the JM-A in KRAA EGFR should favor the TGF-α-type structure because it lacks two EGF-type-specific salt bridges (**Figure. 3.1.A**). As a control for our experiments, we designed a T654D EGFR variant – this mutation occupies the *c* or *e* position of a coiled coil repeat when the JM assembles into the EGF- and TGF-α-type structures, respectively (**Figure. 3.1.A**) and should not affect coiled coil stability. In control experiments, we verified that EGFR variants (containing mutations in the JM) could be expressed in CHO-K1 cells (which express little or no endogenous EGFR [133]), trafficked to the cell surface, and were phosphorylated at multiple tyrosine residues within the C-tail when treated with saturating (16.7 nM) EGF or TGF-α (**Figure. 3.2.C**).

3.3.2. Validating EGFR decoupling mutants. With functional EGFR mutants in hand, we made use of the bipartite tetracysteine display [20], to test the hypothesis that activated E661R and KRAA EGFR dimers would favor an EGF-type or TGF-α-type coiled coil, respectively, regardless of the identity of the activating growth factor. Bipartite tetracysteine display exploits the pro-fluorescent bis-arsenical dye ReAsH [41], which lights up only when bound to four Cys

side chains (two from each EGFR monomer) in a defined array [43]. Previous work identified a CysCys-containing EGFR variant whose dimer binds ReAsH only when its JM-A is assembled into an EGF-type type structure (CC_H-1 EGFR); another CysCys-containing EGFR variant (CC_H-10 EGFR) forms dimers that induce binds ReAsH only when the TGF-α-type coiled coil is formed [21]. For the bipartite tetracysteine display experiments, variants of CC_H-1 and CC_H-10 EGFR containing E661R or KRAA mutations were generated. In control experiments, we verified that all CysCys containing JM mutants were phosphorylated at multiple tyrosine residues within the C-terminal tail when treated with EGF or TGF-α; EGFR T654D was somewhat less active (**Figure. 3.2.D**).

The three sets of EGFR CC_H-1 and CC_H-10 variants were expressed in CHO-K1 cells, stimulated with EGF or TGF-α, incubated with ReAsH, and the level of ReAsH fluorescence relative to EGFR-expression determined using TIRF microscopy (TIRF-M) (**Figure 3.1.B,C**). TIRF-M excites fluorophores in an extremely thin axial region, typically within ~100 nm of the cell surface, thus the measured fold-increases in ReAsH fluorescence provide a read-out of JM coiled coil conformation within EGFR molecules at or near the plasma membrane. As expected [21], a significant fold-increase in ReAsH fluorescence was observed when cells expressing WT EGFR CC_H-1 EGFR are treated with EGF (2.00 ± 0.06) but not TGF-α (1.26 ± 0.03), or when cells expressing WT CC_H-10 EGFR were treated with TGF-α (1.52 ± 0.05) and not EGF (0.97 ± 0.04). By contrast, cells expressing E661R CC_H-1 EGFR showed a significant fold-increase in ReAsH fluorescence regardless of whether the cells were treated with EGF (2.66 ± 0.14) or TGF-α (2.60 ± 0.12), suggesting that the EGF-type structure formed in both cases. Little or no fold-increase in ReAsH fluorescence was observed when cells expressing E661R CC_H-10 EGFR were treated with EGF (1.14 ± 0.08) or TGF-α (1.10 ± 0.07) (**Figure 3.1.B,C**).

In a similar way, cells expressing KRAA CC_H-10 EGFR displayed a significant fold-increase in ReAsH fluorescence regardless of whether the cells were treated with EGF (1.40 ± 0.05) or TGF-α (1.32 ± 0.05), and little increase was observed in cells expressing KRAA CC_H-1 EGFR (1.59 ± 0.19-fold (EGF); 1.21 ± 0.14-fold (TGF-α)) (**Figure 3.1.B,C**). Analogous variants containing T654D mutations behaved like WT EGFR, as expected (**Figure 3.2.E,F**)) and no fold-increase in ReAsH fluorescence was observed in the absence of added growth factor. These data indicate that no matter which growth factor is bound to the EGFR ECD, E661R EGFR assembles into an active dimer containing an EGF-type coiled coil, whereas KRAA EGFR assembles into an active dimer containing a TGF-α-type coiled coil. These results confirm that the mutations embodied by E661R and KRAA EGFR can effectively decouple growth factor identity from coiled coil status.

3.3.3. Trafficking of E661R and KRAA EGFR. A quintessential growth factor-dependent characteristic of EGFR is its path of receptor trafficking following endocytosis [134]. Unactivated EGF receptors at the cell surface are internalized into Rab4-associated early endosomes and recycled back to the cell surface where they accumulate. Activated receptors are trafficked first to EEA1-positive (EEA1+) early endosomes [135]. The pathway then splits, and receptors are sorted into vesicles defined by the presence of either Rab11 (Rab11+) or Rab7 (Rab7+). Rab11+ vesicles deliver EGFR back to the cell surface (recycling pathway) [136] whereas the Rab7+ vesicles deliver EGFR to late endosomes and lysosomes where the receptors are ultimately degraded (degradative pathway) [137]. Trafficking from EEA1+ early endosomes into recycling or degradative endosomes is known to be growth factor-dependent: when stimulated with EGF, EGFR preferentially traffics into Rab7+ endosomes and is ultimately

degraded [137]; when stimulated with TGF-α, EGFR preferentially traffics into Rab11+ endosomes and returns to the cell surface [30].

The dependence of the path of EGFR trafficking on growth factor identity post-endocytosis has been previously attributed to differences in the pH-dependent ligand occupancy of receptors following [28,127]. In particular, TGF-α dissociates from EGFR at higher pH than does EGF; ligand dissociation at earlier points along the endocytic pathway is believed to lead ultimately to receptor sorting. Although the pH-dependent model is simple, it is inconsistent with reports that TGF-α-bound EGFR continues to signal within endosomes [30,138]. We thus asked whether the coiled coil status of the JM-A could also control the pathway of EGFR trafficking. If so, then EGFR mutations that favor the EGF-type (E661R) coiled coil in activated dimers would bias trafficking into Rab7+ endosomes (degradative pathway), whereas those that favor the TGF-α-type structure would bias trafficking into Rab11+ endosomes (recycling pathway).

We used confocal microscopy to trace the time-, mutation, and growth factor-dependent pattern of EGFR trafficking and organelle co-localization following growth factor stimulation. CHO-K1 cells expressing FLAG-tagged WT, E661R, KRAA or T654D EGFR were incubated first on ice with EGF or TGF-α to allow growth factor binding and then at 37 °C in growth factor-free media to initiate endocytosis and receptor trafficking. After 8 or 40 min, the cells were immuno-stained to visualize EGFR and assess the extent of colocalization with EEA1, Rab7, or Rab11. After 8 min, WT EGFR, E661R, KRAA, and T654D EGFR all co-localize with the early endosome marker EEA1 (**Figure 3.3.A,B**) and not with Rab7 (**Figure 3.3.C,D**) or Rab11 (**Figure 3.3.E,F**), regardless of whether the cells were stimulated with EGF or TGF-α. After 40 min, the colocalization of all activated receptors with EEA1 decreases to non-significant levels [29] (**Figure 3.5.A,B**). These results confirm that the growth factor-dependent trafficking of all EGFR

variants studied here proceeds initially through EEA1+ early endosomes regardless of JM coiled coil status or growth factor identity.

We used the same workflow to evaluate the trafficking pattern of FLAG-tagged WT, E661R, KRAA and T654D EGFR at 40 min post growth factor incubation. WT EGFR and T654D EGFR both colocalized preferentially with Rab7 when activated with EGF (MCC = 0.78 ± 0.05 (WT) and 0.71 ± 0.05 (T654D)) (**Figure 3.4.A,C** and **Figure 3.5.C,D**) and with Rab11 when activated with TGF-α (MCC = 0.62 ± 0.06 (WT) and 0.60 ± 0.06 (T654D)) (**Figure 3.4.B,C** and **Figure 3.5.C,D**). In contrast, while E661R still colocalized significantly with Rab7 when activated with EGF, it also colocalized significantly with Rab7 when activated with TGF-α (**Figure 3.4.A-C)**. The extent of EGFR colocalization with Rab7 upon TGF-α activation was low (MCC = 0.09 ± 0.02) for WT EGFR but moderate (MCC = 0.44 ± 0.07) for the E661R variant (**Figure 3.4.A-C**). Similarly, the extent of colocalization with Rab11 upon TGF-α activation was high (MCC = 0.62 ± 0.06) for WT EGFR but only moderate (MCC = 0.34 ± 0.10) for the E661R variant (**Figure 3.4.A-C**). Overall, these results indicate that the E661R mutation biases EGFR trafficking into Rab7+ endosomes independent of whether EGF or TGF-α is used to activate the receptor.

The inverse set of results were obtained when the pathway of KRAA EGFR trafficking was examined: KRAA EGFR colocalized significantly with Rab11 (and not Rab7) whether activated with EGF or TGF-α (**Figure 3.4.A-C**). The extent of EGFR colocalization with Rab11 upon EGF activation was low (MCC = 0.18 ± 0.03) for WT EGFR but moderate (MCC = 0.41 ± 0.08) for the KRAA variant (**Figure 3.4.A-C**). Similarly, the extent of colocalization with Rab7 upon EGF activation was high (MCC = 0.78 ± 0.05) for WT EGFR but only moderate (MCC = 0.29 ± 0.06) for the KRAA variant (**Figure 3.4.A-C**). These results indicate that the KRAA mutation biases EGFR trafficking into Rab11+ endosomes regardless of whether EGF or TGF-α is used to

activate the receptor. Taken together, these results indicate that the pathway of EGFR trafficking is influenced by the structure formed within the JM region that links the TM region to the kinase domain. We note, however, that the biasing of EGFR trafficking is not a perfect "on/off" switch: while the E661R substitution increases the fraction of EGFR that traffics into Rab7+ endosomes in the presence of TGF-α, a small fraction of TGF-α-activated E661R EGFR traffics into Rab11+ endosomes (**Figure 3.4.A-C**). Indeed, the extent of phosphorylation at C-tail residues Y1045, Y1068, and Y1173 did not obviously correlate with JM mutational state (**Figure 3.6.A-C**).

3.3.4. Mutations within the EGFR transmembrane helix that allosterically influence JM coiled coil status control the pathway of receptor trafficking. Mindful of the fact that E661R and KRAA EGFR contain mutations within the JM coiled coil itself which could influence functional intra- or intermolecular protein interactions, we turned to a new set of EGFR decoupling variants in which JM coiled coil identity is controlled allosterically by point mutations in the adjacent transmembrane segment (TM) [17]. Substitution of phenylalanine for a single glycine (G628) at the final position of the N-terminal G-x-x-x-G motif of the EGFR TM (G628F EGFR) generates a receptor dimer with an EGF-type JM coiled coil, regardless of whether the receptor is activated by EGF or TGF-α–just like E661R EGFR [17]. Likewise, substitution of the beta-branched valine residue at position 628 (G628V EGFR) generates a receptor dimer with a TGF-α-type coiled coil, regardless of whether the receptor is activated by EGF or TGF-α–just like KRAA EGFR [17]. Substitution of G628 with alanine (G628A EGFR) generates a receptor that behaves like WT EGFR. Since these TM variants contain an unaltered JM, their functional intra- or intermolecular protein interactions should be preserved. As a result, the trafficking patterns they follow should provide an unadulterated view of the

relationship between JM conformational status and EGFR trafficking. If JM coiled coil structure is both necessary and sufficient to direct the pathway of EGFR trafficking, then G628F and G628V EGFR should traffic into only Rab7+ or Rab11+ endosomes, respectively, regardless of how they are activated, whereas G628A EGFR should behave like WT EGFR and traffic in a growth factor-dependent manner. In control experiments we verified that G628F, G628V, and G628A EGFR colocalize after 8 min with EEA1 (**Figure 3.7.A,B**) and not with Rab7 (**Figure 3.7.C,D**) or Rab11 (**Figure 3.7.E,F**); colocalization with EEA1 falls to expected levels after 40 min (**Figure 3.7.G,H**).

Indeed, after 40 minutes, although the extent of G628A EGFR co-localization with Rab7 and Rab11 was growth factor-dependent, the localization of G628F and G628V EGFR were not (**Figure 3.8.**). When stimulated with EGF, G628A EGFR co-localized preferentially with Rab7 (MCC = 0.38 ± 0.06) (**Figure 3.8.A,C**) and not Rab11 (MCC = 0.13 ± 0.03) (**Figure 3.8.B,C**); when stimulated with TGF-α, G628A EGFR co-localized preferentially with Rab11 (MCC = 0.33 ± 0.03) (**Figure 3.8.B,C**) and not Rab7 (MCC = 0.13 ± 0.03) (**Figure 3.8.A,C**). By contrast, G628F EGFR colocalizes exclusively with Rab7 whether stimulated with EGF (MCC = 0.48 ± 0.05) or TGF-α (MCC = 0.37 ± 0.03) (**Figure 3.8.A,C**) and not with Rab11 (MCC = 0.11 ± 0.05 and 0.14 ± 0.04 for cells stimulated with EGF and TGF-α-, respectively) (**Figure 3.8.B,C**). Conversely, G628V EGFR colocalizes exclusively with Rab11 whether stimulated with EGF (MCC = 0.65 ± 0.03) or TGF-α (MCC = 0.65 ± 0.07) (**Figure 3.8.B,C**) and not with Rab7 (MCC = 0.12 ± 0.02 and 0.16 ± 0.03 for cells stimulated with EGF and TGF-α-, respectively) (**Figure 3.8.A,C**). Here, when the coiled coil status of the JM-A is fixed by distal mutations, the switch in trafficking pattern was observed to be complete: G628F EGFR, whose JM contains an EGF-type coiled coil, trafficks along the degradative pathway whereas G628V EGFR, whose JM

contains a TGF-type coiled coil, trafficks along the recycling pathway. Furthermore, in this case the extent of phosphorylation at C-terminal tail residues Y1045,Y1068, and Y1173 correlates with JM mutational state (**Figure 3.9.A-C**).

3.3.5. Coiled coil control of EGFR degradation. The differences in endocytic trafficking seen with EGFR TM mutants that influence JM structure result in predictable changes in EGFR lifetime (**Figure 3.10.A,B**). The lifetime of WT and G628A EGFR depends on growth factor identity in the expected way [29,30]. Following EGF stimulation, WT and G628A EGFR levels decrease rapidly and the fraction of intact receptor detected after 90 minutes is low (41-45%), whereas the fraction of intact EGFR detected after 90 minutes is high when cells are stimulated with TGF-α (94-92%)(**Figure 3.10.A,B**). By contrast, G628F EGFR is degraded rapidly regardless of whether the receptor was activated with EGF or TGF-α, with 42% and 60% of the intact receptor remaining after 90 min following EGF or TGF-α treatment, respectively (**Figure 3.10.A,B**). Conversely, G628V was degraded slowly following treatment with EGF or TGF-α, with 92% and 95% of the intact receptor remaining after 90 min, respectively (**Figure 3.10.A,B**). Control experiments using inhibitors of either lysosomal or proteasomal function confirmed that EGFR degradation occurred within lysosomes (**Figure 3.10.A,B**). Thus, the presence of a single point mutation in the TM segment and its long-range effect on JM conformation are necessary and sufficient to dictate the pathway of intracellular trafficking (**Figure 3.8**) and the extent of EGFR degradation in lysosomes (**Figure 3.10.**).

3.3.6. Tyrosine kinase inhibitors influence the trafficking path and lifetime of L834R/T766M EGFR. The allosteric network coordinating information transfer between the ECD, TM, and JM regions of EGFR also includes the cytoplasmic kinase domain and its pharmacologic state [31,17,139]. Kinase domain mutations associated with drug-resistant

non-small cell lung cancer (L834R/T766M) [50] generate constitutively active receptors whose JM-A assemble preferentially into the TGF-α-type structure [31]. The structure of the JM coiled coil shifts into the EGF-type structure when L834R/T766M EGFR is inhibited by selective third-generation tyrosine kinase inhibitors (TKIs) such as WZ-4002 [67], CO-1686/ Rociletinib [65], or the clinically approved AZD-9291/ Osimertinib/ Tagrisso [68]. Previous work has shown that L834R/T766M EGFR is constitutively endocytosed and recycled in H1975 cells [140], as predicted by the position of its JM coiled coil switch (preferential assembly into the TGF-α-type JM-A structure). Here we asked whether this pattern of post-endocytic trafficking is also observed in CHO-K1 cells expressing L834R/T766M EGFR, whether it is affected by L834R/T766M EGFR-selective TKIs, and whether differences in trafficking lead to predictable changes in L834R/T766M EGFR lifetime.

Using confocal microscopy, we evaluated the pattern of endocytic trafficking and sub-cellular localization of L834R/T766M EGFR in CHO-K1 cells in the presence and absence of second- (Afatinib), third- (AZD-9291, CO-1686, WZ-4002), and fourth-generation (EAI045) TKIs [117]. These small molecule EGFR inhibitors differ in mechanism of engagement (covalent *vs.* non-covalent), EGFR specificity (WT *vs.* DM; monomer *vs.* dimer-specific), and binding site (ATP *vs.* allosteric) (**Figure 3.11.**). All of these TKIs predictably decreased the levels of EGFR auto-phosphorylation (**Figure 3.12.A**). As anticipated from data in H1975 cells [140], after 40 min uninhibited L834R/T766M EGFR colocalizes with Rab11 (MCC = 0.48 ± 0.03) (**Figure 3.11.C,D**) and not Rab7 (MCC = 0.17 ± 0.01) (**Figure 3.11.A,B**), favoring the recycling pathway as expected for activated receptors that contain a TGF-α-type JM coiled coil [31]. Afatinib-inhibited L834R/T766M EGFR also colocalizes with Rab11 (MCC = 0.46 ± 0.04) (**Figure 3.11.C,D**) and not Rab7 (MCC = 0.14 ± 0.02) (**Figure 3.11.A,B**) after 40 min, again

favoring the recycling pathway expected for activated receptors that contain a TGF-α-type JM coiled coil [31]. By contrast, when covalently inhibited by AZD-9291, CO-1686, or WZ-4002, all third-generation TKIs that selectively and covalently inhibit L834R/T766M EGFR, the extent of L834R/T766M EGFR colocalized with Rab7 increases and colocalization with Rab11 decreases (**Figure 3.11.B,D**). Notably, these changes are not observed in cells expressing L834R/T766M EGFR and treated with the fourth-generation inhibitor EAI045 (**Figure 3.11.B,D**), which binds noncovalently in a pocket adjacent to that of AZD-9291 [117]. EAI045 differs from AZ-9291, CO-1686, and WZ-4002 in both engagement mode and binding site within the EGFR kinase domain, suggesting that the observed differences in receptor trafficking likely result from a common allosteric change in EGFR structure induced by these three small molecules that guides the receptor along the degradative arm of the endocytic pathway.

Finally we asked whether the change in endocytic trafficking induced by AZD-9291, CO-1686, and WZ-4002 also resulted in L834R/T766M EGFR degradation. We observed that treatment of L834R/T766M EGFR with AZD-9291, WZ-4002, and CO-1686 led to markedly (> 75%) reduced receptor levels after 12 hours when compared to untreated samples (**Figure 3.11.E** and **Figure 3.12.B**). In contrast, uninhibited, Afatinib-treated, and EAI045-treated L834R/T766M EGFR levels remained steady (**Figure 3.11.E** and **Figure 3.12.B**). The TKI-induced degradation of L834R/T766M EGFR induced by AZD9291, CO-1686, and WZ-4002 was inhibited completely by chloroquine, while lactacystin had no effect (**Figure 3.11.E** and **Figure 3.12.B**). Neither chloroquine nor lactacystin affected the levels of L834R/T766M EGFR when mock-treated or in the presence of TKIs that failed to induce L834R/T766M EGFR degradation (**Figure 3.11.E** and **Figure 3.12.B**). For all cases inspected, predictable levels [141,65,68,117] of phosphorylated L834R/T766M EGFR were detected at Y1045 (**Figure 3.11.F** and **Figure 3.12.C**) and Y1068

(**Figure 3.11.G** and **Figure 3.12.D**). Thus, third-generation TKIs that engage the ATP-binding pocket [141,65,68], allosterically induce an EGF-type structure within the JM segment [31], and traffic the receptor into Rab7+ endolysosomes (**Figure 3.11.A,B**), also induce significant levels of L834R/T766M EGFR degradation through a lysosomal, as opposed to proteasomal mechanism (**Figure 3.11.E** and **Figure 3.12.B**).

3.3.7. Discussion. EGFR is an essential, membrane-embedded sensor that communicates and integrates growth factor-dependent signals into diverse cellular phenotypes [6,142]. It is also one of the most potent oncogenes in human cancers [11,126] and remains an insufficiently addressed therapeutic target. EGFR is activated by growth factors that bind to the receptor extracellular domain (ECD) and by diverse mutations [6]; in both cases the result is a dimeric receptor with one of two coiled coils within the cytoplasmic juxtamembrane segment (JM) [17,20,21,31] and a catalytically active asymmetric kinase dimer [22]. Despite its clear therapeutic significance, the mechanism by which EGFR decodes growth factor identity and/or mutational status into distinct and dynamic cellular signaling programs has remained elusive. In part, this knowledge gap results from the absence of a high-resolution view of how the full length EGFR acts as an allosteric unit to communicate information across multiple domains and a complex lipid bilayer in cells. But a more complete understanding of EGFR function is also precluded by allostery itself; how can one separate the activities of two or more protein domains whose conformational landscapes are dynamic and themselves tightly coupled?

3.3.8. The JM coiled coil is a rotational toggle switch. In this work, we use structural, biochemical, and chemical biology tools to decouple the conformational landscape of the JM from both the extracellular domain and the kinase domain without loss of EGFR activity. Using these mutants and tools, we identify the cytoplasmic juxtamembrane segment as an essential

EGFR processing center. The JM-A receives inputs from both the TM helices and the kinase domain and assembles into one of two rotationally isomeric coiled coils [17,20,21,31]. Together, these coiled coils contain all of the information necessary to specify both the direction of trafficking along the endocytic pathway and EGFR lifetime. These results support a model in which the pathway of endocytic trafficking following EGFR activation is determined by JM coiled coil status and not by growth factor-dependent differences in the EGFR-ligand complex stability as previously proposed [29,30,127]. The different effects of EGFR-selective growth factors also do not correlate with receptor dimer strength [14], as EGF and TGF-α both induce high affinity ECD dimers but traffic differently. Further corroborating these results are recent findings [26] providing a high-resolution view of how the binding of EGF and TGF-α to the extracellular domain alter the orientation of the dimeric receptor as it tracks into the membrane-embedded transmembrane helix. As changes in transmembrane helix orientation are known to bias JM conformation in cells [17], together these results provide a clear picture of how conformation changes within the EGFR extracellular domain are transduced into alternative JM conformations, and how alternative JM conformations are necessary and sufficient to control fundamental EGFR biology.

The structures of the EGF- and TGF-α-type coiled coils differ not only in the residues that mediate helix-helix interactions but also in the external surface available for intra- and intermolecular interaction. In the EGF-type structure, the residues at the *c*, *f*, and *b* positions of the coiled coil repeat are charged and polar [18], whereas these positions are hydrophobic (all leucine) in the TGF-α-type structure (Figure 1a). A sophisticated molecular dynamics-derived model of the active full-length receptor dimer [16] shows the receiver kinase JM in the EGF-type structure with direct interactions between the receiver kinase JM latch (residues

664-681) and the charged surface of the activator kinase C-lobe. The details of these interactions and/or their dynamics would be different were the JM assembled into the TGF-α-type structure, whose interaction surface is hydrophobic, not polar and charged. The different interaction surfaces could interact differently with the kinase domain to alter the position (and thus accessibility) of the C-terminal tail, which is believed to localize near the JM [6,18,19] or alter the precise arrangement of acceptor and receiver kinase domains relative to one another [16,22,143] and thereby influence their inherent substrate specificity. These different interaction surfaces could also play a direct role by differentially recruiting known JM-interacting factors such as, Nck adaptor protein [77], PKC [79], p38MAPK [86], AP2 [144,145] calmodulin [91] and ARNO [91], which in turn bias EGFR signaling and the consequent trafficking route. The presence of a LeuLeu motif on the outside surface of the TGF-α-type coiled coil is especially intriguing, as LeuLeu motifs elsewhere within EGFR (notably the JM-B region and C-terminal tail) are docking sites for endosomal sorting factors [144,145].

3.3.9. Altered trafficking and degradation as kinase-independent EGFR and TKI activities. Small molecule EGFR inhibitors that bind near or within the ATP binding pocket and monoclonal antibodies targeting the extracellular domain have produced impressive therapeutic benefits to responsive cancers [146]. However, neither therapeutic modality offers sustained patient benefits, in large part because of acquired and innate resistance mechanisms [147,148]. There is a growing realization that EGFR possesses kinase-independent pro-survival functions in cancer cells [149,150] that are insufficiently inhibited by either monoclonal antibodies or small molecules that inhibit kinase activity alone. Our results support a model in which pro-survival kinase-independent EGFR functions are related to JM-dependent differences in

trafficking that avoid lysosomal degradation and receptor downregulation. Indeed, both EGFRvIII (implicated in glioblastoma multiforme) and L834R/T766M EGFR (implicated in NSCLC) avoid Cbl binding, ubiquitination, and degradation [151,152]. In the case of L834R/T766M EGFR, this kinase-independent activity is reversed by TKIs that shift the JM coiled coil equilibrium to promote lysosomal trafficking and degradation. Identification of the as-yet-unknown factors that mediate this trafficking could serve as a new strategy for targeted protein degradation that complements both traditional PROTAC-like strategies and lysosomal targeting strategies based on cell surface receptor engagement [153–155].

3.3.10. Materials and Methods

Materials. Antibodies. Goat polyclonal anti-Rabbit, Horseradish Peroxidase (HRP)-conjugated (#7074), Goat polyclonal anti-Mouse, HRP-conjugated (#7076), Rabbit monoclonal anti-Phospho-EGF ReceptorTyr1173, (53A5) (#4407), Rabbit polyclonal anti-Phospho-EGF Receptor Tyr1086 (#2220), Rabbit polyclonal anti-Phospho-EGF Receptor Tyr1068 (#2234), Rabbit polyclonal anti-Phospho-EGF Receptor Tyr1045 (#2237), Rabbit monoclonal anti-α-Tubulin (#2125), Rabbit monoclonal anti-vinculin (#13901), Rabbit monoclonal anti-EEA1 (C45B10) (#3288), Rabbit monoclonal anti-Rab7 (D95F2) XP (#9367), Rab11 (D4F5) XP Rabbit mAb (#5589), Anti-mouse IgG (H+L) and F(ab')2 Fragment Alexa Fluor® 555-conjugate (#4409) were purchased from Cell Signaling Technologies (CST). Mouse monoclonal (M2) anti-Flag (#F1804), Anti-FLAG® M2 Affinity Gel (#A2220) were purchased from Millipore Sigma. Goat anti-Mouse IgG (H+L) Cross-Adsorbed Secondary Antibody, Alexa Fluor 488®-conjugate (#A11001), IgG (H+L) Cross-Adsorbed Goat anti-Rabbit, Alexa Fluor™ 488 (#A11008), were purchased from ThermoFisher Scientific.

Chemicals and Recombinant Proteins. F-12K Medium (#10-025-CV), Dulbecco's Phosphate Buffered Saline (DPBS) (#14190), Fetal Bovine Serum (FBS)–Heat Inactivated (#11082147), Penicillin/Streptomycin (#1514012), Non-enzymatic Cell Dissociation Solution (#13151014), RestoreTM Western Blot Stripping Buffer (#21059), Hoechst 33342, Trihydrochloride, Trihydrate - 10 mg/mL Solution in Water (#H3570), iBlot PVDF membranes (# IB401031) were purchased from ThermoFisher Scientific. FugeneHD transfection reagent (E2311) was purchased from (Promega). Fetal Bovine Serum (FBS)–Heat Inactivated (#F4135), Bovine Serum Albumin (#9048-46-8), Fibronectin (#F1141) were purchased from Millipore Sigma. cOmplete, Mini Protease Inhibitor Tablets (#11836170001), PhosSTOP Phosphatase Inhibitor Cocktail Tablets

(#04906837001) were purchased from Roche Applied Science. Recombinant Human EGF Protein (#236-EG), Recombinant Human TGF-a Protein (#293-A) were purchased from R&D Systems. Mini-PROTEAN® TGXTM Precast Gels (10% polyacrylamide) (#456-1036), ClarityTM Western ECL reagents (#1705060) were purchased from Bio-Rad Laboratories, Inc. Lactacystin, proteasome inhibitor (#ab141411) and Chloroquine diphosphate, apoptosis and autophagy inhibitor (#ab142116) were purchased from AbCam. Tyrosine Kinase Inhibitors (TKIs) Erlotinib HCl (OSI-744) (#S1023), Afatinib (BIBW2992) (#S1011), Osimertinib (AZD-9291) (#S7297), Rociletinib (CO-1686) (#S7284), WZ4002 (#S1173), EAI045 (#S8242) were purchased from Selleck Chemicals.

Cell culture. CHO-K1 cells (ATCC) were cultured in F12K Medium supplemented with 10% FBS and Pen-Strep (100 I.U./mL penicillin and 100 mg/mL streptomycin) at 37°C in a CO2/air (5%/95%) incubator. Cells were transfected using the TransIT-CHO Transfection Kit (Mirus Bio LLC) (CHO-K1) or using FugeneHD (Promega), according to the manufacturer's instructions. Cell densities for all mammalian cell lines were determined with a Cellometer® Auto T4 automated counter. All cells were bona fide lines and periodically tested for mycoplasma with DNA methods

Cloning and Mutagenesis. All EGFR DNA variants were cloned from a pcDNA3.1 plasmid, generously donated by the Kuriyan Group (University of California, Berkeley), containing the sequence of the full-length EGFR with an N-terminal FLAG tag [18,22]. Mutations were introduced into the wild-type, CCH-1 and CCH-10 EGFR sequences using Quikchange Lightning site-directed mutagenesis kit (Agilent Technologies), according to the manufacturer's instructions, with primers (purchased from Integrated DNA Technologies) listed in Table 3.1. All DNA variants were amplified with XL-10 Gold Ultracompetent cells (Agilent Technologies).

Bipartite Tetracysteine Display Assay i.e. Surface ReAsH Labeling Studies and Total Internal Resonance Fluorescence (TIRF) Microscopy. ReAsH labeling was accomplished as described previously [21,17] by treating CHO-K1 cells expressing EGFR variants with an endocytosis inhibition cocktail (10 mM NaN3, 2 mM NaF, 5 mM 2-deoxy-D-glucose in F12-K media) for 1 hr at 37°C. Cells were stimulated without/with 100 ng/mL of EGF (16.7 nM)) and TGF-α (16.7 nM) prior to labeling. Cells were washed once with endocytosis inhibitor-containing media before incubation with ReAsH labeling solution (2 mM ReAsH (ThermoFisher Scientific), 20 mM BAL (Acros Organics) in F12K media) for 1 hr at 37°C. Cells were washed and incubated with endocytosis inhibitor-containing F12K media supplemented with 100 mM BAL for 10 min at 37°C. The media was removed, and cells fixed using 4% paraformaldehyde (PFA) in DPBS for 25 min at room temperature. Fixed cells were washed with DPBS and blocked with 10% BSA in DPBS for 30 min at 37°C. Cells were then labeled with primary antibody (mouse monoclonal mouse M2 anti-FLAG, 1:1000 dilution in 10% BSA in DPBS) for 1 hr at 37°C, washed thrice with 10% BSA in DPBS, then incubated with secondary antibody (AlexaFluor488- conjugated goat anti-mouse, 1:2000 dilution in 10% BSA in DPBS) for 1 hr at 37°C. Cells were then washed twice with 10% BSA in DPBS, washed once with DPBS, then nuclear-stained with Hoescht 33342 (1.62 mM in DPBS) for 5 min at 37°C. Cells were then washed once with DPBS and stored in DPBS at 4°C, prior to imaging. Labeled cells were monitored via TIRF microscopy, conducted on a Leica microsystems AM TIRF MC DMI6000B fitted with an EM-CCD camera (Hamamatsu) with HCX PL APO 63x/1.47 oil corrective objectives, as described previously[17,21]. Images were analyzed with ImageJ (FIJI) as described previously[17,21].

Immunofluorescent labeling, confocal microscopy and Image analysis.

Immunofluorescent labeling and confocal microscopy to assess localization of EGFR variants expressed in CHO-K1 cells was carried out as described previously[30] with slight modification. CHO-K1 cells expressing FLAG-tagged EGFR variants were incubated without/with 100 ng/mL of EGF (16.7 nM) or TGF-α (16.7 nM) for 1 hr at 4ºC to allow growth factor binding. For experiments with TKIs, instead of growth factor treatment, cells were incubated with 10uM TKI (as indicated) in F12K medium at 4ºC to allow TKI binding. Cells were then washed with DPBS and incubated with serum free media at 37ºC for 8 or 40 minutes as indicated to allow endocytosis. Cells were then fixed using 4% PFA in DPBS for 25 min at room temperature. Cells were washed with DPBS and incubated with blocking buffer (5% normal goat serum (CST), 0.3% Triton X-100 in DPBS) for 1 hr at 37ºC. Cells were then labeled with indicated primary antibodies overnight (~12 hrs) at 4ºC (mouse M2 anti-Flag, 1:1000 dilution and rabbit anti-Rab7, 1:1000 dilution or rabbit anti-EEA1, 1:1000 dilution or rabbit anti-Rab11, 1:1000 dilution in antibody dilution buffer (1% BSA, 0.3 % Triton X-100 in DPBS)). Cells were then washed thrice with DPBS and incubated with secondary antibody (AlexaFluor488- conjugated goat anti-rabbit, 1:500 dilution or AlexaFluor555- conjugated goat anti-mouse, 1:500 dilution in antibody dilution buffer) for 2 hr at room temperature. Cells were then washed twice with DPBS and nuclear-stained with Hoescht 33342 (1.62 mM in DPBS) for 5 min at room temperature. Cells were then washed once with DPBS and stored in DPBS at 4ºC, prior to imaging. Laser-scanning confocal microscopy experiments of labeled immunofluorescent samples were performed at room temperature on an inverted Zeiss LSM 880 laser-scanning confocal microscope equipped with a Plan-Apochromat ×63/1.4 numerical aperture oil immersion lens and a diode 405 nm laser, an Argon 458, 488, 514 nm laser, a diode pumped solid-state 561

nm laser and a 633 nm HeNe laser with standard settings. DAPI and Alexa-488, Alexa Fluor 555, and Alexa Fluor 647 dyes were excited with 405-, 488-, 546-, and 633-nm laser lines, and emitted light was collected through band pass filters transmitting wavelengths of 420–480 nm, 505–530 nm and 560–615 nm and a long-pass filter transmitting 615 nm, respectively. The pinhole size was set to 1 airy unit. Images were acquired at a nuclear section with fixed thresholds. Image acquisition was performed with ZEN software (Carl Zeiss). Raw images were exported as .lsm files. Images were analyzed using ImageJ software[125]. Colocalization of EGFR with indicated endocytic marker (Rab7, Rab11, EEA1) was evaluated as Manders' Colocalization Coefficient (MCC)[156] which represents the sum of intensities of green pixels (due to Rab11 or Rab7 or EEA1) that also contain red (due to FLAG-tagged EGFR) divided by the total sum of green intensities. Colocalization was evaluated using JACoP (Just Another Colocalization Plugin)[157] in ImageJ. MCC values for each condition obtained from multiple cells collected over at least 2 biological replicates were pooled and represented as Mean with S.E.M using Prism 8.4.3

Western Blot Analysis of EGFR Expression and Autophosphorylation. Western blot analysis of EGFR expression and autophosphorylation in transfected CHO-K1 cells was accomplished as described previously with slight modification [17,21]. CHO-K1 cells expressing FLAG-tagged EGFR variants were serum starved overnight (~12 hours). 48 hr post seeding cells were stimulated without/with 100 ng/mL of EGF (16.7 nM) or TGF-α (16.7 nM) for 5 min at 37°C, washed with serum free F12K media, and lysed in 100 mL of lysis buffer (50 mM Tris,150 mM NaCl, 1 mM EDTA, 1 mM NaF, 1% Triton X-100, pH 7.5, 1x cOmplete protease inhibitor cocktail, 1x Phos-Stop) for 1 hr. For experiments investigating the time dependent changes in intracellular EGFR levels, CHO-K1 cells were incubated without/with 100 ng/mL of EGF (16.7

nM) or TGF-α (16.7 nM) for 15 min following which, growth factor solution was washed with DPBS and cells were incubated at 37°C with serum free media for 0-90 minutes and cell lysis was carried out as described previously. For experiments investigating the time dependent changes in EGFR phosphorylation, CHO-K1 cells were incubated without/with 100 ng/mL of EGF (16.7 nM) or TGF-α (16.7 nM) for 15 min following which, growth factor solution was washed with DPBS and cells were incubated at 37°C with serum free media for 0-8 minutes and cell lysis was carried out as described previously. Clarified cell lysates were subjected to reducing 4-15% polyacrylamide SDS-PAGE electrophoresis and transferred to immuno-blot PVDF membranes. Membranes were blocked with 5% milk in TBS-T Buffer (50 mM Tris, 150 mM NaCl, 0.1% Tween, pH 7.4) for 1 hr followed by an overnight incubation at 4°C of indicated primary (rabbit or mouse) antibodies. Blots were washed with TBS-T and incubated with either anti-rabbit or anti-mouse goat horseradish peroxidase conjugate secondary antibodies for 1 hr at room temperature, then washed with TBS-T. Blots were then visualized using Clarity Western ECL reagents on a ChemiDoc XRS+/ ChemiDocMP instrument, and intensities of immuno-stained bands measured with ImageJ 64[125]. When assessing phosphorylation of EGFR/ gel loading at multiple positions using the same samples, the blots obtained with a given phospho-EGFR antibody were stripped with Restore Western Blot Stripping Buffer/ and antibody stripping buffer (Tris-HCl (62.5 mM), SDS (2%w/v), 2-mercaptoethanol (0.7%v/v)) and re-probed with a different phospho-EGFR antibody. For experiments investigating the time dependent changes in intracellular EGFR levels, the FLAG signal (total EGFR) was normalized to the vinculin loading control and normalized signal for the condition without any growth factor/ inhibitor treatment. For experiments investigating the time dependent changes in EGFR phosphorylation, the phospho-EGFR signal (pY1045, pY1068, pY1173) was normalized to the

total EGFR (FLAG signal) and vinculin/ tubulin was used as a loading control. For western blot experiments with the tyrosine kinase inhibitors (TKI), CHO-K1 cells expressing L834R/ T766M EGFR were pre-treated with serum free F12K medium containing 10uM of TKI at 37°C for 30 minutes, washed once with DPBS followed by incubation with serum free DMEM for 12 hrs, prior to cell lysis. FLAG, pY1045 and pY1068 signal was normalized to the vinculin loading control and corresponding signal detected at 12 hours without inhibitor/ TKI treatment. For all experiments with proteasomal/ lysosomal inhibitors, the experiments were carried out with CHO-K1 cells as described before in the methods, involving a pretreatment with 10uM Lactacystin or 100uM Chloroquine for 1 hr at 37°C prior to growth factor or TKI treatment.

Table 3.1. List of mutagenesis primers used to design JM decoupling mutants

EGFR Target Mutation	**Primer sequence (5'-3')**
E661R	forward: 5'- ggaggctgctgcagaggagggagcttgtgg -3' reverse: 5'- ccacaagctccctcctctgcagcagcctcc -3'
K652A/ R656A (or KRAA)	forward: 5'- cacatcgttcgggcgcgcacgctggcgaggctgctgca -3' reverse: 5'- tgcagcagcctcgccagcgtgcgcgcccgaacgatgtg -3'
T654D	forward: 5'- gcagcagcctccgcagatcgcgcttccgaacgatg -3' reverse: 5'- catcgttcggaagcgcgatctgcggaggctgctgc -3'

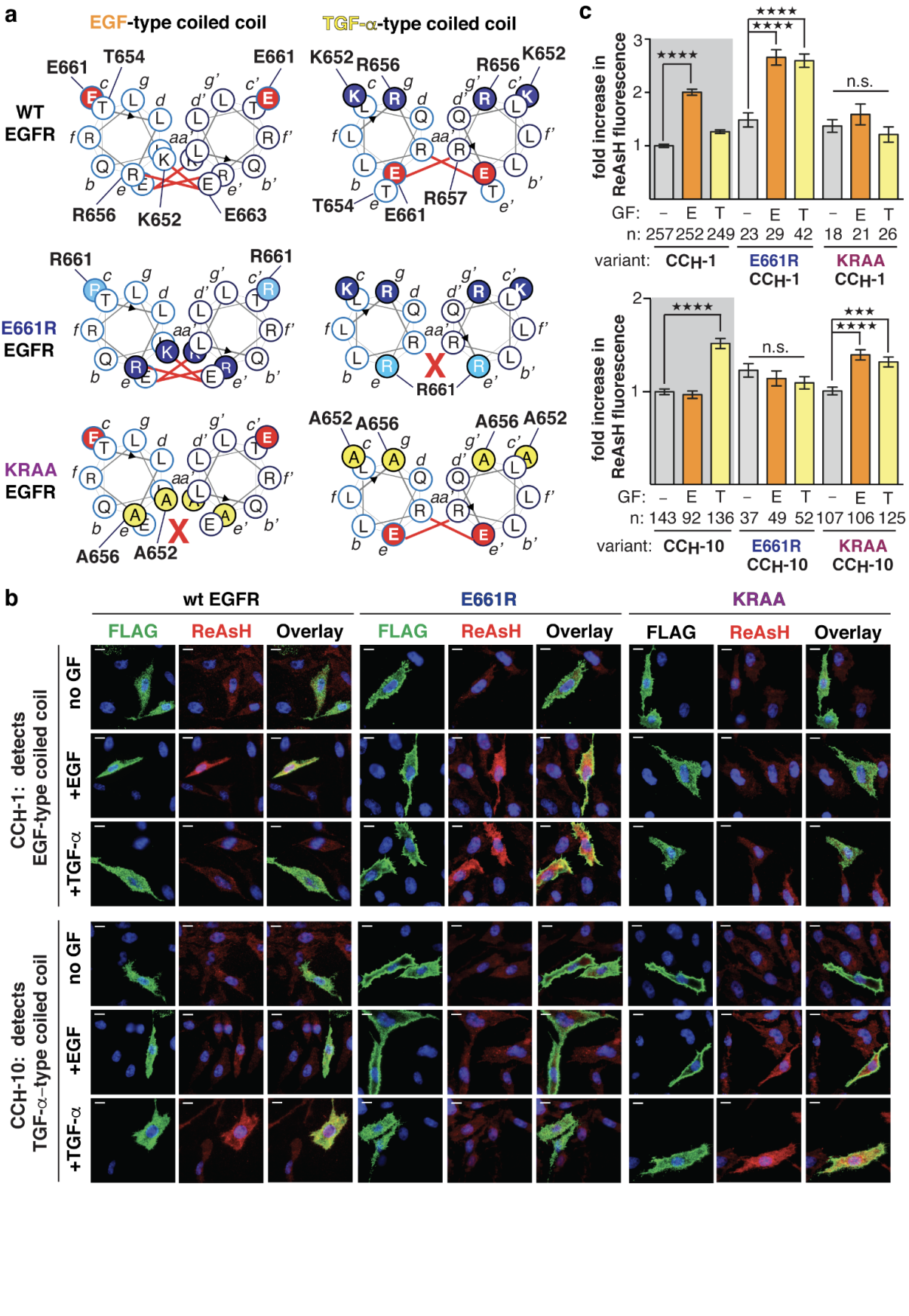
a
EGF-type coiled coil
TGF-α-type coiled coil
WT EGFR
E661R EGFR
KRAA EGFR
E661
T654
E661
K652
R656
R656
K652
R656
K652
E663
T654
R657
E661
R661
R661
R661
A656
A652
A652
A656
A656
A652
c
b
fold increase in ReAsH fluorescence
GF: – E T – E T – E T
n: 257 252 249 23 29 42 18 21 26
variant: CCH-1 E661R CCH-1 KRAA CCH-1
n: 143 92 136 37 49 52 107 106 125
variant: CCH-10 E661R CCH-10 KRAA CCH-10
n.s.
b
wt EGFR
E661R
KRAA
FLAG
ReAsH
Overlay
no GF
+EGF
+TGF-α
CCH-1: detects EGF-type coiled coil
CCH-10: detects TGF-α–type coiled coil

Figure. 3.1. Design of E661R and KRAA EGFR decoupling mutants. (A) Helical wheel diagrams illustrating relative positions of residues within the N-terminal region of the EGFR JM segment of WT, E661R, and KRAA EGFR when assembled into an EGF-type (left) or TGF-α-type (right) coiled-coil. Bold red lines identify potential salt bridge interactions referred to in the text. **(B)** Representative TIRF-M images of CHO-K1 cells illustrating ReAsH labeling (red fluorescence) and expression (green fluorescence) of FLAG-tagged CC_H-1 and CC_H-10 variants of WT, E661R, or KRAA EGFR with or without EGF or TGF-α stimulation (16.7 nM). Scale bars = 10 μm. **(C)** Bar plots illustrating the fold increase in expression-corrected ReAsH fluorescence over background. n = # of cells. Error bars = s.e.m. ****$p<0.0001$, ***$p<0.001$, **$p<0.01$, *$p<0.1$ from one-way ANOVA with Bonferroni post-analysis accounting for multiple comparisons. n.s., not significant.

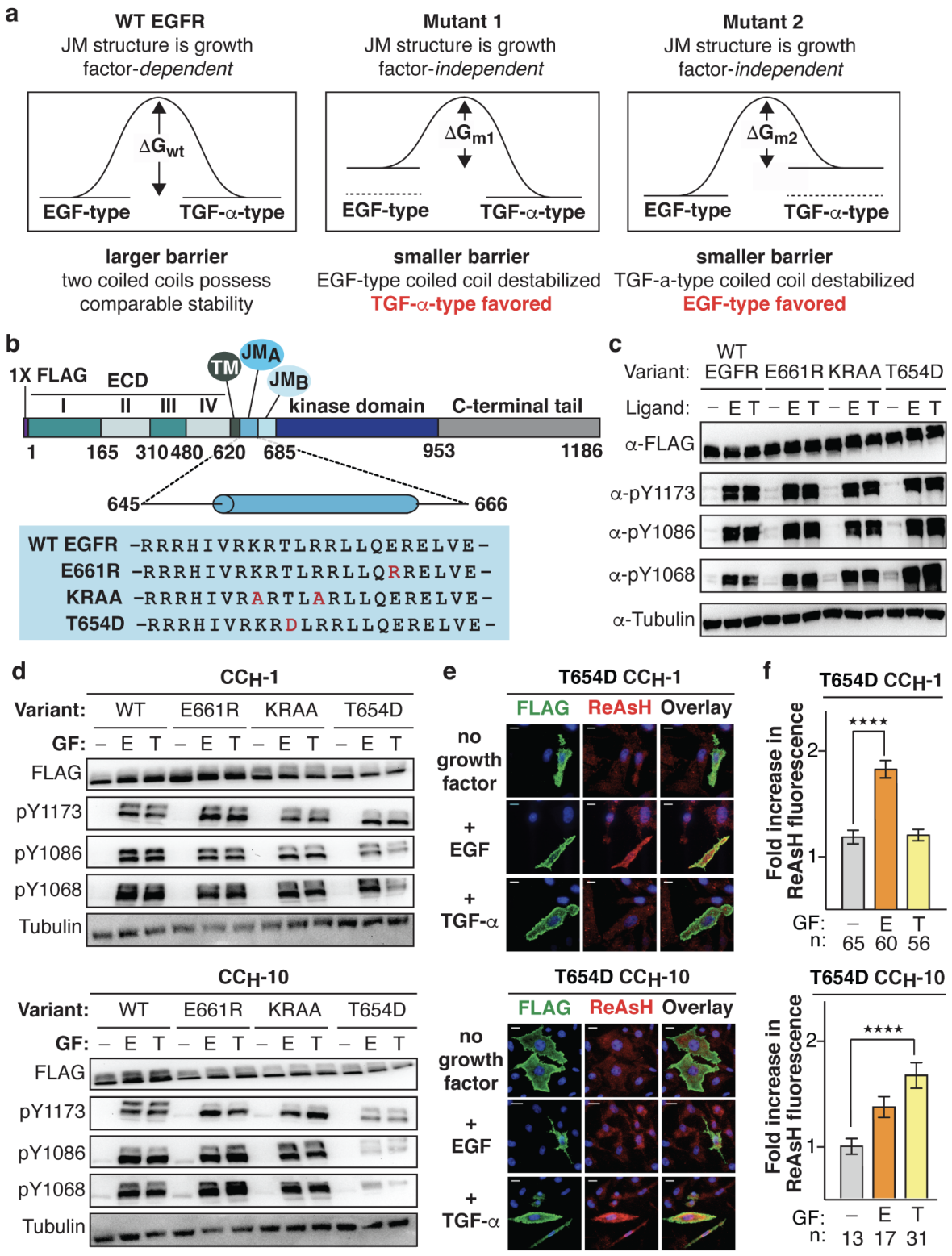
a
WT EGFR
JM structure is growth factor-dependent
Mutant 1
JM structure is growth factor-independent
Mutant 2
JM structure is growth factor-independent
ΔGwt
ΔGm1
ΔGm2
EGF-type
TGF-α-type
larger barrier
two coiled coils possess comparable stability
smaller barrier
EGF-type coiled coil destabilized
TGF-α-type favored
smaller barrier
TGF-a-type coiled coil destabilized
EGF-type favored
b
1X FLAG
ECD
I
II
III
IV
TM
JMA
JMB
kinase domain
C-terminal tail
1
165
310
480
620
645
666
685
953
1186
WT EGFR -RRRHIVRKRTLRRLLQERELVE-
E661R -RRRHIVRKRTLRRLLQRRELVE-
KRAA -RRRHIVRARTLARLLQERELVE-
T654D -RRRHIVRKRDLRRLLQERELVE-
c
WT
Variant: EGFR E661R KRAA T654D
Ligand: – E T – E T – E T – E T
α-FLAG
α-pY1173
α-pY1086
α-pY1068
α-Tubulin
d
CCH-1
Variant: WT E661R KRAA T654D
GF: – E T – E T – E T – E T
FLAG
pY1173
pY1086
pY1068
Tubulin
CCH-10
Variant: WT E661R KRAA T654D
GF: – E T – E T – E T – E T
FLAG
pY1173
pY1086
pY1068
Tubulin
e
T654D CCH-1
FLAG ReAsH Overlay
no growth factor
+ EGF
+ TGF-α
T654D CCH-10
FLAG ReAsH Overlay
no growth factor
+ EGF
+ TGF-α
f
T654D CCH-1
Fold increase in ReAsH fluorescence
****
GF: – E T
n: 65 60 56
T654D CCH-10
Fold increase in ReAsH fluorescence
****
GF: – E T
n: 13 17 31

Figure 3.2.: **Design of EGFR decoupling mutants (KRAA, E661R) and controls (T654D) and TIRF microscopy images and western blots related to Bipartite tetracysteine display experiments. (A)** Influencing coiled coil preferences by design. In WT EGFR, both coiled coil conformations are energetically accessible, and the identity of the bound growth factor influences which conformation is adopted. In Mutant 1, the EGF-type coiled coil is destabilized and the TGF-α-type structure is favored; in Mutant 2, the TGF-α-type coiled coil is destabilized and the EGF-type structure is favored. **(B)** Domain diagram of FLAG-tagged EGFR illustrating sequences of WT EGFR as well as E661R and KRAA decoupling mutants that favor the EGF-type or TGF-α-type coiled coil, respectively; T654D EGFR also contains a mutation within the JM but at a location predicted to not affect relative coiled coil stability (light blue box). E661R, KRAA, and T654D EGFR respond like WT EGFR to growth factor stimulation. Representative western blots illustrating expression and extent of Y1173, Y1086, and Y1068 phosphorylation of **(C)** FLAG-tagged WT, E661R, KRAA, and T654D EGFR and **(D)** FLAG-tagged CC_H-1 and CC_H-10 variants of WT, E661R, KRAA, and T654D EGFR in CHO-K1 cells stimulated continuously without/with EGF and TGF-α (16.7 nM) for 5 minutes 37oC. Alpha-tubulin is used as loading control. **(E)** Representative TIRF-M images of CHO-K1 cells illustrating ReAsH labeling (red fluorescence) and expression (green fluorescence) of FLAG-tagged CC_H-1 and CC_H-10 variants of T654D without/ with EGF/ TGF-α stimulation (16.7 nM). Scale bars = 10 μm. **(F)** Bar plots illustrating the quantification of TIRF-M results from 'n' cells expressing FLAG-tagged T654D EGFR as fold increase in expression-corrected ReAsH fluorescence over background. Error bars = s.e.m. ****$p<0.0001$, n.s. $p>0.05$ from one-way ANOVA with Dunnett's post-analysis accounting for comparisons within individual mutants to no growth factor treated control. n.s., not significant. Scale bars = 10 μm.

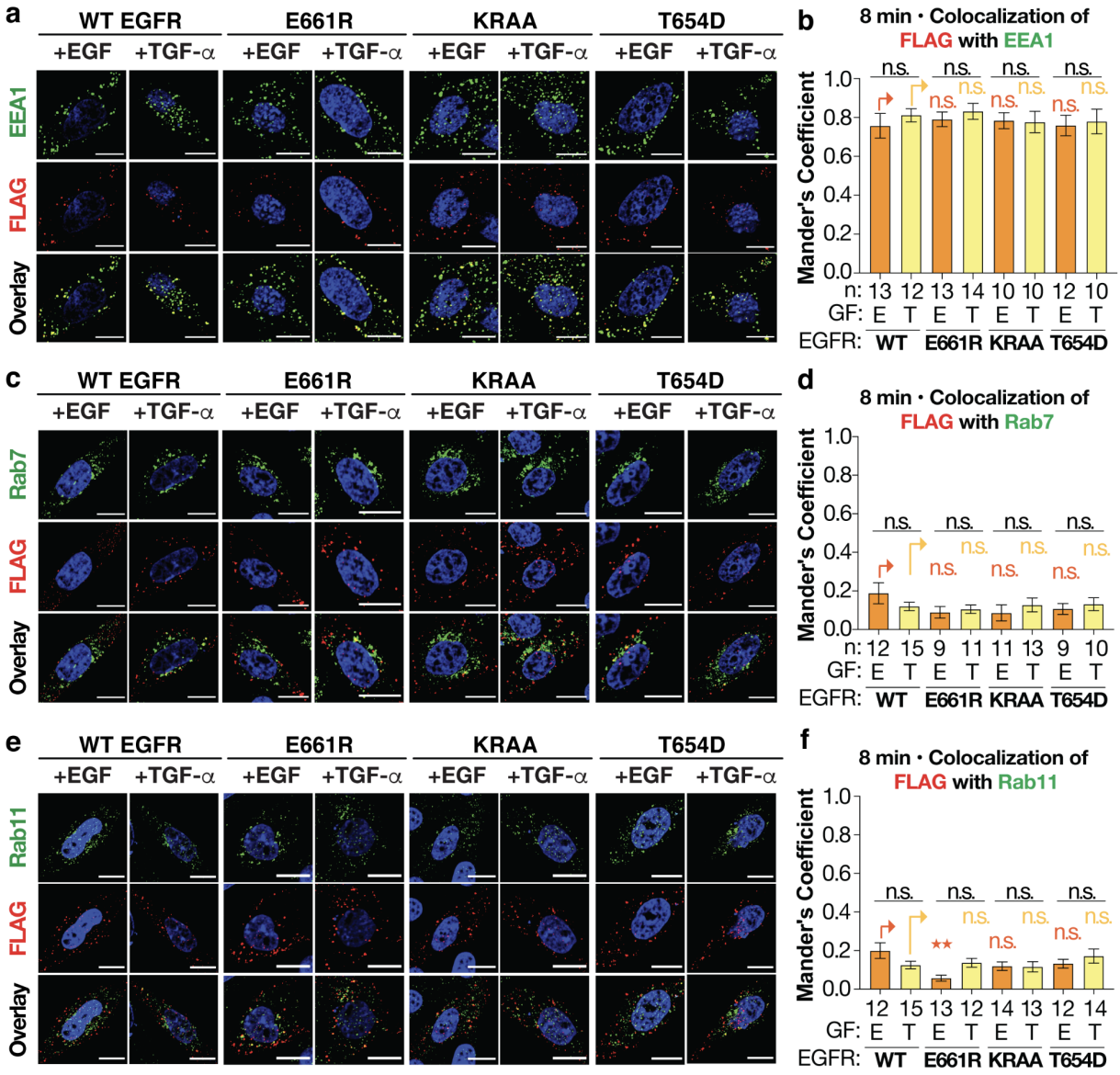
a
WT EGFR
E661R
KRAA
T654D
+EGF
+TGF-α
EEA1
FLAG
Overlay
b
8 min · Colocalization of
FLAG with EEA1
Mander's Coefficient
n.s.
n: 13 12 13 14 10 10 12 10
GF: E T E T E T E T
EGFR: WT E661R KRAA T654D
c
Rab7
d
8 min · Colocalization of
FLAG with Rab7
n: 12 15 9 11 11 13 9 10
e
Rab11
f
8 min · Colocalization of
FLAG with Rab11
12 15 13 12 14 13 12 14

Figure 3.3. FLAG-tagged WT, E661R, and KRAA EGFR colocalize with EEA1 and not with Rab7 or Rab11 respectively, 8 minutes after stimulation with EGF or TGF-α. (A, C, E) Representative confocal microscopy images of CHO-K1 cells expressing FLAG-tagged WT, E661R, KRAA and T654D EGFR (false-colored red) 8 minutes after stimulation with EGF or TGF-α (16.7 nM). **(A)** Early endosomes (false-colored green) are identified using anti-EEA1 antibody. **(C)** Degradative endosomes (false-colored green) are identified using an anti-Rab7 antibody. **(E)** Recycling endosomes (false-colored green) are identified using an anti-Rab11 antibody. **(A, C, E)** Scale bars = 10 μm. Bar plots illustrating the quantified Mander's co-localization coefficient (MCC) values of FLAG-tagged WT, E661R, KRAA and T654D EGFR with **(B)** EEA1 **(D)** Rab7 **(F)** Rab11 8 minutes after stimulation with EGF/ TGF-α (16.7 nM) for 'n' cells. Error bars, s.e.m., n.s. not-significant from one-way ANOVA with Tukey's multiple comparison test.

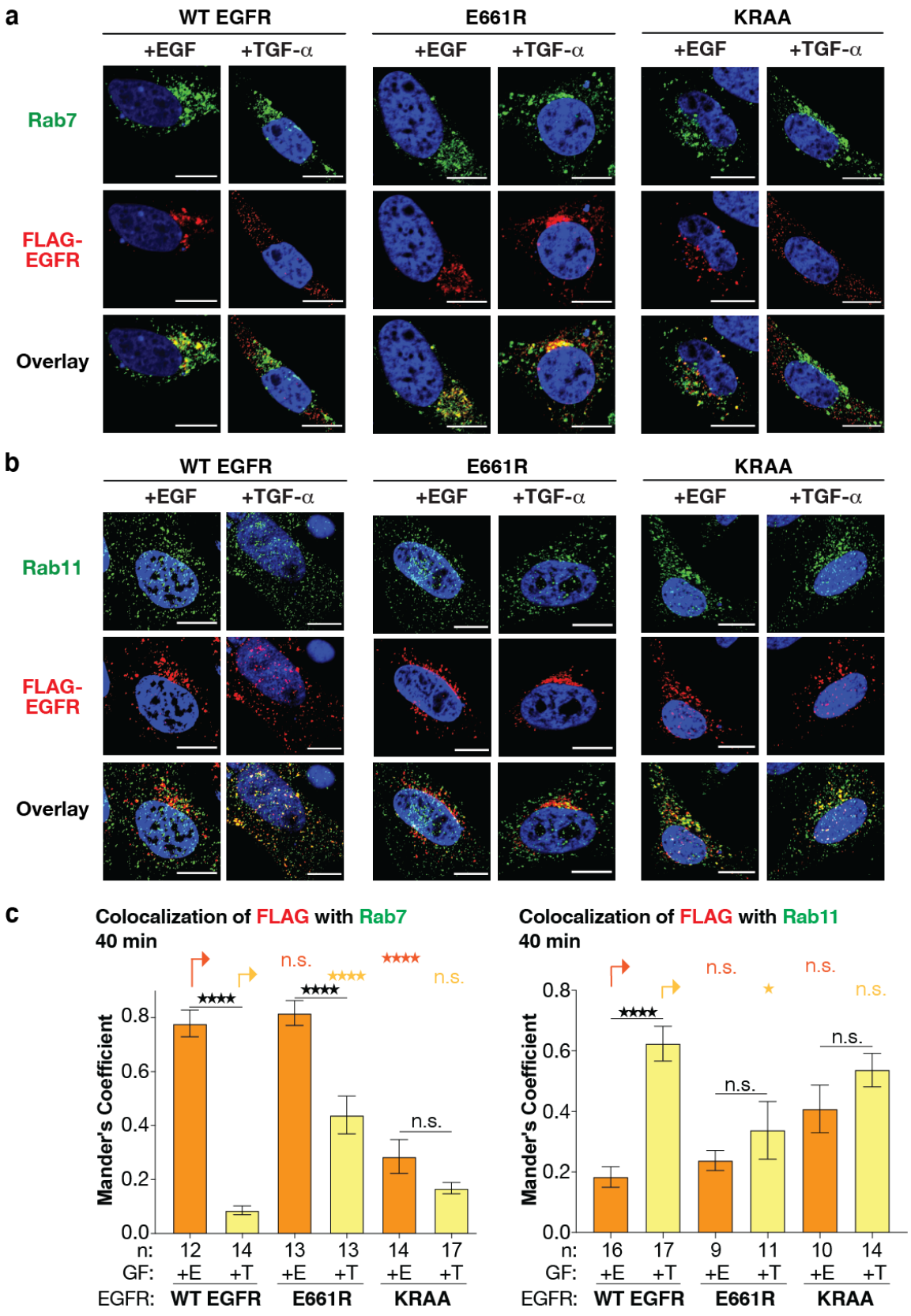
a
WT EGFR
E661R
KRAA
+EGF
+TGF-α
Rab7
FLAG-EGFR
Overlay
b
WT EGFR
E661R
KRAA
+EGF
+TGF-α
Rab11
FLAG-EGFR
Overlay
c
Colocalization of FLAG with Rab7
40 min
Mander's Coefficient
0.0
0.2
0.4
0.6
0.8
n.s.
****
n: 12 14 13 13 14 17
GF: +E +T +E +T +E +T
EGFR: WT EGFR E661R KRAA
Colocalization of FLAG with Rab11
40 min
Mander's Coefficient
0.0
0.2
0.4
0.6
0.8
n.s.
*
****
n: 16 17 9 11 10 14
GF: +E +T +E +T +E +T
EGFR: WT EGFR E661R KRAA

Figure 3.4. The path of EGFR trafficking in CHO-K1 cells is controlled by JM coiled coil identity. Confocal microscopy of CHO-K1 cells expressing FLAG-tagged WT, E661R, or KRAA EGFR (false colored red), immuno-labeled with **(A)** Rab7 (false colored green) as a marker for degradative endosomes or **(B)** Rab11 (false colored green) as a marker for recycling endosomes, 40 minutes after stimulation with EGF (E) or TGF-α (T). Scale bars = 10 μm. **(C)** Bar plots illustrating the Manders colocalization coefficient (MCC) of FLAG-tagged WT, E661R and KRAA EGFR with either Rab7 or Rab11 40 minutes after stimulation with EGF/TGF-α. n = # of cells. Error bars = s.e.m. ****$p<0.0001$, ***$p<0.001$, **$p<0.01$, *$p<0.1$, n.s. not significant, from one-way ANOVA with Tukey's multiple comparison test.

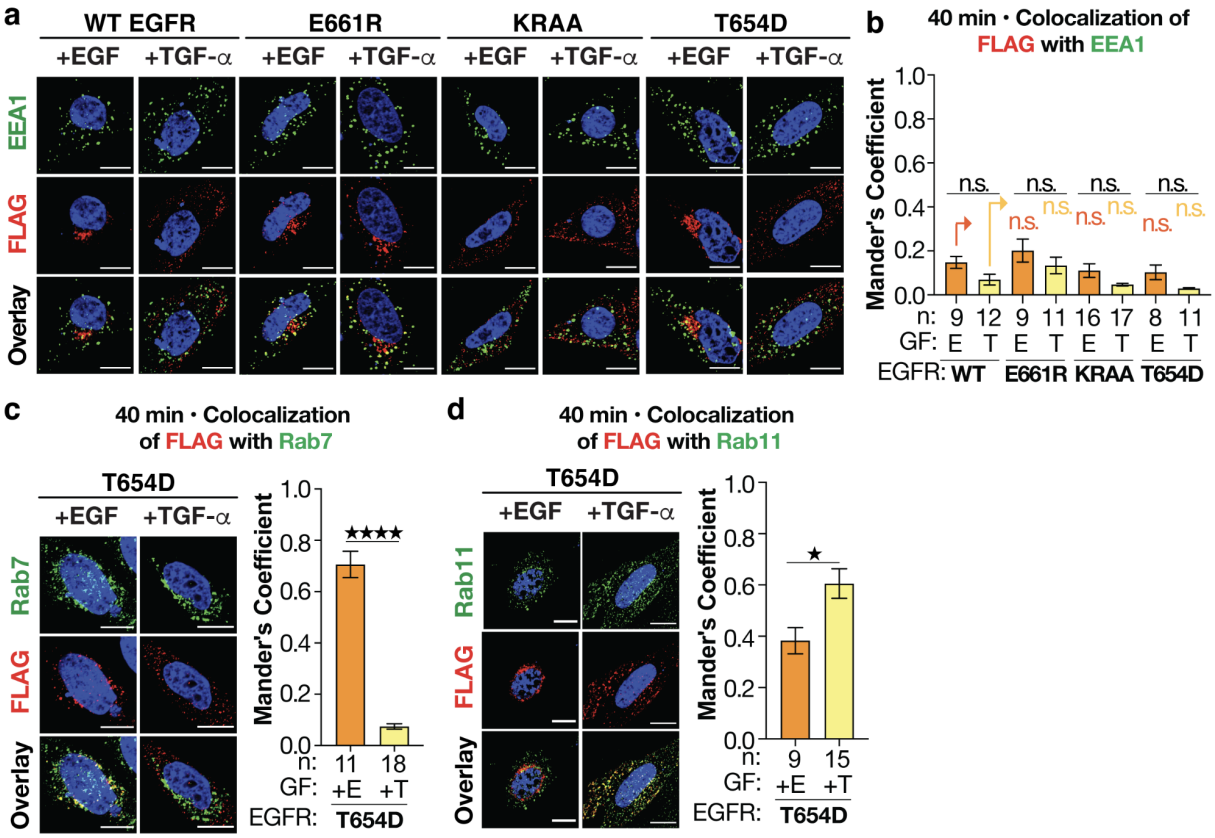
a
WT EGFR
E661R
KRAA
T654D
+EGF
+TGF-α
EEA1
FLAG
Overlay
b
40 min · Colocalization of FLAG with EEA1
Mander's Coefficient
n.s.
n: 9 12 9 11 16 17 8 11
GF: E T E T E T E T
EGFR: WT E661R KRAA T654D
c
40 min · Colocalization of FLAG with Rab7
T654D
Rab7
****
n: 11 18
GF: +E +T
EGFR: T654D
d
40 min · Colocalization of FLAG with Rab11
Rab11
*
n: 9 15
GF: +E +T
EGFR: T654D

Figure 3.5. Co-localization of FLAG-tagged WT, E661R, KRAA and T654D EGFR with EEA1, 40 minutes after stimulation with EGF/TGF-α and co-localization of FLAG-tagged T654D EGFR with Rab7, Rab11, 40 minutes after stimulation with EGF/TGF-α. (A) Representative confocal microscopy images of CHO-K1 cells expressing FLAG-tagged WT, E661R, KRAA and T654D EGFR (false colored red) 40 minutes after stimulation with EGF or TGF-α (16.7 nM). Early endosomes (false colored green) are identified using an anti-EEA1 antibody. Scale bars = 10 μm. **(B)** Bar plots illustrating the quantified MCC values of FLAG-tagged WT, E661R, KRAA and T654D EGFR with EEA1 40 minutes after stimulation with EGF or TGF-α (16.7 nM) for 'n' cells. Error bars, s.e.m., n.s. not significant from one-way ANOVA with Tukey's multiple comparison test. **(C, D)** Confocal microscopy of CHO-K1 cells expressing FLAG-tagged T654D EGFR (false-colored red) 40 minutes after stimulation with EGF/ TGF-α. **(C)** Degradative endosomes are identified using an anti-Rab7 antibody (false-colored green). **(D)** Recycling endosomes are identified using an anti-Rab11 antibody (false-colored green). Scale bars = 10 μm**.** Bar plots illustrating the quantified MCC values of FLAG-tagged T654D (green) with either **(C)** Rab7 or **(D)** Rab11 40 minutes after stimulation with EGF or TGF-α (16.7 nM) for 'n' cells. Error bars, s.e.m. ****$p<0.0001$, *$p<0.1$, from t-test.

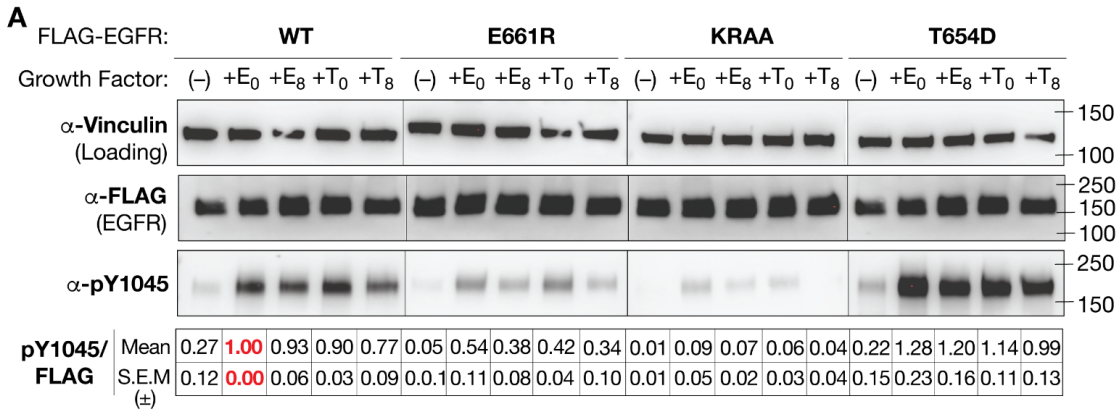

pY1045/FLAG		WT (–)	WT +E0	WT +E8	WT +T0	WT +T8	E661R (–)	E661R +E0	E661R +E8	E661R +T0	E661R +T8	KRAA (–)	KRAA +E0	KRAA +E8	KRAA +T0	KRAA +T8	T654D (–)	T654D +E0	T654D +E8	T654D +T0	T654D +T8
	Mean	0.27	1.00	0.93	0.90	0.77	0.05	0.54	0.38	0.42	0.34	0.01	0.09	0.07	0.06	0.04	0.22	1.28	1.20	1.14	0.99
	S.E.M (±)	0.12	0.00	0.06	0.03	0.09	0.01	0.11	0.08	0.04	0.10	0.01	0.05	0.02	0.03	0.04	0.15	0.23	0.16	0.11	0.13

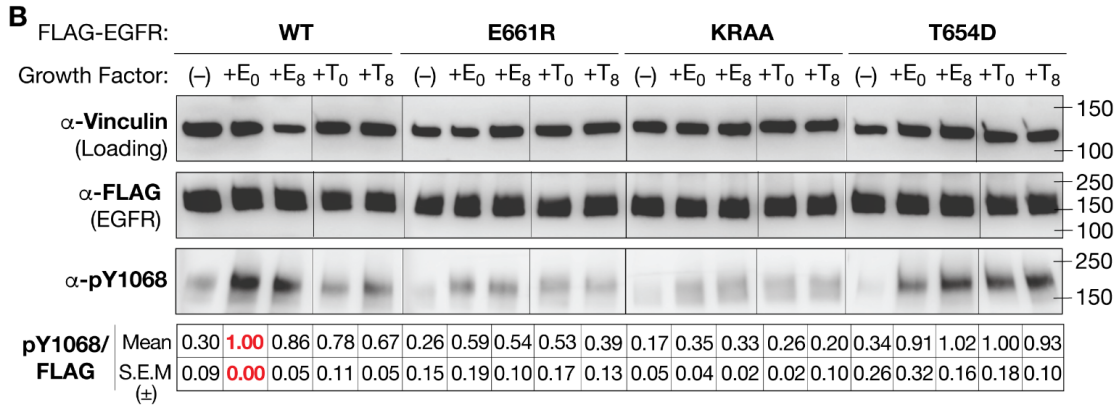

pY1068/FLAG		WT (–)	WT +E0	WT +E8	WT +T0	WT +T8	E661R (–)	E661R +E0	E661R +E8	E661R +T0	E661R +T8	KRAA (–)	KRAA +E0	KRAA +E8	KRAA +T0	KRAA +T8	T654D (–)	T654D +E0	T654D +E8	T654D +T0	T654D +T8
	Mean	0.30	1.00	0.86	0.78	0.67	0.26	0.59	0.54	0.53	0.39	0.17	0.35	0.33	0.26	0.20	0.34	0.91	1.02	1.00	0.93
	S.E.M (±)	0.09	0.00	0.05	0.11	0.05	0.15	0.19	0.10	0.17	0.13	0.05	0.04	0.02	0.02	0.10	0.26	0.32	0.16	0.18	0.10

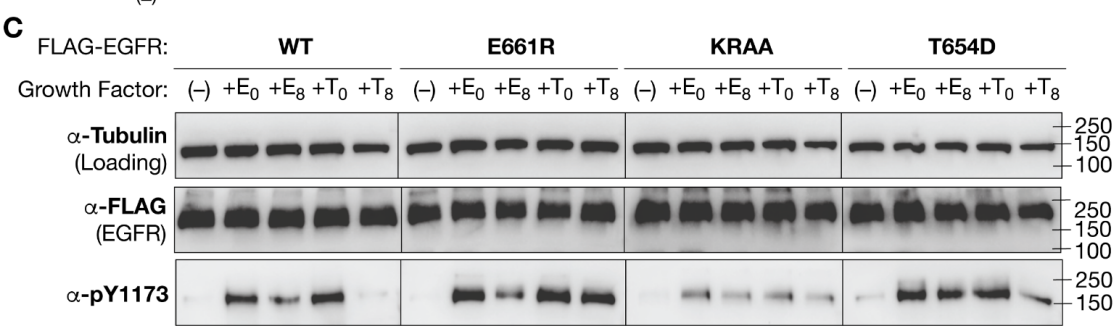

pY1173/FLAG		WT (–)	WT +E0	WT +E8	WT +T0	WT +T8	E661R (–)	E661R +E0	E661R +E8	E661R +T0	E661R +T8	KRAA (–)	KRAA +E0	KRAA +E8	KRAA +T0	KRAA +T8	T654D (–)	T654D +E0	T654D +E8	T654D +T0	T654D +T8
	Mean	0.22	1.00	0.84	1.01	0.70	0.09	0.83	0.68	0.87	0.66	0.06	0.40	0.34	0.34	0.27	0.14	1.26	1.30	1.16	0.96
	S.E.M (±)	0.13	0.00	0.11	0.06	0.27	0.04	0.31	0.24	0.37	0.31	0.01	0.13	0.14	0.13	0.14	0.04	0.18	0.19	0.05	0.18

Figure 3.6. Time dependent decay in phosphorylation of FLAG-tagged WT, E661R, KRAA and T654D EGFR at Y1045, Y1068, Y1173. Immunoblots illustrating the time-dependent change in **(A)** pY1045; **(B)** pY1068; and **(C)** pY1173 0-8 minutes after stimulation with EGF or TGF-α (16.7 nM). FLAG blot indicates levels of total EGFR. Vinculin is used as a loading control. Blots represent data pooled from at least 3 biological replicates and densitometric quantification of signal pYEGFR/ FLAG (Mean and S.E.M.) is included below the immunoblots.

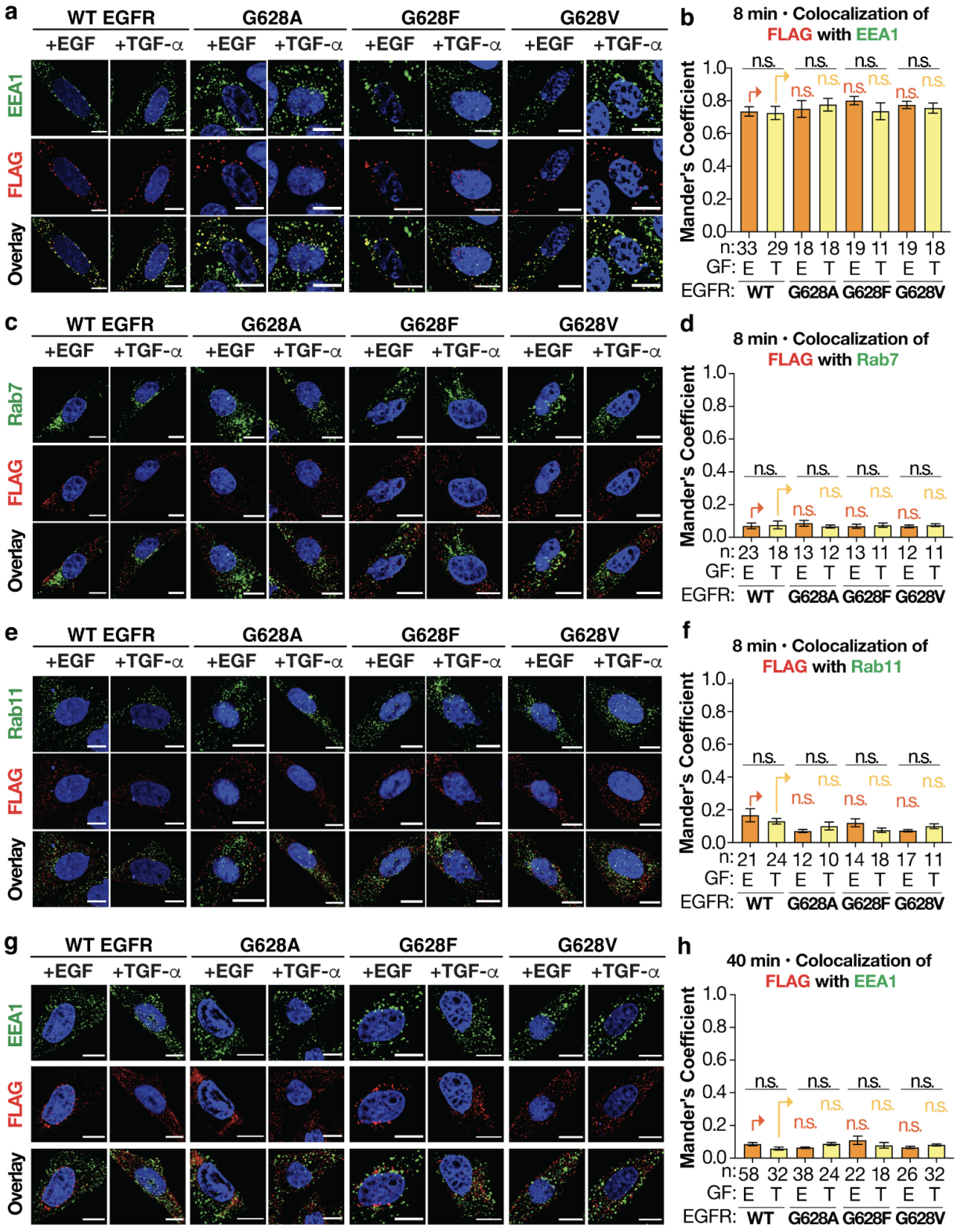
a
WT EGFR
G628A
G628F
G628V
+EGF
+TGF-α
EEA1
FLAG
Overlay
b
8 min · Colocalization of
FLAG with EEA1
Mander's Coefficient
n.s.
n: 33 29 18 18 19 11 19 18
GF: E T E T E T E T
EGFR: WT G628A G628F G628V
c
Rab7
d
8 min · Colocalization of
FLAG with Rab7
n: 23 18 13 12 13 11 12 11
e
Rab11
f
8 min · Colocalization of
FLAG with Rab11
n: 21 24 12 10 14 18 17 11
g
h
40 min · Colocalization of
FLAG with EEA1
n: 58 32 38 24 22 18 26 32

Figure 3.7. Co-localization of FLAG-tagged G628A, G628F, and G628V EGFR with EEA1 (8 and 40 min) and Rab7 or Rab11 (8 min) after stimulation with EGF or TGF-α. Representative confocal microscopy images of CHO-K1 cells expressing FLAG-tagged WT, G628A, G628F, and G628V EGFR (false colored red) stimulated for **(A, C, E)** 8 minutes; and **(G)** 40 minutes with EGF/ TGF-α (16.7 nM). **(A, G)** Early endosomes (false-colored green) are identified using an anti-EEA1 antibody. **(C)** Degradative endosomes (false-colored green) are identified using an anti-Rab7 antibody. **(E)** Recycling endosomes (false-colored green) are identified using an anti-Rab11 antibody. **(A, C, E, G)** Scale bars = 10 μm. Bar plots illustrating the quantified MCC values of FLAG-tagged WT, G628A, G628F, G628V EGFR with **(B)** EEA1 or **(D)** Rab7 or **(F)** Rab11, 8 min or **(H)** EEA1, 40 min; after stimulation with EGF/ TGF-α (16.7 nM) for 'n' cells. Error bars, s.e.m., n.s. not significant from one-way ANOVA with Tukey's multiple comparison test.

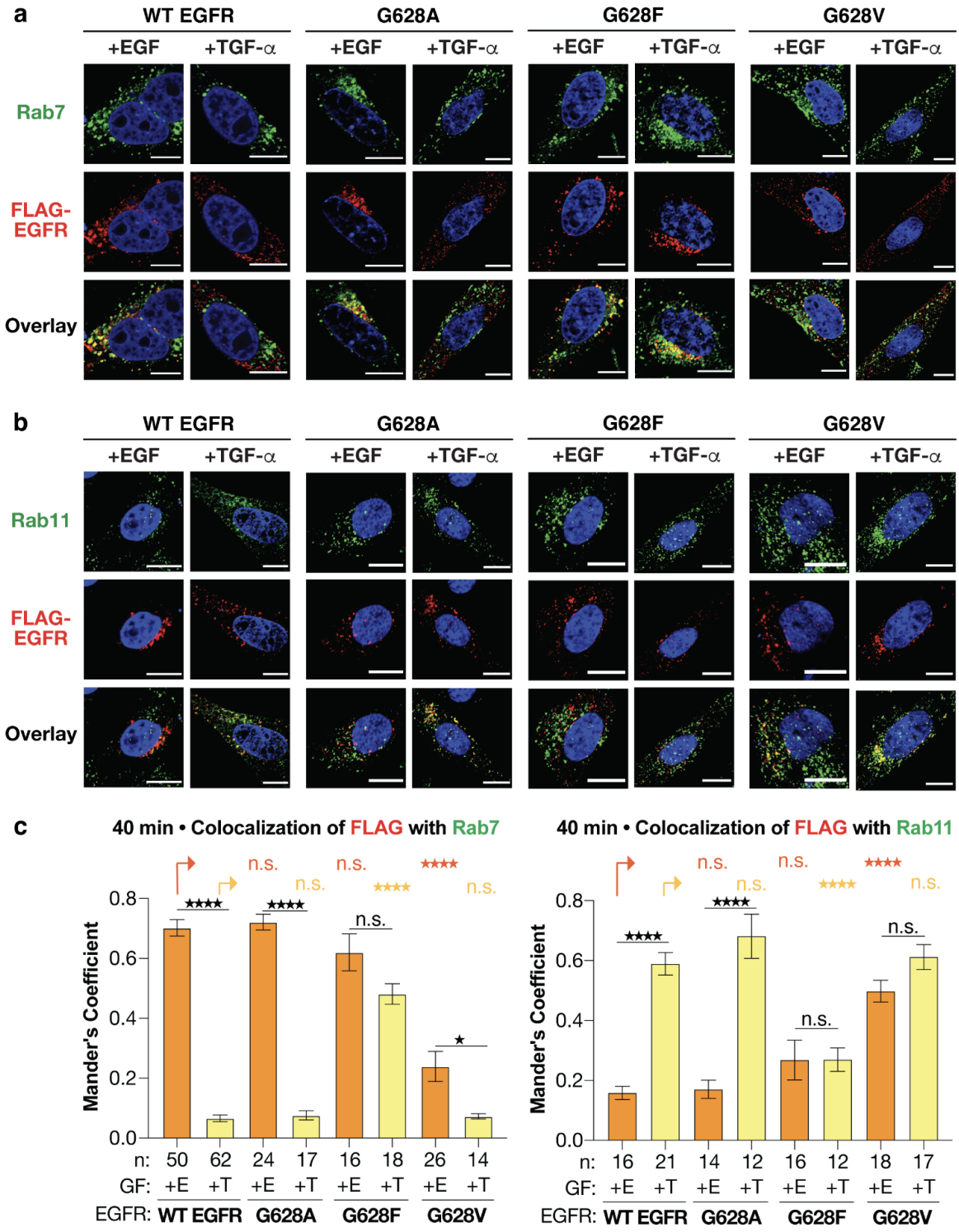
a
WT EGFR
G628A
G628F
G628V
+EGF
+TGF-α
Rab7
FLAG-EGFR
Overlay
b
Rab11
c
40 min • Colocalization of FLAG with Rab7
40 min • Colocalization of FLAG with Rab11
Mander's Coefficient
n.s.
n: 50 62 24 17 16 18 26 14
GF: +E +T +E +T +E +T +E +T
EGFR: WT EGFR G628A G628F G628V
n: 16 21 14 12 16 12 18 17

Figure 3.8. Point mutations within the EGFR transmembrane helix allosterically influence the pathway of receptor trafficking. Confocal microscopy of CHO-K1 cells expressing FLAG-tagged G628A, G628F and G628V EGFR (false colored red) and immuno-labeled with **(A)** Rab7 (false colored green) as a marker for degradative endosomes or **(B)** Rab11 (false colored green) as a marker for recycling endosomes, 40 minutes after stimulation with EGF (E) or TGF-α (T). Scale bars = 10 μm. **(C)** Bar Plots illustrating colocalization of FLAG-tagged G628A, G628F and G628V EGFR with either Rab7 or Rab11-GFP 40 minutes after stimulation with EGF/TGF-α (16.7 nM). n = # of cells. Error bars = s.e.m.. ****$p<0.0001$, ***$p<0.001$, **$p<0.01$, *$p<0.1$, n.s. not significant from one-way ANOVA with Tukey's multiple comparison test.

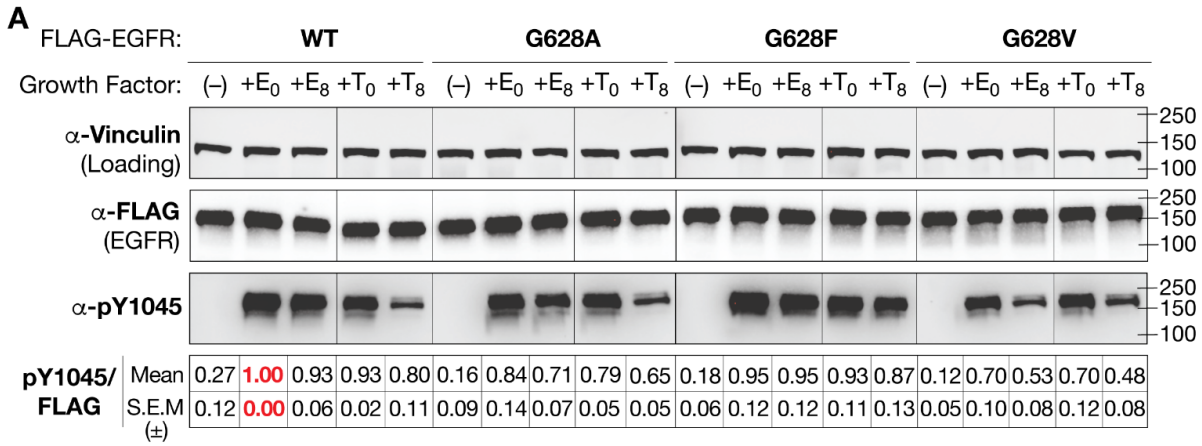

pY1045/FLAG		WT					G628A					G628F					G628V				
		(–)	+E0	+E8	+T0	+T8	(–)	+E0	+E8	+T0	+T8	(–)	+E0	+E8	+T0	+T8	(–)	+E0	+E8	+T0	+T8
	Mean	0.27	1.00	0.93	0.93	0.80	0.16	0.84	0.71	0.79	0.65	0.18	0.95	0.95	0.93	0.87	0.12	0.70	0.53	0.70	0.48
	S.E.M (±)	0.12	0.00	0.06	0.02	0.11	0.09	0.14	0.07	0.05	0.05	0.06	0.12	0.12	0.11	0.13	0.05	0.10	0.08	0.12	0.08

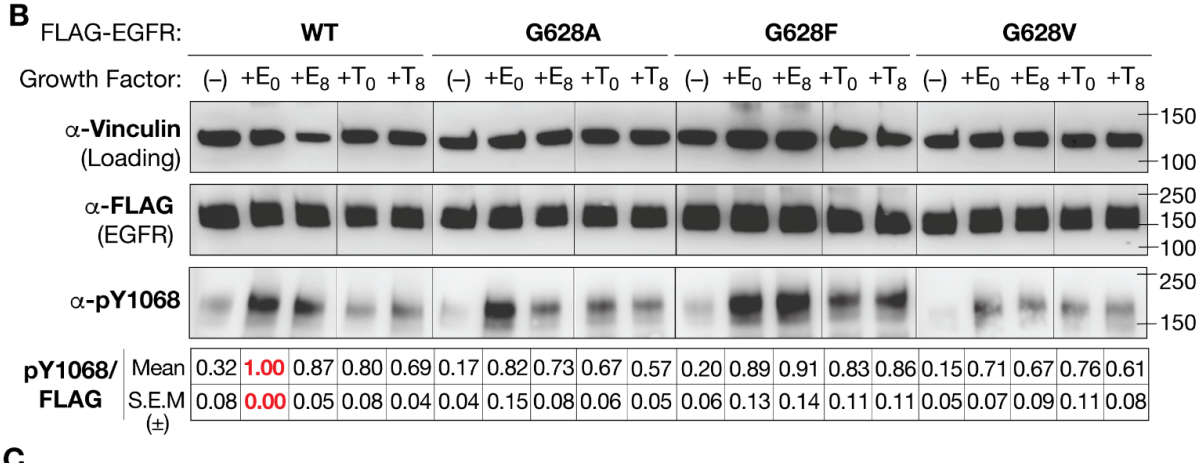

pY1068/FLAG		WT					G628A					G628F					G628V				
		(–)	+E0	+E8	+T0	+T8	(–)	+E0	+E8	+T0	+T8	(–)	+E0	+E8	+T0	+T8	(–)	+E0	+E8	+T0	+T8
	Mean	0.32	1.00	0.87	0.80	0.69	0.17	0.82	0.73	0.67	0.57	0.20	0.89	0.91	0.83	0.86	0.15	0.71	0.67	0.76	0.61
	S.E.M (±)	0.08	0.00	0.05	0.08	0.04	0.04	0.15	0.08	0.06	0.05	0.06	0.13	0.14	0.11	0.11	0.05	0.07	0.09	0.11	0.08

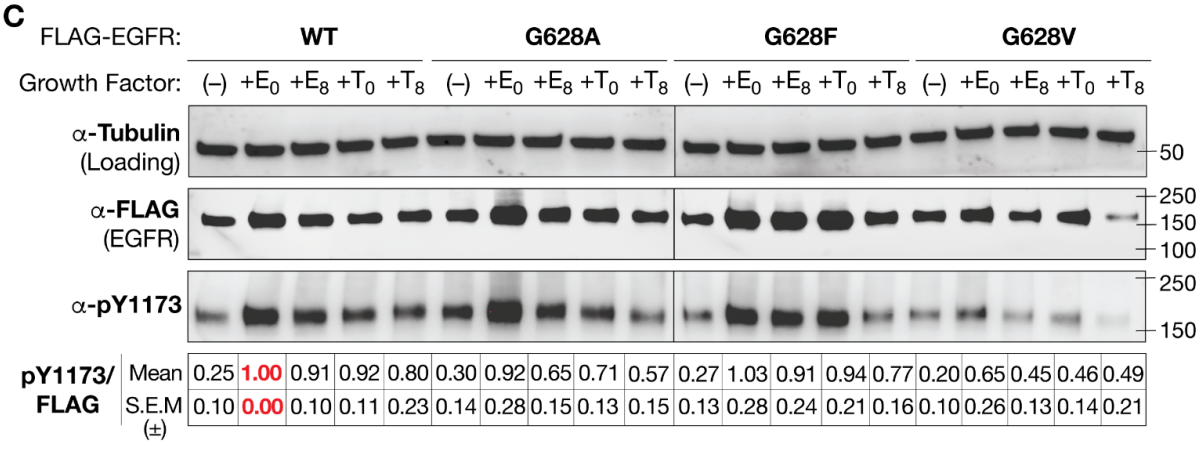

pY1173/FLAG		WT					G628A					G628F					G628V				
		(–)	+E0	+E8	+T0	+T8	(–)	+E0	+E8	+T0	+T8	(–)	+E0	+E8	+T0	+T8	(–)	+E0	+E8	+T0	+T8
	Mean	0.25	1.00	0.91	0.92	0.80	0.30	0.92	0.65	0.71	0.57	0.27	1.03	0.91	0.94	0.77	0.20	0.65	0.45	0.46	0.49
	S.E.M (±)	0.10	0.00	0.10	0.11	0.23	0.14	0.28	0.15	0.13	0.15	0.13	0.28	0.24	0.21	0.16	0.10	0.26	0.13	0.14	0.21

Figure 3.9. Time dependent decay in phosphorylation of FLAG-tagged WT, G628A, G628F and G628V EGFR at Y1045, Y1068, Y1173. Immunoblots illustrating the time-dependent change in **(a)** pY1045; **(b)** pY1068; and **(c)** pY1173 for FLAG-tagged WT EGFR, G628A, G628F and G628V 0-8 minutes after stimulation with EGF or TGF-α (16.7 nM). FLAG blot indicates levels of total EGFR. Vinculin/ Alpha-Tubulin is used as a loading control. Blots represent data pooled from at least 3 biological replicates and densitometric quantification of pYEGFR/FLAG signal (Mean and S.E.M.) is included below the immunoblots.

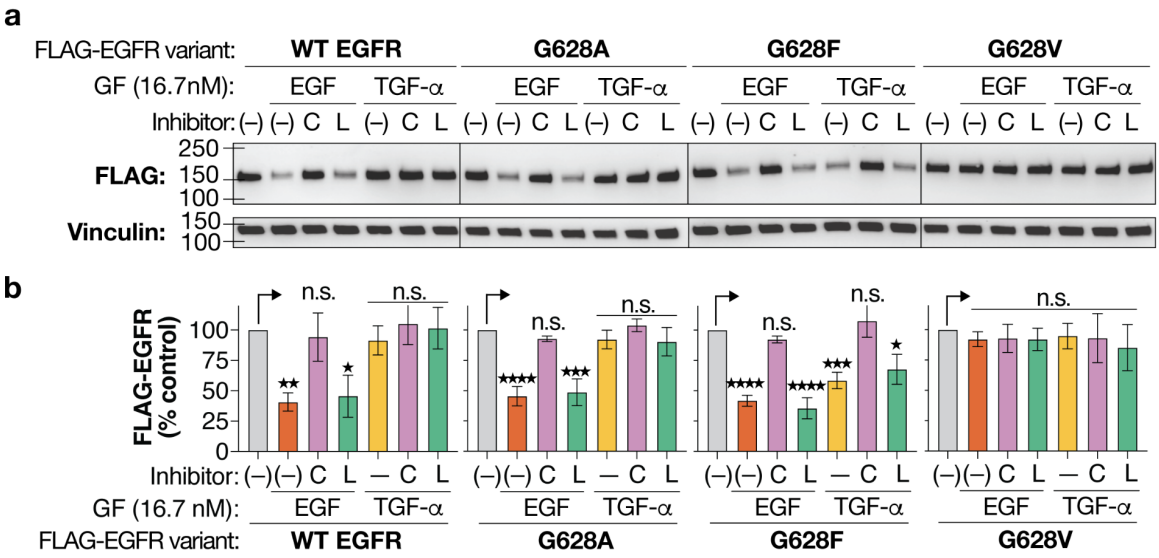

Figure 3.10.. Coiled coil control of EGFR degradation. (A) Immunoblots illustrating the level of FLAG-tagged WT, G628A, G628F, and G628V EGFR detected in CHO-K1 cells 90 minutes after stimulation with or without EGF/TGF-α (16.7 nM) and without/with pre-incubation with the lysosomal inhibitor chloroquine, C (100 μM) [158] or the proteasomal inhibitor lactacystin, L (10 μM)[159] for 1 hour at 37 °C. **(B)** Plot illustrating the normalized percent of intact FLAG-tagged WT, G628A, G628F, and G628V EGFR as shown in **3.10.A**. Vinculin is used as loading control. Error bars = s.e.m.. ****p<0.0001, ***p<0.001, **p<0.01, *p<0.1, n.s. not significant from one-way ANOVA with Dunnett's multiple comparison test.

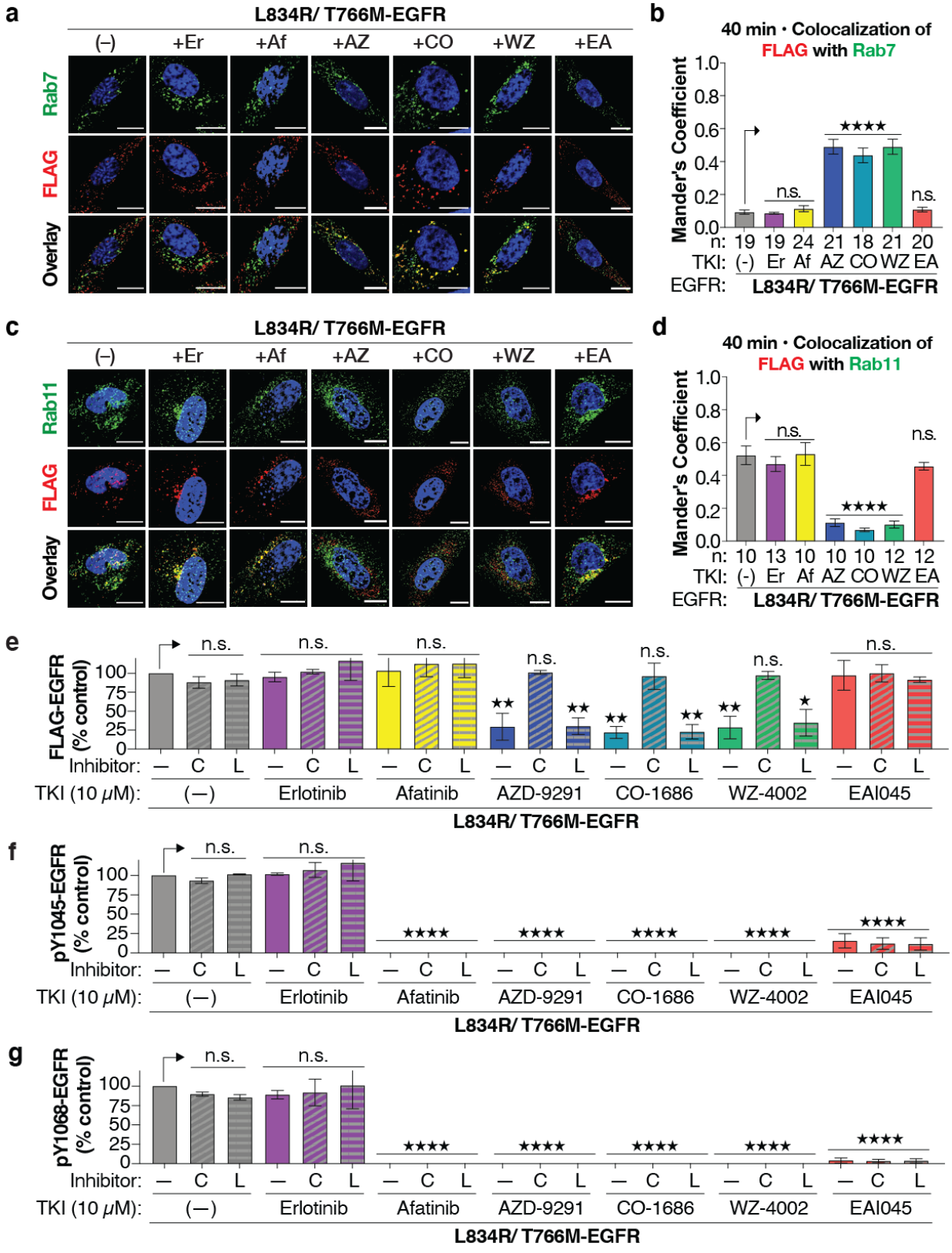
a
L834R/ T766M-EGFR
(–)
+Er
+Af
+AZ
+CO
+WZ
+EA
Rab7
FLAG
Overlay
b
40 min · Colocalization of
FLAG with Rab7
Mander's Coefficient
1.0
0.8
0.6
0.4
0.2
0.0
★★★★
n.s.
n.s.
n: 19 19 24 21 18 21 20
TKI: (-) Er Af AZ CO WZ EA
EGFR: L834R/ T766M-EGFR
c
L834R/ T766M-EGFR
(–)
+Er
+Af
+AZ
+CO
+WZ
+EA
Rab11
FLAG
Overlay
d
40 min · Colocalization of
FLAG with Rab11
Mander's Coefficient
1.0
0.8
0.6
0.4
0.2
0.0
n.s.
★★★★
n.s.
n: 10 13 10 10 10 12 12
TKI: (-) Er Af AZ CO WZ EA
EGFR: L834R/ T766M-EGFR
e
FLAG-EGFR (% control)
100
75
50
25
0
n.s.
★★
★
★★★★
Inhibitor: — C L
TKI (10 μM): (—) Erlotinib Afatinib AZD-9291 CO-1686 WZ-4002 EAI045
L834R/ T766M-EGFR
f
pY1045-EGFR (% control)
100
75
50
25
0
n.s.
★★★★
Inhibitor: — C L
TKI (10 μM): (—) Erlotinib Afatinib AZD-9291 CO-1686 WZ-4002 EAI045
L834R/ T766M-EGFR
g
pY1068-EGFR (% control)
100
75
50
25
0
n.s.
★★★★
Inhibitor: — C L
TKI (10 μM): (—) Erlotinib Afatinib AZD-9291 CO-1686 WZ-4002 EAI045
L834R/ T766M-EGFR

Figure 3.11. Clinically relevant, third-generation tyrosine kinase inhibitors influence L834R/T766M EGFR trafficking and induce EGFR degradation. Confocal microscopy of CHO-K1 cells expressing FLAG-tagged L834R/T766M EGFR (false colored red) and and immuno-labeled with **(A)** Rab7 (false colored green) as a marker for degradative endosomes or **(C)** Rab11 (false colored green) as a marker for recycling endosomes, 30 minutes after pre-incubation without/with 10 μM of indicated TKI. Scale bars = 10 μm. Bar plots illustrating the MCC value representing the colocalization of FLAG-tagged L834R/T766M EGFR with **(B)** Rab7 or **(D)** Rab11 without/with the indicated TKI. n = # of cells. Error bars = s.e.m. ****p<0.0001, ***p<0.001, **p<0.01, *p<0.1, n.s. not significant, from one-way ANOVA with Tukey's multiple comparison test. **(E)** Normalized loss of FLAG-tagged L834R/T766M EGFR in CHO-K1 cells 12 hours following pre-incubation without/with 100 μM chloroquine (C) or lactacystin (L) (10 μM) and/or 10 μM Erlotinib (Er), afatinib (Af), AZD9291 (AZ), CO-1686 (CO), WZ-4002 (WZ), or EAI045 (EA). Phosphorylation of L834R/T766M EGFR at **(F)** Y1045; and **(G)** Y1068 in CHO-K1 cell lysates prepared as described in **3.11.E**. In **3.11. E, F, G,** Error bars = s.e.m.. ****p<0.0001, ***p<0.001, **p<0.01, *p<0.1, n.s. not significant from one-way ANOVA with Dunnett's multiple comparison test.

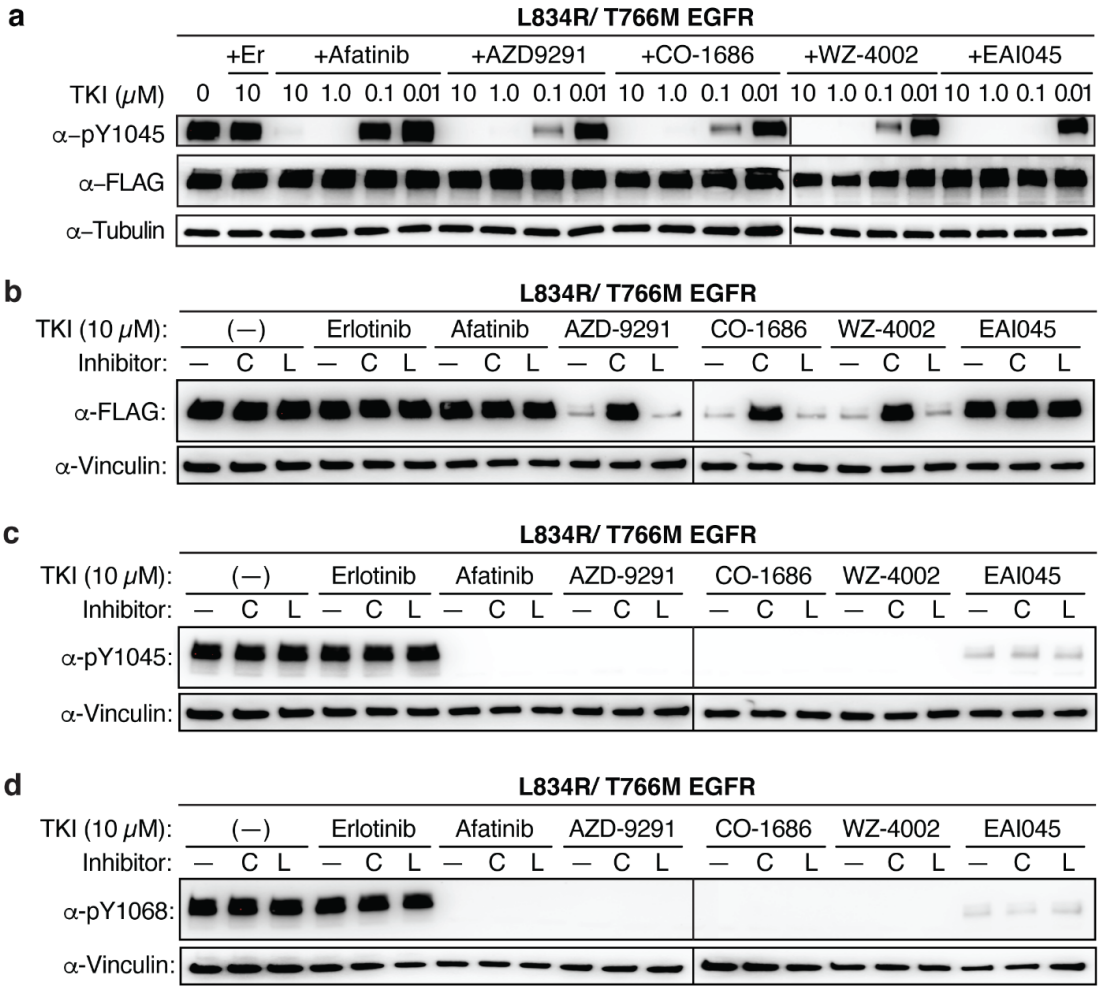
a
L834R/ T766M EGFR
+Er
+Afatinib
+AZD9291
+CO-1686
+WZ-4002
+EAI045
TKI (μM)
0 10 10 1.0 0.1 0.01 10 1.0 0.1 0.01 10 1.0 0.1 0.01 10 1.0 0.1 0.01 10 1.0 0.1 0.01
α–pY1045
α–FLAG
α–Tubulin
b
L834R/ T766M EGFR
TKI (10 μM):
(—)
Erlotinib
Afatinib
AZD-9291
CO-1686
WZ-4002
EAI045
Inhibitor:
— C L — C L — C L — C L — C L — C L — C L
α-FLAG:
α-Vinculin:
c
L834R/ T766M EGFR
TKI (10 μM):
(—)
Erlotinib
Afatinib
AZD-9291
CO-1686
WZ-4002
EAI045
Inhibitor:
— C L — C L — C L — C L — C L — C L — C L
α-pY1045:
α-Vinculin:
d
L834R/ T766M EGFR
TKI (10 μM):
(—)
Erlotinib
Afatinib
AZD-9291
CO-1686
WZ-4002
EAI045
Inhibitor:
— C L — C L — C L — C L — C L — C L — C L
α-pY1068:
α-Vinculin:

Figure 3.12. Immunoblots illustrating the intracellular levels of FLAG-tagged and phosphorylated EGFR detected at various time points post treatment with EGFR TKIs (A) Immunoblots illustrating the cellular expression (FLAG) and dose-dependent phosphorylation of FLAG-tagged L858R/T790M EGFR at Y1045, detected in CHO-K1 cells 30 minutes following pre-incubation without/ with 10, 1.0, 0.1 and 0.01 uM of TKIs erlotinib (+Er), afatinib, AZD9291, CO-1686, WZ-4002 and EAI045. Alpha-tubulin is used as loading control. **(B)** Immunoblots illustrating the loss of FLAG-tagged L834R/T766M EGFR detected in CHO-K1 cells lysed 12 hours following pre-incubation without/with 100 μM chloroquine, C or lactacystin, L (10 μM) for 1 hour followed by pre-incubation without/with 10 μM erlotinib, afatinib, AZD9291, CO-1686, WZ-4002, or EAI045. Immunoblots illustrating the phosphorylation of L834R/T766M EGFR at **(C)** Y1045; and **(D)** Y1068 in CHO-K1 cell lysates prepared as described in **3.12.C**. Vinculin is used as loading control.

Chapter 4. Summary and Analysis of partially completed projects and future directions

This chapter describes preliminary experiments that were performed on two projects that were initiated in the early and later parts of Ph.D. research. The aim of the first project was to investigate the role of receptor multimerization on the JM structure of EGFR. This work was performed with Dr. Amy E. Doerner. The aim of the second ongoing project is to investigate the effect of JM structure on the interactome of WT and oncogenic EGFR using APEX2-based proximity labeling and mass spectrometry. This work has been performed with Sol H.-H. Chang.

Chapter 4. Summary and Analysis of partially completed projects and future directions.

4.1. Investigating the role of receptor multimerization on the JM structure of EGFR. In the canonical view of growth factor induced EGFR activation, the receptor transitions from an equilibrium between an inactive monomeric structure and inactive dimeric structure to active dimeric structure [6,160]. High resolution structures of the ECD [12,13,23,45,122], TM [15,18], JM [15,18] and Kinase [22] domains reveal that in its active dimeric structure, dimerization of the monomeric units is mediated by interactions arising from all four of these domains. In addition to forming active dimeric structures, there is also evidence that EGFR can assemble into catalytically competent higher order oligomers in cells [161–163]. More recently, two independent studies from the Kuriyan [164] and Shaw/ Fernandez [165] research groups have illuminated structural details for the mechanisms by which receptor oligomerization may occur.

In the study from the Kuriyan lab, Huang and colleagues used single molecule imaging combined with photobleaching experiments in Xenopus oocytes to observe clustering of fluorescently labeled particles of EGFR [164]. In their studies they found that following treatment with EGF, fluorescently labeled EGFR particles appear as clusters on the surface of Xenopus cells [164]. To characterize the number of particles present in individual clusters, the authors used photobleaching experiments to sequentially bleach out fluorescence arising from individual fluorescently labeled EGFR particles within a cluster in a field of view. The authors observed that for nearly 50% of these clusters complete photobleaching would occur following a multi-step photobleaching procedure, which the authors suggested was on account of receptor oligomerization (as opposed to photobleaching in a single step (25%) observed for monomers or in two steps (25%) for dimers) [164]. To characterize the surface of EGFR used for the assembly of these oligomers the authors used a combination of structural modeling and

mutagenesis studies in combination with these single molecule photobleaching experiments. From their studies, the authors determined that oligomerization is primarily mediated by interactions arising from the domain IV of the EGFR ECD [164]. The authors identified multiple combinations of domain IV mutations that were demonstrated via single molecule photobleaching experiments to inhibit multimerization of EGFR – (i) I544K/ I556K/ I562R/ V592E dubbed IIIV/KKRE; (ii) V526E/ E527R/ N528R dubbed VEN/ERR; (iii) T548N/ N554R – and a domain IV control mutant mutant I544A/ I556A/ I562R/ V592E dubbed IIIV/AARE that did not inhibit multimerization [164].

In the Schepartz lab, the focus of research has been to study how chemical information encoded by diverse growth factors is communicated through the allosteric network of EGFR to mediate diverse signaling outcomes [17,20,21]. The focus of this research has been the JM region that plays a critical role in diverse aspects of EGFR biology. Work in the Schepartz lab has demonstrated that upon activation by growth factors, the JM-A of EGFR can assemble into distinct coiled coil conformations that allosterically encode growth factor identity and are necessary and sufficient for modulating intracellular EGFR biology [17,20,21]. In this particular project, my efforts were focused towards exploring whether inhibiting EGFR multimerization had any effect on altering the allosteric network that communicates growth factor identity in terms of affecting the JM-A coiled coil structure.

To investigate the effect of inhibiting multimerization [164] on the JM-A structure of growth factor activated EGFR, we made use of bipartite tetracysteine display [39,40]. For our experiments, we cloned CysCys containing (CC_H-1 and CC_H-10) versions of the EGFR variants that were reported to inhibit multimerization (IIIV/KKRE, VEN/ERR, TN/RR) or not (IIIV/AARE); CC_H-1 and CC_H-10 variants probe for the assembly of EGF-type or TGF-α-type JM-A coiled

coil respectively [17,20,21]. In control experiments I was able to verify that all the CC_H-1 variants namely IIIV/KKRE-CC_H-1, VEN/ERR-CC_H-1, TN/RR-CC_H-1 and IIIV/AARE-CC_H-1 were all expressed in CHO-K1 cells and responded to treatment with saturating concentrations (16.7nM) of EGF/ TGF-α (phosphorylation at Y1173/ Y1068 and Erk phosphorylation) analogous to the WT-CC_H-1 variant (**Figure 4.1. C**).

In the bipartite tetracysteine display experiments, CHO-K1 cells expressing IIIV/KKRE-CC_H-1, VEN/ERR-CC_H-1, TN/RR-CC_H-1 and IIIV/AARE-CC_H-1 or WT-CC_H-1 were stimulated with growth factor (or not), incubated with ReAsH, washed, and immuno-stained. Receptor expression was monitored using a fluorescently labeled antibody to an N-terminal FLAG epitope. Using TIRF microscopy, the level of both cell surface ReAsH fluorescence (red) and EGFR expression (green) was quantified across multiple cells (40-109) expressing either EGFR or EGFRvIII variants. The cell-surface ReAsH fluorescence detected (over background) was normalized to the surface EGFR-expression detected (over background) to calculate the fold-increase in ReAsH fluorescence [17,20,21] (**Figure 4.1.A,B**). Cells expressing WT-CC_H-1 displayed levels of normalized ReAsH fluorescence relative to background that mirrored previous reports (1.76 ± 0.13 with EGF treatment; 1.21 ± 0.05 with TGF-α) [17,20,21] (**Figure 4.1.A,B**). In an analogous manner the other four EGFR variants also showed an almost 2-fold increase in normalized ReAsH fluorescence relative to background only when treated with EGF (IIIV/AARE-CC_H-1: 1.80 ± 0.14; IIIV/KKRE-CC_H-1: 2.10 ± 0.13; VEN/ERR-CC_H-1: 2.30 ± 0.19; TN/RR-CC_H-1: 2.33 ± 0.13) and not with TGF-α (IIIV/AARE-CC_H-1: 1.20 ± 0.11; IIIV/KKRE-CC_H-1: 1.25 ± 0.09; VEN/ERR-CC_H-1: 1.45 ± 0.11; TN/RR-CC_H-1: 1.26 ± 0.09) (**Figure 4.1.A,B**). The results of my initial experiments suggest that inhibiting multimerization does not have any obvious effect on assembly of the EGF-type structure. Future experiments

would need to evaluate (i) whether or not inhibiting multimerization affects the TGF-α-type structure and (ii) that the multimerization phenotype of the variants IIIV/AARE, IIIV/KKRE, VEN/ERR, TN/RR is not affected by the incorporation of cysteine residues to generate the CC_H-1/ CC_H-10 versions of these constructs.

4.2. Efforts towards understanding the effect of JM structure on the interactome of EGFR using APEX2-based proximity labeling and mass spectrometry.

Rationale: A research direction that directly follows from my work discussed in Chapter 3 is to elucidate the mechanism by which alternate JM-A coiled coil structures modulate EGFR biology. In chapter 3 we hypothesized that differences in EGFR biology may result partly from the altered patterns of EGFR C-tail phosphorylation that is responsible for recruiting diverse intracellular down regulatory mechanisms (**Figure 4.2.A**). While this hypothesis can explain the observed biological effects with WT EGFR, they are insufficient for explaining the observations with oncogenic L834R/ T766M EGFR treated with different classes of TKI. In this latter case, we observed that treatment with the different classes of TKI lead to differences in the biology of L834R/ T766M EGFR in a manner that is independent of C-tail phosphorylation but correlates directly with JM-A coiled coil structure. This suggests that additional down-regulatory mechanisms that are dependent on JM-A structure may be involved. It is possible that the assembly of the alternate JM-A coiled coil structures can directly alter the interactome of EGFR between the two states (**Figure 4.2.B**). In order to probe those differences in interactome, we would need to use a robust methodology to isolate and reliably characterize the protein partners of EGFR in the different coiled coil states using mass spectroscopy. Mass spectrometric methods have been previously used to characterize the interacting partners EGFR following activation with growth factors EGF and TGF-α [30,166,167]. Proximity labeling

using the engineered peroxidase APEX2 and mass spectrometric characterization is a robust methodology for detecting protein protein interactions and spatiotemporally resolving interaction networks in mammalian cells [168–171]. **Here we propose** to use a an APEX2-based proximity labeling followed mass spectrometric characterization strategy to isolate and identify the interacting partners of (i) WT EGFR and G628F-EGFR or G628V EGFR that fix the JM-A coiled coil structure into the EGF-type or TGF-α-structure respectively and (ii) L834R/ T766M EGFR treated with different TKIs classes (**Figure 4.2.C**).

Approach and preliminary results: For our proximity labeling/ MS experiment workflow, we first generated fusions of the engineered peroxidase APEX2 with (i) WT EGFR (ii) JM decoupling mutants: G628A-EGFR, G628F-EGFR and G628V-EGFR (iii) L834R/ T766M EGFR. Mammalian cells expressing these fusion constructs would be treated with biotin-phenol followed by either (i) activation with EGFR specific growth factors EGF or TGF-α or (ii) inhibition with L834R/ T766M EGFR-specific TKIs. Thereafter the cells would be treated with H_2O_2 to initiate the rapid biotinylation reaction after specific periods of time (0-8 min: to identify for early interactors; 40-90min: to identify to later interactors). Cells would be subsequently lysed and the biotinylated proteins (by virtue of their interaction to EGFR and thus APEX2) will be purified and enriched for using streptavidin pulldown. Thereafter, the isolated proteins would be identified using LC-MS/MS and mapping onto the mammalian cell proteome.

In this section I describe my efforts in preliminary experiments to ensure that EGFR-APEX2 (i) was expressed in CHO-K1 mammalian cells (ii) had growth factor dependent auto-phosphorylation activity comparable to WT EGFR (that did not bear an APEX2 fusion) (iii) had APEX-2 enzymatic activity comparable to APEX2 (that was not fused to EGFR). The proximity labeling/ MS experiments will be carried out by fellow graduate student Sol Chang. For these

initial experiments in addition to WT EGFR, EGFR-APEX2 and APEX2, we designed two additional control constructs K721M-EGFR (where EGFR kinase activity is abrogated) and D208N APEX2 (where APEX2 peroxidase activity is abrogated) (**Figure 4.3.A**). We first sought to evaluate the expression and activity of EGFR-APEX2 in CHO-K1 cells. CHO-K1 cells were transiently transfected with FLAG-tagged WT-EGFR, EGFR-APEX2, APEX-2, K721M-EGFR and D208N APEX2. Using western blot assays we probed for the expression of the FLAG-tagged variants using an anti-FLAG antibody. We observed that all FLAG-tagged variants were expressed in CHO-K1 cells (**Figure 4.3.B-D**). We next sought to evaluate the growth factor dependent auto-phosphorylation activity of WT EGFR-APEX2. CHO-K1 cells expressing FLAG-tagged WT EGFR, EGFR-APEX2 and a negative control K721M-EGFR were treated with saturating amounts (16.7 nM) of EGF/ TGF-α). Using western blot analysis we evaluated the auto-phosphorylation activity of the FLAG-tagged EGFR variants at C-tail tyrosine residues Y1045 and Y1068 (**Figure 4.3. C-F**). As expected, WT EGFR was robustly phosphorylated at both Y1045 (**Figure 4.3. C,E**) and Y1068 (**Figure 4.3. D,F**) following treatment with either EGF or TGF-α (and not in the absence of growth factor treatment). In an analogous fashion EGFR-APEX2 was phosphorylated at both Y1045 (**Figure 4.3. C,E**) and Y1068 (**Figure 4.3. D,F**) following treatment with both EGF or TGF-α at levels comparable to WT EGFR. With K721M EGFR no auto-phosphorylation activity was detected at either tyrosine residues both in the absence and presence of EGF or TGF-α. Overall we observed that the fusion of APEX2 to WT EGFR did not significantly affect its growth factor dependent phosphorylation at C-tail residues Y1045 and Y1068 (**Figure 4.3. C-F**). We next sought to evaluate the peroxidase activity of EGFR-APEX2. For this we used a fluorescence based assay that makes use of the peroxidase mediated conversion of Amplex red to Resorufin [168]. Amplex red that is ambiently non

fluorescent, upon treatment with H_2O_2 and peroxidase (in this case APEX2) is spontaneously converted to brightly fluorescent dye resorufin. The time dependent change in fluorescence provides a robust and instantaneous readout of the enzymatic activity of the peroxidase enzyme (APEX2) (**Figure 4.3.G**). Clarified cellular lysates from CHO-K1 cells expressing APEX-2, EGFR-APEX2 and a negative control D208N APEX2 were diluted in DPBS and treated individually with H_2O_2 and Amplex Red. Immediately following H_2O_2 and Amplex Red addition, the resulting fluorescence of the reaction mixture was recorded at regular time intervals. From the time dependent changes in fluorescence, the activity of the APEX2 constructs was evaluated. From our experiments, we observed that both APEX2 and EGFR-APEX2 were active, albeit the activity of EGFR-APEX2 was both slightly lesser and slightly slower as compared to APEX2 (**Figure 4.3.H**). No detectable peroxidase activity was observed with the negative control D208N APEX2 (where peroxidase activity is abrogated) (**Figure 4.3.H**). Overall we observe that although APEX2 fused to EGFR with a flexible GGS linker retains considerable enzymatic activity, its extent and velocity is slightly reduced (**Figure 4.3.H**). Given that the proper enzymatic activity of APEX2 in the fusion construct is critical for the subsequent proximity labeling experiments, it may be worthwhile to investigate if extending the flexible linker between EGFR and APEX2 restores the enzymatic activity of APEX2 to level comparable to APEX2. Nonetheless, it is encouraging that the EGFR-APEX2 fusion is expressed in mammalian cells and retains enzymatic activity both in the EGFR and APEX2 parts. I am excited to see how this project develops in the future and what all we learn about the interactome of EGFR when its JM is fixed either by mutations in the TM or treatment with TKIs.

4.3. Materials and Methods

Materials. Antibodies. Goat polyclonal anti-Rabbit, Horseradish Peroxidase (HRP)-conjugated (#7074), Goat polyclonal anti-Mouse, HRP-conjugated (#7076), Rabbit monoclonal anti-Phospho-EGF ReceptorTyr1173, (53A5) (#4407), Rabbit polyclonal anti-Phospho-EGF Receptor Tyr1086 (#2220), Rabbit polyclonal anti-Phospho-EGF Receptor Tyr1068 (#2234), Rabbit polyclonal anti-Phospho-EGF Receptor Tyr1045 (#2237), Rabbit monoclonal anti-α-Tubulin (#2125) were purchased from Cell Signaling Technologies (CST). Mouse monoclonal (M2) anti-Flag (#F1804), was purchased from Millipore Sigma. Goat anti-Mouse IgG (H+L) Cross-Adsorbed Secondary Antibody, Alexa Fluor 488®-conjugate (#A11001), was purchased from ThermoFisher Scientific.

Chemicals and Recombinant Proteins. F-12K Medium (#10-025-CV), Dulbecco's Phosphate Buffered Saline (DPBS) (#14190), Fetal Bovine Serum (FBS)–Heat Inactivated (#11082147), Penicillin/Streptomycin (#1514012), Non-enzymatic Cell Dissociation Solution (#13151014), RestoreTM Western Blot Stripping Buffer (#21059), Hoechst 33342, Trihydrochloride, Trihydrate 10 mg/mL Solution in Water (#H3570), iBlot PVDF membranes (# IB401031), Amplex Red Hydrogen Peroxide/Peroxidase Assay Kit (A22188) were purchased from ThermoFisher Scientific. TransIT-CHO transfection kit was purchased from Mirus Bio LLC. Fetal Bovine Serum (FBS)–Heat Inactivated (#F4135), Bovine Serum Albumin (#9048-46-8), Fibronectin (#F1141) were purchased from Millipore Sigma. cOmplete, Mini Protease Inhibitor Tablets (#11836170001), PhosSTOP Phosphatase Inhibitor Cocktail Tablets (#04906837001) were purchased from Roche Applied Science. Recombinant Human EGF Protein (#236-EG), Recombinant Human TGF-a Protein (#293-A) were purchased from R&D Systems. Mini-PROTEAN® TGX Precast Gels (10% polyacrylamide) (#456-1036), Clarity Western ECL

reagents (#1705060) were purchased from Bio-Rad Laboratories, Inc.

Cell culture. CHO-K1 cells (ATCC) were cultured in F12K Medium supplemented with 10% FBS and Pen-Strep (100 I.U./mL penicillin and 100 mg/mL streptomycin) at 37°C in a CO2/air (5%/95%) incubator. Cells were transfected using the TransIT-CHO Transfection Kit (Mirus Bio LLC) (CHO-K1), according to the manufacturer's instructions. Cell densities for all mammalian cell lines were determined with a Cellometer® Auto T4 automated counter. All cells were bona fide lines and periodically tested for mycoplasma with DNA methods

Cloning and Mutagenesis. All EGFR DNA variants were cloned from a pcDNA3.1 plasmid, generously donated by the Kuriyan Group (University of California, Berkeley), containing the sequence of the full-length EGFR with an N-terminal FLAG tag [18,22]. Mutations were introduced into the wild-type, CCH-1 and CC_H-10 EGFR sequences using Quikchange Lightning site-directed mutagenesis kit (Agilent Technologies)/ Gibson assembly (NEB) of G-Blocks and linearized backbone fragments according to the manufacturer's instructions, with primers (purchased from Integrated DNA Technologies) listed in Table 4.1. All DNA variants were amplified with XL-10 Gold Ultracompetent cells (Agilent Technologies).

Bipartite Tetracysteine Display Assay i.e. Surface ReAsH Labeling Studies and Total Internal Resonance Fluorescence (TIRF) Microscopy. ReAsH labeling was accomplished as described previously [21,17] by treating CHO-K1 cells expressing EGFR variants with an endocytosis inhibition cocktail (10 mM NaN_3, 2 mM NaF, 5 mM 2-deoxy-D-glucose in F12-K media) for 1 hr at 37°C. Cells were stimulated without/with 100 ng/mL of EGF (16.7 nM)) and TGF-α (16.7 nM) prior to labeling. Cells were washed once with endocytosis inhibitor-containing media before incubation with ReAsH labeling solution (2 mM ReAsH

(ThermoFisher Scientific), 20 mM BAL (Acros Organics) in F12K media) for 1 hr at 37ºC. Cells were washed and incubated with endocytosis inhibitor-containing F12K media supplemented with 100 mM BAL for 10 min at 37ºC. The media was removed, and cells fixed using 4% paraformaldehyde (PFA) in DPBS for 25 min at room temperature. Fixed cells were washed with DPBS and blocked with 10% BSA in DPBS for 30 min at 37ºC. Cells were then labeled with primary antibody (mouse monoclonal mouse M2 anti-FLAG, 1:1000 dilution in 10% BSA in DPBS) for 1 hr at 37ºC, washed thrice with 10% BSA in DPBS, then incubated with secondary antibody (AlexaFluor488-conjugated goat anti-mouse, 1:2000 dilution in 10% BSA in DPBS) for 1 hr at 37ºC. Cells were then washed twice with 10% BSA in DPBS, washed once with DPBS, then nuclear-stained with Hoescht 33342 (1.62 mM in DPBS) for 5 min at 37ºC. Cells were then washed once with DPBS and stored in DPBS at 4ºC, prior to imaging. Labeled cells were monitored via TIRF microscopy, conducted on a Leica microsystems AM TIRF MC DMI6000B fitted with an EM-CCD camera (Hamamatsu) with HCX PL APO 63x/1.47 oil corrective objectives, as described previously[17,21]. Images were analyzed with ImageJ (FIJI) as described previously[17,21].

Western Blot Analysis of EGFR Expression and Autophosphorylation. Western blot analysis of EGFR expression and autophosphorylation in transfected CHO-K1 cells was accomplished as described previously with slight modification [17,21]. CHO-K1 cells expressing FLAG-tagged EGFR variants were serum starved overnight (~12 hours). 48 hr post seeding cells were stimulated without/with 100 ng/mL of EGF (16.7 nM) or TGF-α (16.7 nM) for 5 min at 37ºC, washed with serum free F12K media, and lysed in 100 uL of lysis buffer (50 mM Tris,150 mM NaCl, 1 mM EDTA, 1 mM NaF, 1% Triton X-100, pH 7.5, 1x cOmplete protease inhibitor cocktail, 1x Phos-Stop) for 1 hr. Clarified cell lysates were subjected to reducing 4-15%

polyacrylamide SDS-PAGE electrophoresis and transferred to immuno-blot PVDF membranes. Membranes were blocked with 5% milk in TBS-T Buffer (50 mM Tris, 150 mM NaCl, 0.1% Tween, pH 7.4) for 1 hr followed by an overnight incubation at 4°C of indicated primary (rabbit or mouse) antibodies. Blots were washed with TBS-T and incubated with either anti-rabbit or anti-mouse goat horseradish peroxidase conjugate secondary antibodies for 1 hr at room temperature, then washed with TBS-T. Blots were then visualized using Clarity Western ECL reagents on a ChemiDoc XRS+/ ChemiDocMP instrument, and intensities of immuno-stained bands measured with ImageJ 64[125]. When assessing phosphorylation of EGFR/ gel loading at multiple positions using the same samples, the blots obtained with a given phospho-EGFR antibody were stripped with Restore Western Blot Stripping Buffer/ and antibody stripping buffer (Tris-HCl (62.5 mM), SDS (2%w/v), 2-mercaptoethanol (0.7%v/v)) and re-probed with a different phospho-EGFR antibody.

Amplex red assay to detect peroxidase activity. Cellular lysates from CHO-K1 cells expressing FLAg tagged variants were prepared as described for western blot analyses. Clarified cell lysates were quantified for total protein content using Pierce™ 660nm Protein Assay Reagent according to the manufacturer's instructions. 20ug of the clarified cellular lysate from each sample was diluted in 100 uL of DPBS pH 7.4 and was set up in Corning 96-Well x 360µL clear flat bottom assay microplate, non-treated black polystyrene. A 2X reaction mixture was prepared by mixing 25 uL of 10mM Amplex UltraRed stock (50 uM final conc.), 11.4 uL of 3% H_2O_2 (1mM final conc.) and 2.5 mL of DPBS pH 7.4. Using a multichannel pipette, 100 uL of reaction mixture was added to a 100 uL cell lysate solution and the fluorescence at 530/590 nm ex/em was recorded at regular intervals of 5 min for 1 hour on a Synergy HTX microplate plate reader.

Table 4.1. List of mutagenesis primers/ G-blocks used for cloning in Chapter 4

S.No.	Name	Primer/ G-block sequence
Project 1: Investigating the role of multimerization on JM structure		
1.	VEN/ERR forward (V562E, E527R, N528R)	5'-gtggcactgtatgcactcagacctcctctcaaactcccttggctcaccct-3'
2.	VEN/ERR reverse (V562E, E527R, N528R)	5'-agggtgagccaagggagtttgagaggaggtctgagtgcatacagtgccac-3'
3.	I562R forward	5'-ccagtgtgcccactacagggacggcccccac-3'
4.	I562R reverse	5'-gtgggggccgtccctgtagtgggcacactgg-3'
5.	V592E forward	5'-cacaggtggcactcatggccggcgt-3'
6.	V592E reverse	5'-acgccggccatgagtgccacctgtg-3'
7.	I545A forward	5'-cgtcctgtgcaggtggcgttcatggcctgagg-3'
8.	I545A reverse	5'-cctcaggccatgaacgccacctgcacaggacg-3'
9.	I556A forward	5'-gggcacactgggcacagttgtctggtccccgtcc-3'
10.	I556A reverse	5'-ggacggggaccagacaactgtgcccagtgtgccc-3'
11.	I545K forward	5'-cctgtgcaggtcttgttcatggcctgaggcag-3'
12.	I545K reverse	5'-ctgcctcaggccatgaacaagacctgcacagg-3'
13.	I556K forward	5'-tgggcacactgcttacagttgtctggtccccgt-3'
14.	I556K reverse	5'-acggggaccagacaactgtaagcagtgtgccca-3'
15.	T548R forward	5'-tccccgtcctctgcaggtgatgttcatgg-3'
16.	T548R reverse	5'-ccatgaacatcacctgcagaggacgggga-3'
17.	N554R forward	5'-gcacactggatacacctgtctggtccccgtcctg-3'
18.	N554R reverse	5'-caggacggggaccagacaggtgtatccagtgtgc-3'
19.	EGFR lin. forward	5’-GGCCTGAGGCAGGCACTCT-3’
20.	EGFR lin. reverse	5’-CTGTGCCATCCAAACTGCACC-3’

21.	G-Block (AARE) I545A/ I556A/ I562R/ V592E	5’-AGAGTGCCTGCCTCAGGCCatgaacgcaacctgcacaggacggggaccagac aactgtgcacagtgtgcccactacagagacggcccccactgcgtcaagacctgcccggcag gagtcatgggagaaaacaacaccctggtctggaagtacgcagacgccggccatgagtgcca cCTGTGCCATCCAAACTGCACC-3’
22.	G-Block (KKRE) I545K/ I556K/ I562R/ V592E	5’-AGAGTGCCTGCCTCAGGCCatgaacaagacctgcacaggacggggaccagac aactgtaagcagtgtgcccactacagagacggcccccactgcgtcaagacctgcccggcag gagtcatgggagaaaacaacaccctggtctggaagtacgcagacgccggccatgagtgcca cCTGTGCCATCCAAACTGCACC-3’
23.	G-Block (RR) (T548R, N554R)	5’-AGAGTGCCTGCCTCAGGCCatgaacatcacctgcagaggacggggaccagac agatgtatccagtgtgcccactacattgacggcccccactgcgtcaagacctgcccggcagg agtcatgggagaaaacaacaccctggtctggaagtacgcagacgccggccatgtgtgccac CTGTGCCATCCAAACTGCACC-3’
Project 2: Evaluating the interactome of EGFR using APEX2 proximity labeling and MS		
1.	APEX2 lin. fwd	5’-ATGTATATCTCCTTCTTAAAGTTAAACAAAATTATT-3’
2.	APEX2 lin. revs	5’-taacaaagcccgaaaggaag-3’
3.	EGFR lin. fwd	5’-GTCTAGAGGGCCCGTTTAAACCCG-3’
4.	EGFR lin. revs	5’-GCTCCAATAAATTCACTGCTTTGTGGCG-3’
5.	EGFR-APEX2 forward	5’-GCGCCACAAAGCAGTGAATTTATTGGAGCAGGCTCGGGCgg aaagtcttacccaactgtgagtgctgat-3'
6.	EGFR-APEX2 reverse	5’-TGATCAGCGGGTTTAAACGGGCCCTCTAGACTAggcatcagcaa acccaagctcggaaagctt-3’
7.	D208N-APEX2 (f)	5’-CTTCAGCTACCTTCTaacAAGGCTCTTTTGTC-3’
8.	D208N-APEX2 (r)	5’-GACAAAAGAGCCTTgttAGAAGGTAGCTGAAG-3’
9.	G628A-EGFR (f)	5’-ACTGGGATGGTGgccGCCCTCCTCTTG-3’
10.	G628A-EGFR (r)	5’-CAAGAGGAGGGCggcCACCATCCCAGT-3’
11.	G628F-EGFR (f)	5’-GCCACTGGGATGGTGttcGCCCTCCTCTTGCTG-3’
12.	G628F-EGFR (r)	5’-CAGCAAGAGGAGGGCgaaCACCATCCCAGTGGC-3’
13.	G628V-EGFR (f)	5’-ACTGGGATGGTGgtgGCCCTCCTCTTG-3’
14.	G628V-EGFR (r)	5’-CAAGAGGAGGGCcacCACCATCCCAGT-3’
15.	K721M-EGFR (f)	5’-GTTAAAATTCCCGTCGCTATCgctGAATTAAGA-3’
16.	K721M-EGFR (r)	5’-CTCTTAATTCagcGATAGCGACGGGAATTTTAAC-3’

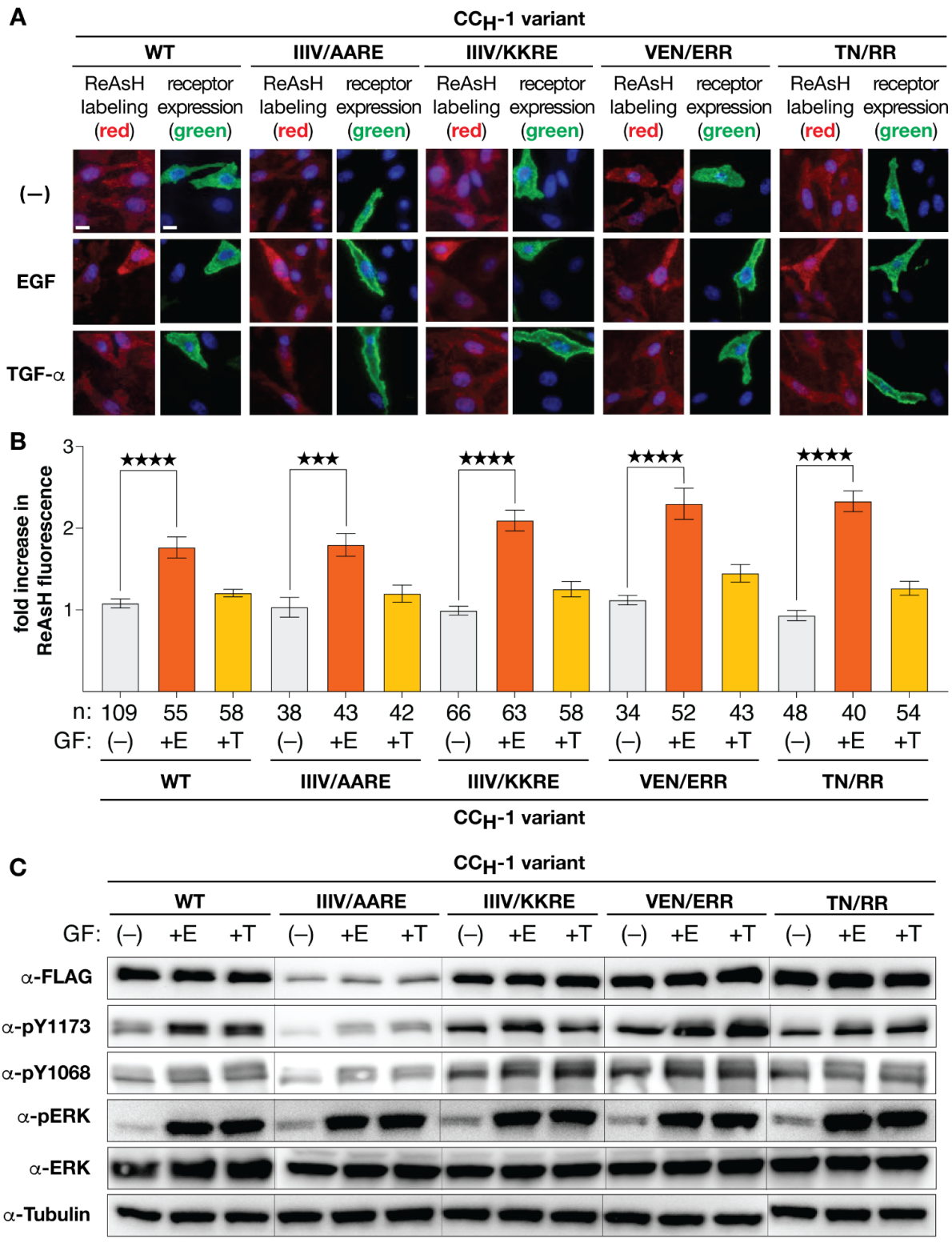
A
CCH-1 variant
WT
IIIV/AARE
IIIV/KKRE
VEN/ERR
TN/RR
ReAsH labeling (red)
receptor expression (green)
(–)
EGF
TGF-α
B
fold increase in ReAsH fluorescence
3
2
1
★★★★
★★★
★★★★
★★★★
★★★★
n: 109 55 58 38 43 42 66 63 58 34 52 43 48 40 54
GF: (–) +E +T (–) +E +T (–) +E +T (–) +E +T (–) +E +T
WT
IIIV/AARE
IIIV/KKRE
VEN/ERR
TN/RR
CCH-1 variant
C
CCH-1 variant
WT
IIIV/AARE
IIIV/KKRE
VEN/ERR
TN/RR
GF: (–) +E +T (–) +E +T (–) +E +T (–) +E +T (–) +E +T
α-FLAG
α-pY1173
α-pY1068
α-pERK
α-ERK
α-Tubulin

Figure 4.1. Inhibiting EGFR multimerization does not affect the EGF-type JM-A coiled coil structure (A) Representative TIRF-M images of CHO-K1 cells illustrating ReAsH labeling (red fluorescence) and expression (green fluorescence) of FLAG-tagged CC_H-1 variants of WT EGFR, IIIV/AARE, IIIV/KKRE, VEN/ERR, TN/RR in the absence and presence of EGF or TGF-α stimulation (16.7 nM). Scale bars represent 10 μm. **(B)** Bar Plots illustrating the quantification of TIRF-M results from 'n' cells as a fold-increase in expression-corrected ReAsH fluorescence over background. Error bars represent s.e.m., ****$p<0.0001$, ***$p<0.001$, from one-way ANOVA with Dunnett's post-analysis accounting comparison to the control for each case without growth factor treatment. n.s., not significant. **(C)** Representative western blots illustrating expression (FLAG) and extent of Y1173, Y1068 and Erk phosphorylation of FLAG-tagged CC_H-1 variants of WT EGFR, IIIV/AARE, IIIV/KKRE, VEN/ERR, TN/RR in the absence and presence of EGF or TGF-α stimulation (16.7 nM). Tubulin was used as a loading control.

A

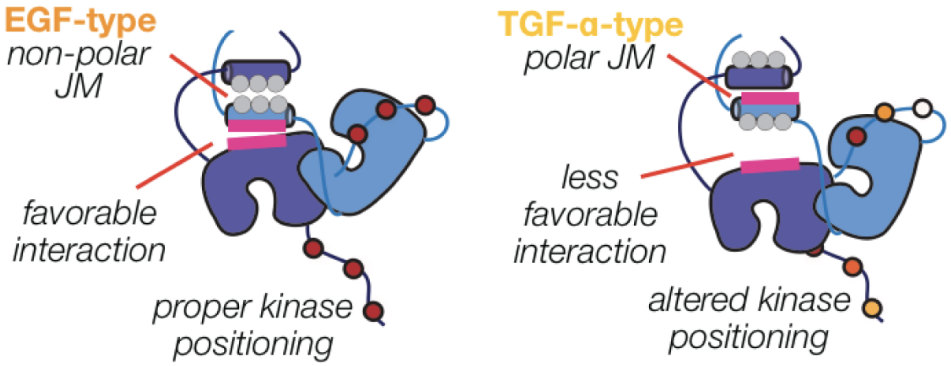

Kinase positioning and EGFR activity is altered between discrete coiled coil states

B

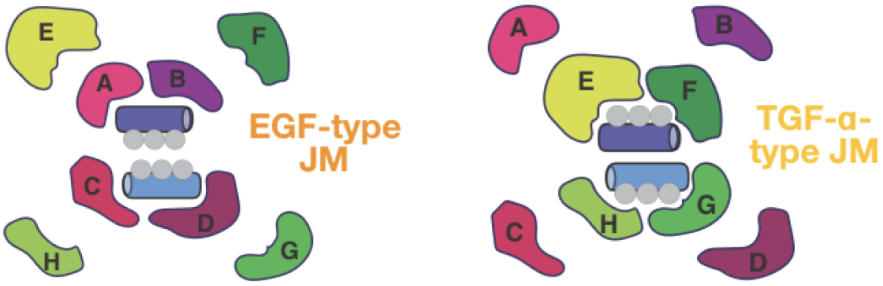

JM-A interactome is altered between dicrete coiled coil states

C

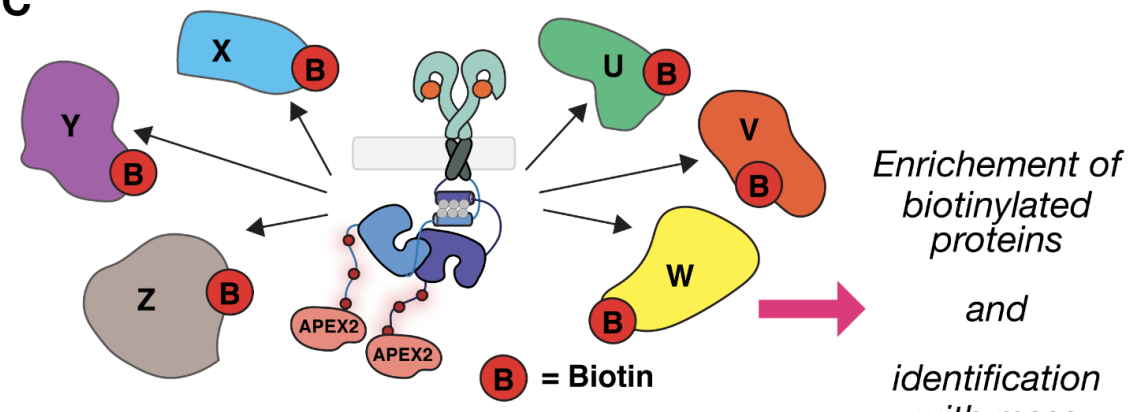

Proximity labeling with biotin using APEX-2

Figure 4.2. Mechanism of coiled coil mediated control of EGFR biology and methods to dissect the EGFR interactome. The alternate JM-A coiled coil structures can regulate EGFR biology by two possible mechanisms. **(A)** The two JM-A structures can alter the JM-A surface that interacts with the EGFR kinase thereby altering kinase positioning and activity thereby affecting the recruitment of diverse intracellular adaptors and down regulatory proteins. **(B)** Alternately the two JM-A surface can directly alter the interactome of EGFR. **(C)** The coiled coil dependent interactome of EGFR can be dissected using proximity labeling methodology (utilizing the engineered peroxidase APEX2) followed by identification and characterization with mass spectrometry.

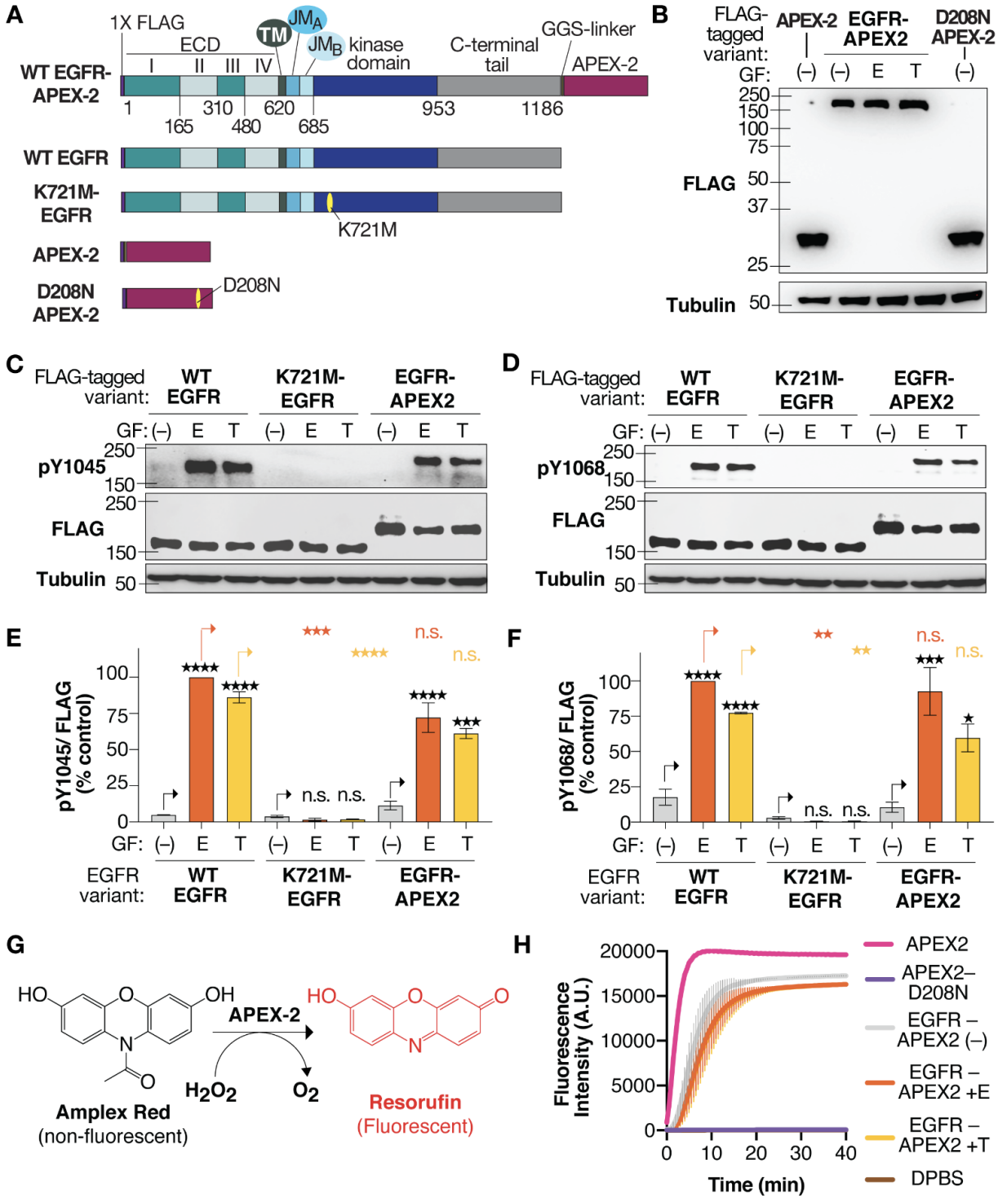
A
1X FLAG
ECD
I
II
III
IV
TM
JMA
JMB
kinase domain
C-terminal tail
GGS-linker
APEX-2
WT EGFR-APEX-2
1
165
310
480
620
685
953
1186
WT EGFR
K721M-EGFR
K721M
APEX-2
D208N APEX-2
D208N
B
FLAG-tagged variant:
APEX-2
EGFR-APEX2
D208N APEX-2
GF:
(–) (–) E T (–)
250
150
100
75
FLAG
50
37
25
Tubulin
50
C
FLAG-tagged variant:
WT EGFR
K721M-EGFR
EGFR-APEX2
GF: (–) E T (–) E T (–) E T
pY1045
250
150
FLAG
Tubulin
50
D
FLAG-tagged variant:
WT EGFR
K721M-EGFR
EGFR-APEX2
GF: (–) E T (–) E T (–) E T
pY1068
FLAG
Tubulin
E
pY1045/ FLAG (% control)
100
75
50
25
0
n.s.
GF: (–) E T (–) E T (–) E T
EGFR variant:
WT EGFR
K721M-EGFR
EGFR-APEX2
F
pY1068/ FLAG (% control)
G
HO
O
OH
N
O
APEX-2
H2O2
O2
Amplex Red
(non-fluorescent)
HO
O
O
N
Resorufin
(Fluorescent)
H
Fluorescence Intensity (A.U.)
20000
15000
10000
5000
0
0 10 20 30 40
Time (min)
APEX2
APEX2–D208N
EGFR – APEX2 (–)
EGFR – APEX2 +E
EGFR – APEX2 +T
DPBS

Figure 4.3. EGFR-APEX2 fusion retains enzymatic activity in both EGFR and APEX2 parts. **(A)** Domain diagram of FLAG-tagged EGFR/ APEX constructs illustrating sequences of EGFR-APEX2, WT EGFR, K721M-EGFR (whose EGFR kinase activity is abrogated), APEX2 and D208N-APEX2 (whose peroxidase activity is abrogated). EGFR is fused to APEX2 with a short flexible GGS linker. Location of K721M or D208N mutations is indicated in the domain diagram with a yellow oval. **(B)** Representative western blot illustrating the expression of FLAG-tagged APEX2, EGFR-APEX2 and D208N-APEX2 as detected with an anti-FLAG antibody. Tubulin was used as a loading control. Representative western blots illustrating the expression (FLAG) and autophosphorylation activity of WT EGFR, EGFR-APEX2 and K721M-EGFR (negative control) at C-tail tyrosine residues **(C)** Y1045 and **(D)** Y1068. Tubulin was used as a loading control. Bar plots illustrating the normalized percent of **(E)** pY1045/ FLAG or **(F)** pY1068/ FLAG for western blots shown in **(C)** or **(D)** respectively. In each case, pY-EGFR/ FLAG signal is normalized to the signal for WT EGFR treated with EGF. Error bars represent S.E.M. ****$p<0.0001$, ***$p<0.001$, from one-way ANOVA with Dunnett's post-analysis accounting comparison to no growth factor treated control for each mutant case (black symbols) and comparison among variants to WT EGFR treated with EGF (orange symbols) or WT EGFR treated with TGF-α (yellow symbols) n.s., not significant. **(G)** Reaction schematic illustrating the peroxidase (APEX2) mediated conversion of Amplex Red (non-fluorescent) to Resorufin (fluorescent) in the presence of hydrogen peroxide. **(H)** Results of amplex red assay illustrating the time dependent change in fluorescence intensity detected from reaction of Amplex Red and H_2O_2 with cellular lysate from CHO-K1 cells expressing APEX2 (pink), EGFR-APEX2 (without/ with 16.7 nM EGF /TGF-α treatment; represented by grey, orange and yellow lines respectively), D208N-APEX2 (purple; negative control).

References

1 Carpenter, G. and Cohen, S. (1979) Epidermal Growth Factor. *Annu. Rev. Biochem.* 48, 193–216

2 Kawamoto, T. *et al.* (1983) Growth stimulation of A431 cells by epidermal growth factor: identification of high-affinity receptors for epidermal growth factor by an anti-receptor monoclonal antibody. *Proc. Natl. Acad. Sci.* 80, 1337–1341

3 Yarden, Y. and Sliwkowski, M.X. (2001) Untangling the ErbB signalling network. *Nat. Rev. Mol. Cell Biol.* 2, 127–137

4 Lemmon, M.A. and Schlessinger, J. (2010) Cell signaling by receptor tyrosine kinases. *Cell* 141, 1117–34

5 Lemmon, M.A. *et al.* (2014) The EGFR Family: Not So Prototypical Receptor Tyrosine Kinases. *Cold Spring Harb. Perspect. Biol.* 6,

6 Kovacs, E. *et al.* (2015) A structural perspective on the regulation of the epidermal growth factor receptor. *Annu Rev Biochem* 84, 739–64

7 Harris, R.C. *et al.* (2003) EGF receptor ligands. *Exp Cell Res* 284, 2–13

8 Kochupurakkal, B.S. *et al.* (2005) Epigen, the Last Ligand of ErbB Receptors, Reveals Intricate Relationships between Affinity and Mitogenicity*. *J. Biol. Chem.* 280, 8503–8512

9 da Cunha Santos, G. *et al.* (2011) EGFR Mutations and Lung Cancer. *Annu. Rev. Pathol. Mech. Dis.* 6, 49–69

10 Yarden, Y. and Pines, G. (2012) The ERBB network: at last, cancer therapy meets systems biology. *Nat. Rev. Cancer* 12, 553–563

11 Sigismund, S. *et al.* (2018) Emerging functions of the EGFR in cancer. *Mol. Oncol.* 12, 3–20

12 Garrett, T.P.J. *et al.* (2002) Crystal Structure of a Truncated Epidermal Growth Factor Receptor Extracellular Domain Bound to Transforming Growth Factor α. *Cell* 110, 763–773

13 Ogiso, H. *et al.* (2002) Crystal Structure of the Complex of Human Epidermal Growth Factor and Receptor Extracellular Domains. *Cell* 110, 775–787

14 Freed, D.M. *et al.* (2017) EGFR Ligands Differentially Stabilize Receptor Dimers to Specify Signaling Kinetics. *Cell* 171, 683-695 e18

15 Endres, N.F. *et al.* (2013) Conformational coupling across the plasma membrane in activation of the EGF receptor. *Cell* 152, 543–56

16 Arkhipov, A. *et al.* (2013) Architecture and membrane interactions of the EGF receptor. *Cell* 152, 557–69

17 Sinclair, J.K.L. *et al.* (2018) Mechanism of Allosteric Coupling into and through the Plasma Membrane by EGFR. *Cell Chem Biol* 25, 857-870 e7

18 Jura, N. *et al.* (2009) Mechanism for activation of the EGF receptor catalytic domain by the

juxtamembrane segment. *Cell* 137, 1293–307

19 Brewer, M.R. *et al.* (2009) The Juxtamembrane Region of the EGF Receptor Functions as an Activation Domain. *Mol. Cell* 34, 641–651

20 Scheck, R.A. *et al.* (2012) Bipartite tetracysteine display reveals allosteric control of ligand-specific EGFR activation. *ACS Chem Biol* 7, 1367–76

21 Doerner, A. *et al.* (2015) Growth Factor Identity Is Encoded by Discrete Coiled-Coil Rotamers in the EGFR Juxtamembrane Region. *Chem Biol* 22, 776–84

22 Zhang, X. *et al.* (2006) An Allosteric Mechanism for Activation of the Kinase Domain of Epidermal Growth Factor Receptor. *Cell* 125, 1137–1149

23 Ferguson, K.M. *et al.* (2003) EGF Activates Its Receptor by Removing Interactions that Autoinhibit Ectodomain Dimerization. *Mol. Cell* 11, 507–517

24 Bocharov, E.V. *et al.* (2018) Structural basis of the signal transduction via transmembrane domain of the human growth hormone receptor. *Biochim Biophys Acta Gen Subj* 1862, 1410–1420

25 Mi, L.-Z. *et al.* (2011) Simultaneous visualization of the extracellular and cytoplasmic domains of the epidermal growth factor receptor. *Nat. Struct. Mol. Biol.* 18, 984–989

26 Huang, Y. *et al.* (2020) *A structural mechanism for the generation of biased agonism in the epidermal growth factor receptor*,

27 Ferguson, K.M. (2008) Structure-Based View of Epidermal Growth Factor Receptor Regulation. *Annu. Rev. Biophys.* 37, 353–373

28 French, A.R. *et al.* (1995) Intracellular trafficking of epidermal growth factor family ligands is directly influenced by the pH sensitivity of the receptor/ligand interaction. *J Biol Chem* 270, 4334–40

29 Roepstorff, K. *et al.* (2009) Differential effects of EGFR ligands on endocytic sorting of the receptor. *Traffic* 10, 1115–27

30 Francavilla, C. *et al.* (2016) Multilayered proteomics reveals molecular switches dictating ligand-dependent EGFR trafficking. *Nat Struct Mol Biol* 23, 608–18

31 Lowder, M.A. *et al.* (2015) Structural Differences between Wild-Type and Double Mutant EGFR Modulated by Third-Generation Kinase Inhibitors. *J Am Chem Soc* 137, 6456–9

32 Aifa, S. *et al.* (2005) A basic peptide within the juxtamembrane region is required for EGF receptor dimerization. *Exp. Cell Res.* 302, 108–114

33 Thiel, K.W. and Carpenter, G. (2007) Epidermal growth factor receptor juxtamembrane region regulates allosteric tyrosine kinase activation. *Proc. Natl. Acad. Sci.* 104, 19238–19243

34 He, L. and Hristova, K. (2012) Consequences of replacing EGFR juxtamembrane domain with an unstructured sequence. *Sci. Rep.* 2, 854

35 Macdonald-Obermann, J.L. and Pike, L.J. (2009) The Intracellular Juxtamembrane Domain

of the Epidermal Growth Factor (EGF) Receptor Is Responsible for the Allosteric Regulation of EGF Binding*♦. *J. Biol. Chem.* 284, 13570–13576

36 Choowongkomon, K. *et al.* (2005) A Structural Model for the Membrane-bound Form of the Juxtamembrane Domain of the Epidermal Growth Factor Receptor. *J. Biol. Chem.* 280, 24043–24052

37 Wood, E.R. *et al.* (2008) 6-Ethynylthieno[3,2-d]- and 6-ethynylthieno[2,3-d]pyrimidin-4-anilines as tunable covalent modifiers of ErbB kinases. *Proc. Natl. Acad. Sci.* 105, 2773–2778

38 Nick Pace, C. and Martin Scholtz, J. (1998) A Helix Propensity Scale Based on Experimental Studies of Peptides and Proteins. *Biophys. J.* 75, 422–427

39 Luedtke, N.W. *et al.* (2007) Surveying polypeptide and protein domain conformation and association with FlAsH and ReAsH. *Nat Chem Biol* 3, 779–84

40 Scheck, R.A. and Schepartz, A. (2011) Surveying protein structure and function using bis-arsenical small molecules. *Acc Chem Res* 44, 654–65

41 Adams, S.R. *et al.* (2002) New biarsenical ligands and tetracysteine motifs for protein labeling in vitro and in vivo: synthesis and biological applications. *J Am Chem Soc* 124, 6063–76

42 Griffin, B.A. *et al.* (1998) Specific covalent labeling of recombinant protein molecules inside live cells. *Science* 281, 269–272

43 Walker, A.S. *et al.* (2016) Rotamer-Restricted Fluorogenicity of the Bis-Arsenical ReAsH. *J. Am. Chem. Soc.* 138, 7143–7150

44 Gray, J.J. *et al.* (2003) Protein–Protein Docking with Simultaneous Optimization of Rigid-body Displacement and Side-chain Conformations. *J. Mol. Biol.* 331, 281–299

45 Lu, C. *et al.* (2010) Structural Evidence for Loose Linkage between Ligand Binding and Kinase Activation in the Epidermal Growth Factor Receptor. *Mol. Cell. Biol.* 30, 5432–5443

46 Barth, P. *et al.* (2007) Toward high-resolution prediction and design of transmembrane helical protein structures. *Proc. Natl. Acad. Sci.* 104, 15682–15687

47 Alford, R.F. *et al.* (2015) An Integrated Framework Advancing Membrane Protein Modeling and Design. *PLOS Comput. Biol.* 11, e1004398

48 Yarov-Yarovoy, V. *et al.* (2006) Multipass membrane protein structure prediction using Rosetta. *Proteins* 62, 1010–1025

49 Rotow, J. and Bivona, T.G. (2017) Understanding and targeting resistance mechanisms in NSCLC. *Nat. Rev. Cancer* 17, 637–658

50 Lynch, T.J. *et al.* (2004) Activating Mutations in the Epidermal Growth Factor Receptor Underlying Responsiveness of Non–Small-Cell Lung Cancer to Gefitinib. *N. Engl. J. Med.*

51 Pao, W. *et al.* (2004) EGF receptor gene mutations are common in lung cancers from “never smokers” and are associated with sensitivity of tumors to gefitinib and erlotinib. *Proc. Natl. Acad. Sci.* 101, 13306–13311

52 COSMIC (2020) Catalogue of Somatic Mutations in Cancer, release version 92. at <https://cancer.sanger.ac.uk/cosmic>

53 Graham, R.P. *et al.* (2017) Worldwide Frequency of Commonly Detected EGFR Mutations. *Arch. Pathol. Lab. Med.* 142, 163–167

54 Sharma, S.V. *et al.* (2007) Epidermal growth factor receptor mutations in lung cancer. *Nat. Rev. Cancer* 7, 169–181

55 Hidalgo, M. *et al.* (2001) Phase I and Pharmacologic Study of OSI-774, an Epidermal Growth Factor Receptor Tyrosine Kinase Inhibitor, in Patients With Advanced Solid Malignancies. *J. Clin. Oncol.* 19, 3267–3279

56 Rosell, R. *et al.* (2012) Erlotinib versus standard chemotherapy as first-line treatment for European patients with advanced EGFR mutation-positive non-small-cell lung cancer (EURTAC): a multicentre, open-label, randomised phase 3 trial. *Lancet Oncol.* 13, 239–246

57 Wakeling, A.E. *et al.* (2002) ZD1839 (Iressa): an orally active inhibitor of epidermal growth factor signaling with potential for cancer therapy. *Cancer Res.* 62, 5749–5754

58 Maemondo, M. *et al.* (2010) Gefitinib or Chemotherapy for Non–Small-Cell Lung Cancer with Mutated EGFR. *N. Engl. J. Med.* 362, 2380–2388

59 Ferguson, F.M. and Gray, N.S. (2018) Kinase inhibitors: the road ahead. *Nat. Rev. Drug Discov.* 17, 353–377

60 Eck, M.J. and Yun, C. (2010) Structural and Mechanistic Underpinnings of the Differential Drug Sensitivity of EGFR Mutations in Non-Small Cell Lung Cancer. *Biochim. Biophys. Acta* 1804, 559–566

61 Kosaka, T. *et al.* (2006) Analysis of Epidermal Growth Factor Receptor Gene Mutation in Patients with Non–Small Cell Lung Cancer and Acquired Resistance to Gefitinib. *Clin. Cancer Res.* 12, 5764–5769

62 Yun, C.-H. *et al.* (2008) The T790M mutation in EGFR kinase causes drug resistance by increasing the affinity for ATP. *Proc. Natl. Acad. Sci. U. S. A.* 105, 2070–2075

63 Li, D. *et al.* (2008) BIBW2992, an irreversible EGFR/HER2 inhibitor highly effective in preclinical lung cancer models. *Oncogene* 27, 4702–4711

64 Sequist, L.V. *et al.* (2013) Phase III Study of Afatinib or Cisplatin Plus Pemetrexed in Patients With Metastatic Lung Adenocarcinoma With *EGFR* Mutations. *J. Clin. Oncol.* 31, 3327–3334

65 Walter, A.O. *et al.* (2013) Discovery of a Mutant-Selective Covalent Inhibitor of EGFR that Overcomes T790M-Mediated Resistance in NSCLC. *Cancer Discov.* 3, 1404–1415

66 Sequist, L.V. *et al.* (2015) Rociletinib in EGFR-Mutated Non–Small-Cell Lung Cancer. *N. Engl. J. Med.* 372, 1700–1709

67 Zhou, W. *et al.* (2009) Novel mutant-selective EGFR kinase inhibitors against EGFR T790M. *Nature* 462, 1070–1074

68 Cross, D.A.E. *et al.* (2014) AZD9291, an Irreversible EGFR TKI, Overcomes T790M-Mediated Resistance to EGFR Inhibitors in Lung Cancer. *Cancer Discov.* 4, 1046–1061

69 Soria, J.-C. *et al.* (2017) Osimertinib in Untreated EGFR-Mutated Advanced Non–Small-Cell Lung Cancer. *N. Engl. J. Med.* DOI: 10.1056/NEJMoa1713137

70 Ramalingam, S.S. *et al.* (2020) Overall Survival with Osimertinib in Untreated, EGFR-Mutated Advanced NSCLC. *N. Engl. J. Med.* 382, 41–50

71 Hedger, G. *et al.* (2015) The juxtamembrane regions of human receptor tyrosine kinases exhibit conserved interaction sites with anionic lipids. *Sci. Rep.* 5, 9198

72 McLaughlin, S. *et al.* (2005) An Electrostatic Engine Model for Autoinhibition and Activation of the Epidermal Growth Factor Receptor (EGFR/ErbB) Family. *J. Gen. Physiol.* 126, 41–53

73 Martín-Nieto, J. and Villalobo, A. (1998) The Human Epidermal Growth Factor Receptor Contains a Juxtamembrane Calmodulin-Binding Site †. *Biochemistry* 37, 227–236

74 Sengupta, P. *et al.* (2009) EGFR Juxtamembrane Domain, Membranes, and Calmodulin: Kinetics of Their Interaction. *Biophys. J.* 96, 4887–4895

75 Li, H. *et al.* (2012) Regulation of the Ligand-dependent Activation of the Epidermal Growth Factor Receptor by Calmodulin*. *J. Biol. Chem.* 287, 3273–3281

76 Sato, T. *et al.* (2006) Structure of the Membrane Reconstituted Transmembrane−Juxtamembrane Peptide EGFR(622−660) and Its Interaction with Ca2+/Calmodulin. *Biochemistry* 45, 12704–12714

77 Hake, M.J. *et al.* (2008) Specificity Determinants of a Novel Nck Interaction with the Juxtamembrane Domain of the Epidermal Growth Factor Receptor †,‡. *Biochemistry* 47, 3096–3108

78 Poppleton, H.M. *et al.* (2000) The Juxtamembrane Region of the Epidermal Growth Factor Receptor Is Required for Phosphorylation of GαS. *Arch. Biochem. Biophys.* 383, 309–317

79 Hunter, T. *et al.* (1984) Protein kinase C phosphorylation of the EGF receptor at a threonine residue close to the cytoplasmic face of the plasma membrane. *Nature* 311, 480–483

80 Cochet, C. *et al.* (1984) C-kinase phosphorylates the epidermal growth factor receptor and reduces its epidermal growth factor-stimulated tyrosine protein kinase activity. *J. Biol. Chem.* 259, 2553–2558

81 Friedman, B. *et al.* (1984) Tumor promoters block tyrosine-specific phosphorylation of the epidermal growth factor receptor. *Proc. Natl. Acad. Sci. U. S. A.* 81, 3034–3038

82 Davis, R.J. and Czech, M.P. (1985) Tumor-promoting phorbol diesters cause the phosphorylation of epidermal growth factor receptors in normal human fibroblasts at threonine-654. *Proc. Natl. Acad. Sci.* 82, 1974–1978

83 Lin, C.R. *et al.* (1986) Protein kinase C phosphorylation at Thr 654 of the unoccupied EGF receptor and EGF binding regulate functional receptor loss by independent mechanisms.

Cell 44, 839–848

84 Morrison, P. *et al.* (1993) Role of threonine residues in regulation of the epidermal growth factor receptor by protein kinase C and mitogen-activated protein kinase. *J. Biol. Chem.* 268, 15536–15543

85 Takishima, K. *et al.* (1988) Thapsigargin, a novel promoter, phosphorylates the epidermal growth factor receptor at threonine 669. *Biochem. Biophys. Res. Commun.* 157, 740–746

86 Winograd-Katz, S.E. and Levitzki, A. (2006) Cisplatin induces PKB/Akt activation and p38 MAPK phosphorylation of the EGF receptor. *Oncogene* 25, 7381–7390

87 Cochet, C. *et al.* (1991) Interaction between the epidermal growth factor receptor and phosphoinositide kinases. *J. Biol. Chem.* 266, 637–644

88 Kil, S.J. *et al.* (1999) A Leucine-based Determinant in the Epidermal Growth Factor Receptor Juxtamembrane Domain Is Required for the Efficient Transport of Ligand-Receptor Complexes to Lysosomes. *J. Biol. Chem.* 274, 3141–3150

89 Kil, S.J. and Carlin, C. (2000) EGF receptor residues Leu679, Leu680 mediate selective sorting of ligand-receptor complexes in early endosomal compartments. *J. Cell. Physiol.* 185, 47–60

90 Cai, G. *et al.* (2018) TRAF4 binds to the juxtamembrane region of EGFR directly and promotes kinase activation. *Proc. Natl. Acad. Sci.* 115, 11531–11536

91 Viegas, A. *et al.* (2020) Molecular Architecture of a Network of Potential Intracellular EGFR Modulators: ARNO, CaM, Phospholipids, and the Juxtamembrane Segment. *Structure* 28, 54-62.e5

92 Kluba, M. *et al.* (2015) Inhibition of Receptor Dimerization as a Novel Negative Feedback Mechanism of EGFR Signaling. *PLOS ONE* 10, e0139971

93 He, C. *et al.* (2002) The epidermal growth factor receptor juxtamembrane domain has multiple basolateral plasma membrane localization determinants, including a dominant signal with a polyproline core. *J. Biol. Chem.* 277, 38284–38293

94 Cotton, C.U. *et al.* (2013) Basolateral EGF receptor sorting regulated by functionally distinct mechanisms in renal epithelial cells. *Traffic Cph. Den.* 14, 337–354

95 Hsu, S.-C. and Hung, M.-C. (2007) Characterization of a novel tripartite nuclear localization sequence in the EGFR family. *J. Biol. Chem.* 282, 10432–10440

96 Lin, S.Y. *et al.* (2001) Nuclear localization of EGF receptor and its potential new role as a transcription factor. *Nat. Cell Biol.* 3, 802–808

97 Gan, H.K. *et al.* (2009) The EGFRvIII variant in glioblastoma multiforme. *J. Clin. Neurosci.* 16, 748–754

98 Gan, H.K. *et al.* (2013) The epidermal growth factor receptor variant III (EGFRvIII): where wild things are altered. *FEBS J.* 280, 5350–5370

99 Brennan, C.W. *et al.* (2013) The Somatic Genomic Landscape of Glioblastoma. *Cell* 155, 462–477

100 An, Z. *et al.* (2018) Epidermal growth factor receptor and EGFRvIII in glioblastoma: signaling pathways and targeted therapies. *Oncogene* 37, 1561–1575

101 Yamazaki, H. *et al.* (1988) Amplification of the structurally and functionally altered epidermal growth factor receptor gene (c-erbB) in human brain tumors. *Mol. Cell. Biol.* 8, 1816–1820

102 Sugawa, N. *et al.* (1990) Identical splicing of aberrant epidermal growth factor receptor transcripts from amplified rearranged genes in human glioblastomas. *Proc. Natl. Acad. Sci.* 87, 8602–8606

103 Ekstrand, A.J. *et al.* (1992) Amplified and rearranged epidermal growth factor receptor genes in human glioblastomas reveal deletions of sequences encoding portions of the N- and/or C-terminal tails. *Proc. Natl. Acad. Sci.* 89, 4309–4313

104 Ymer, S.I. *et al.* (2011) Glioma Specific Extracellular Missense Mutations in the First Cysteine Rich Region of Epidermal Growth Factor Receptor (EGFR) Initiate Ligand Independent Activation. *Cancers* 3, 2032–2049

105 Mozumdar, D. *et al.* (2020) Discrete Coiled Coil Rotamers Form within the EGFRvIII Juxtamembrane Domain. *Biochemistry* 59, 3965–3972

106 Nishikawa, R. *et al.* (1994) A mutant epidermal growth factor receptor common in human glioma confers enhanced tumorigenicity. *Proc. Natl. Acad. Sci.* 91, 7727–7731

107 Nagane, M. *et al.* (1996) A Common Mutant Epidermal Growth Factor Receptor Confers Enhanced Tumorigenicity on Human Glioblastoma Cells by Increasing Proliferation and Reducing Apoptosis. *Cancer Res.* 56, 5079–5086

108 Huang, H.-J.S. *et al.* (1997) The Enhanced Tumorigenic Activity of a Mutant Epidermal Growth Factor Receptor Common in Human Cancers Is Mediated by Threshold Levels of Constitutive Tyrosine Phosphorylation and Unattenuated Signaling. *J. Biol. Chem.* 272, 2927–2935

109 Frederick, L. *et al.* (2000) Diversity and Frequency of Epidermal Growth Factor Receptor Mutations in Human Glioblastomas. *Cancer Res.* 60, 1383–1387

110 Hanif, F. *et al.* (2017) Glioblastoma Multiforme: A Review of its Epidemiology and Pathogenesis through Clinical Presentation and Treatment. *Asian Pac. J. Cancer Prev. APJCP* 18, 3–9

111 Shinojima, N. *et al.* (2003) Prognostic Value of Epidermal Growth Factor Receptor in Patients with Glioblastoma Multiforme. *Cancer Res.* 63, 6962–6970

112 Heimberger, A.B. *et al.* (2005) Prognostic Effect of Epidermal Growth Factor Receptor and EGFRvIII in Glioblastoma Multiforme Patients. *Clin. Cancer Res.* 11, 1462–1466

113 Paez, J.G. *et al.* (2004) EGFR Mutations in Lung Cancer: Correlation with Clinical Response to Gefitinib Therapy. *Science* 304, 1497–1500

114 Kobayashi, S. *et al.* (2005) EGFR Mutation and Resistance of Non–Small-Cell Lung Cancer to Gefitinib. *N. Engl. J. Med.* 352, 786–792

115 Pao, W. *et al.* (2005) Acquired Resistance of Lung Adenocarcinomas to Gefitinib or

Erlotinib Is Associated with a Second Mutation in the EGFR Kinase Domain. *PLOS Med.* 2, e73

116 Moyer, J.D. *et al.* (1997) Induction of apoptosis and cell cycle arrest by CP-358,774, an inhibitor of epidermal growth factor receptor tyrosine kinase. *Cancer Res.* 57, 4838–4848

117 Jia, Y. *et al.* (2016) Overcoming EGFR(T790M) and EGFR(C797S) resistance with mutant-selective allosteric inhibitors. *Nature* 534, 129–132

118 Brandes, A.A. *et al.* (2008) Epidermal Growth Factor Receptor Inhibitors in Neuro-oncology: Hopes and Disappointments. *Clin. Cancer Res.* 14, 957–960

119 van den Bent, M.J. *et al.* (2009) Randomized Phase II Trial of Erlotinib Versus Temozolomide or Carmustine in Recurrent Glioblastoma: EORTC Brain Tumor Group Study 26034. *J. Clin. Oncol.* 27, 1268–1274

120 Peereboom, D.M. *et al.* (2010) Phase II trial of erlotinib with temozolomide and radiation in patients with newly diagnosed glioblastoma multiforme. *J. Neurooncol.* 98, 93–99

121 Reardon, D.A. *et al.* (2015) Phase I/randomized phase II study of afatinib, an irreversible ErbB family blocker, with or without protracted temozolomide in adults with recurrent glioblastoma. *Neuro-Oncol.* 17, 430–439

122 Dawson, J.P. *et al.* (2005) Epidermal Growth Factor Receptor Dimerization and Activation Require Ligand-Induced Conformational Changes in the Dimer Interface. *Mol. Cell. Biol.* 25, 7734–7742

123 Moscatello, D.K. *et al.* (1996) Transformational and altered signal transduction by a naturally occurring mutant EGF receptor. *Oncogene* 13, 85–96

124 Okamoto, I. *et al.* (2003) Expression of constitutively activated EGFRvIII in non-small cell lung cancer. *Cancer Sci.* 94, 50–56

125 Schneider, C.A. *et al.* (2012) NIH Image to ImageJ: 25 years of Image Analysis. *Nat. Methods* 9, 671–675

126 Pines, G. *et al.* (2010) Oncogenic mutant forms of EGFR: lessons in signal transduction and targets for cancer therapy. *FEBS Lett.* 584, 2699–2706

127 Ebner, R. and Derynck, R. (1991) Epidermal growth factor and transforming growth factor-alpha: differential intracellular routing and processing of ligand-receptor complexes. *Cell Regul* 2, 599–612

128 Ronan, T. *et al.* (2016) Different Epidermal Growth Factor Receptor (EGFR) Agonists Produce Unique Signatures for the Recruitment of Downstream Signaling Proteins. *J Biol Chem* 291, 5528–40

129 Freed, D.M. *et al.* (2017) EGFR Ligands Differentially Stabilize Receptor Dimers to Specify Signaling Kinetics. *Cell* 171, 683-695 e18

130 Macdonald-Obermann, J.L. and Pike, L.J. (2014) Different epidermal growth factor (EGF) receptor ligands show distinct kinetics and biased or partial agonism for homodimer and heterodimer formation. *J Biol Chem* 289, 26178–88

131 O'Shea, E.K. *et al.* (1993) Peptide "Velcro": design of a heterodimeric coiled coil. *Curr Biol* 3, 658–67

132 Harbury, P.B. *et al.* (1993) A switch between two-, three-, and four-stranded coiled coils in GCN4 leucine zipper mutants. *Science* 262, 1401–7

133 Krug, A.W. *et al.* (2003) Aldosterone Stimulates Epidermal Growth Factor Receptor Expression *. *J. Biol. Chem.* 278, 43060–43066

134 Bakker, J. *et al.* (2017) The EGFR odyssey - from activation to destruction in space and time. *J Cell Sci* 130, 4087–4096

135 Mu, F.T. *et al.* (1995) EEA1, an early endosome-associated protein. EEA1 is a conserved alpha-helical peripheral membrane protein flanked by cysteine "fingers" and contains a calmodulin-binding IQ motif. *J Biol Chem* 270, 13503–11

136 Ullrich, O. *et al.* (1996) Rab11 regulates recycling through the pericentriolar recycling endosome. *J Cell Biol* 135, 913–24

137 Ceresa, B.P. and Bahr, S.J. (2006) rab7 activity affects epidermal growth factor:epidermal growth factor receptor degradation by regulating endocytic trafficking from the late endosome. *J Biol Chem* 281, 1099–106

138 Fortian, A. and Sorkin, A. (2014) Live-cell fluorescence imaging reveals high stoichiometry of Grb2 binding to the EGF receptor sustained during endocytosis. *J. Cell Sci.* 127, 432–444

139 Macdonald-Obermann, J.L. and Pike, L.J. (2018) Allosteric regulation of epidermal growth factor (EGF) receptor ligand binding by tyrosine kinase inhibitors. *J. Biol. Chem.* 293, 13401–13414

140 Chung, B.M. *et al.* (2009) Aberrant trafficking of NSCLC-associated EGFR mutants through the endocytic recycling pathway promotes interaction with Src@. *BMC Cell Biol.* 10, 84

141 Zhou, W. *et al.* (2009) Novel mutant-selective EGFR kinase inhibitors against EGFR T790M. *Nature* 462, 1070–1074

142 Lemmon, M.A. and Schlessinger, J. (2010) Cell signaling by receptor tyrosine kinases. *Cell* 141, 1117–34

143 Wilson, K.J. *et al.* (2009) Functional selectivity of EGF family peptide growth factors: implications for cancer. *Pharmacol Ther* 122, 1–8

144 Kil, S.J. *et al.* (1999) A Leucine-based Determinant in the Epidermal Growth Factor Receptor Juxtamembrane Domain Is Required for the Efficient Transport of Ligand-Receptor Complexes to Lysosomes. *J. Biol. Chem.* 274, 3141–3150

145 Huang, F. *et al.* (2003) Tyrosine Phosphorylation of the β2 Subunit of Clathrin Adaptor Complex AP-2 Reveals the Role of a Di-leucine Motif in the Epidermal Growth Factor Receptor Trafficking. *J. Biol. Chem.* 278, 43411–43417

146 Yuan, M. *et al.* (2019) The emerging treatment landscape of targeted therapy in non-small-cell lung cancer. *Signal Transduct. Target. Ther.* 4, 1–14

147 Thress, K.S. *et al.* (2015) Acquired EGFR C797S mutation mediates resistance to AZD9291 in non–small cell lung cancer harboring EGFR T790M. *Nat. Med.* 21, 560–562

148 Westover, D. *et al.* (2018) Mechanisms of acquired resistance to first- and second-generation EGFR tyrosine kinase inhibitors. *Ann. Oncol.* 29, i10–i19

149 Liu, Q. *et al.* (2018) EGFR-TKIs resistance via EGFR-independent signaling pathways. *Mol. Cancer* 17, 53

150 Thomas, R. and Weihua, Z. (2019) Rethink of EGFR in Cancer With Its Kinase Independent Function on Board. *Front. Oncol.* 9,

151 Grandal, M.V. *et al.* (2007) EGFRvIII escapes down-regulation due to impaired internalization and sorting to lysosomes. *Carcinogenesis* 28, 1408–1417

152 Shtiegman, K. *et al.* (2007) Defective ubiquitinylation of EGFR mutants of lung cancer confers prolonged signaling. *Oncogene* 26, 6968–6978

153 Banik, S.M. *et al.* (2020) Lysosome-targeting chimaeras for degradation of extracellular proteins. *Nature* 584, 291–297

154 Ahn, G. *et al.* (2021) LYTACs that engage the asialoglycoprotein receptor for targeted protein degradation. *Nat. Chem. Biol.* DOI: 10.1038/s41589-021-00770-1

155 Cotton, A.D. *et al.* (2021) Development of Antibody-Based PROTACs for the Degradation of the Cell-Surface Immune Checkpoint Protein PD-L1. *J. Am. Chem. Soc.* 143, 593–598

156 Bolte, S. and Cordelières, F.P. (2006) A guided tour into subcellular colocalization analysis in light microscopy. *J. Microsc.* 224, 213–232

157 Dunn, K.W. *et al.* (2011) A practical guide to evaluating colocalization in biological microscopy. *Am. J. Physiol. - Cell Physiol.* 300, C723–C742

158 Homewood, C.A. *et al.* (1972) Lysosomes, p H and the Anti-malarial Action of Chloroquine. *Nature* 235, 50–52

159 Fenteany, G. *et al.* (1995) Inhibition of proteasome activities and subunit-specific amino-terminal threonine modification by lactacystin. *Science* 268, 726–731

160 Schlessinger, J. (2002) Ligand-Induced, Receptor-Mediated Dimerization and Activation of EGF Receptor. *Cell* 110, 669–672

161 Yarden, Y. and Schlessinger, J. (1987) Epidermal growth factor induces rapid, reversible aggregation of the purified epidermal growth factor receptor. *Biochemistry* 26, 1443–1451

162 Clayton, A.H.A. *et al.* (2005) Ligand-induced dimer-tetramer transition during the activation of the cell surface epidermal growth factor receptor-A multidimensional microscopy analysis. *J. Biol. Chem.* 280, 30392–30399

163 Kozer, N. *et al.* (2013) Exploring higher-order EGFR oligomerisation and phosphorylation—a combined experimental and theoretical approach. *Mol. Biosyst.* 9, 1849–1863

164 Huang, Y. *et al.* (2016) Molecular basis for multimerization in the activation of the

epidermal growth factor receptor. *eLife* 5, e14107

165 Needham, S.R. *et al.* (2016) EGFR oligomerization organizes kinase-active dimers into competent signalling platforms. *Nat. Commun.* 7, 13307

166 Tong, J. *et al.* (2014) Proteomic Analysis of the Epidermal Growth Factor Receptor (EGFR) Interactome and Post-translational Modifications Associated with Receptor Endocytosis in Response to EGF and Stress. *Mol. Cell. Proteomics MCP* 13, 1644–1658

167 Chen, Y. *et al.* (2019) A Cross-Linking-Aided Immunoprecipitation/Mass Spectrometry Workflow Reveals Extensive Intracellular Trafficking in Time-Resolved, Signal-Dependent Epidermal Growth Factor Receptor Proteome. *J. Proteome Res.* 18, 3715–3730

168 Lam, S.S. *et al.* (2015) Directed evolution of APEX2 for electron microscopy and proximity labeling. *Nat. Methods* 12, 51–54

169 Hung, V. *et al.* (2016) Spatially resolved proteomic mapping in living cells with the engineered peroxidase APEX2. *Nat. Protoc.* 11, 456–475

170 Hung, V. *et al.* (2017) Proteomic mapping of cytosol-facing outer mitochondrial and ER membranes in living human cells by proximity biotinylation. *eLife* 6, e24463

171 Lobingier, B.T. *et al.* (2017) An Approach to Spatiotemporally Resolve Protein Interaction Networks in Living Cells. *Cell* 169, 350-360.e12